A deep Westerbork survey of areas with multicolor Mayall 4 M plates. I - The 1412 MHz catalogue, source counts and angular size statistics

Windhorst, R.A.; Heerde, G.M. van; Katgert, P.

ASTRONOMY & ASTROPHYSICS
SUPPLEMENT SERIES

OCTOBER 1984, PAGE 1

Astron. Astrophys. Suppl. Ser. **58,** 1-37 (1984)

A deep Westerbork survey of areas with multicolor Mayall 4 m plates. I. The 1412 MHz catalogue, source counts and angular size statistics

R. A. Windhorst (*), G. M. van Heerde and P. Katgert

Sterrewacht Leiden, Postbus 9513, 2300 RA Leiden, The Netherlands

Received January 2, accepted April 20, 1984

Summary. — A deep 21 cm Westerbork radio survey is presented of nine fields, selected in four high latitude areas (SA57, SA68, SA28 and an area in Hercules) for which deep multicolor Kitt Peak 4 m plates are available.
The Westerbork observations have been done with the 3 km array at 1412 MHz with an east-west beam of 12.″5 and yielding a noise of 0.12-0.20 mJy in 12^h. Careful calibration of the data, including self-calibration, yielded high dynamic range, noise limited maps with absolute uncertainties in position of order 0.″4 and in flux of order 3-5 %.
At 12.″5 resolution about 30 % of all sources is resolved, requiring a complicated algorithm to calculate source positions, fluxes, angular sizes and position angles. Due to noise, fluxes and angular sizes are generally overestimated, but corrections to the parameter estimates are derived that make them statistically unbiassed. Special attention is paid to the empirical derivation of the position and flux errors.
In total 471 sources are tabulated, out of which 306 form a well defined complete sample within 5.52 deg^2, having a peak signal-to-noise $\geqslant$ 5.0 and lying within the $-$ 7 dB attenuation radius (0.°464) of each field. The influence of the selection criteria on the sample completeness is discussed, taking the angular size and component flux ratio distribution into account. The latter is independent of flux density over three decades.
The angular size distribution could be derived precisely with the WSRT 3 km resolution and shows that in the range 1-10 mJy a smaller fraction of large ($\psi \geqslant 20''$) sources is seen than in the 10-100 mJy range. It is possible that faint radio sources have smaller intrinsic linear sizes than the brighter ones. The median angular size is $\sim$ 10″ in the range 1-200 mJy.
The 1412 MHz source counts are consistent at different cut-off levels, showing that the statistical corrections for population and resolution bias are reliable. The presented counts are consistent with previously observed 1.4 GHz counts of which a summary is given in the flux range 1-10^5 mJy.

Key words : radio source : general — surveys catalogues — cosmology.

1. Introduction.

1.1 BACKGROUND. — Several systematic deep surveys of extragalactic radio sources have been made with the Westerbork Synthesis Radio Telescope, mostly at 1.4 GHz and with a maximum baseline of 1.5 km. Among these are : the 1st Westerbork survey (Katgert *et al.*, 1973) covering 18 deg^2 down to $\sim$ 10 mJy; the 2nd Westerbork survey (Katgert and Spinrad, 1974), covering $\sim$ 4.5 deg^2 down to $\sim$ 7 mJy; and the 3rd Westerbork survey (Katgert, 1975; hereafter K75) covering 18 deg^2 down to 6 mJy. The so-called « Background Survey » (BGS) was constructed by Willis, Oosterbaan, and de Ruiter (1976; hereafter WOR) from the WSRT data-bank and covered $\sim$ 90 deg^2 down to 4-10 mJy. All surveys yielded 21 cm source counts, but only for the 3rd WBK survey and the BGS corrections for resolution bias were applied. These surveys were also the first to produce angular size statistics at such low flux levels (Katgert, 1976; Oosterbaan, 1978).

Optical identification programs were carried out for all four surveys mentioned : on Palomar Schmidt plates of varying depth for the 1st (Katgert *et al.*, 1973) and 3rd (Katgert *et al.*, 1979) Westerbork Survey and the BGS (Willis and de Ruiter, 1977), on deep Lick 3 m plates for the 2nd Westerbork survey (Katgert and Spinrad, 1974) and on deep IIIaJ Mayall 4 m plates for the BGS (de Ruiter *et al.*, 1977).

Unfortunately, all these programs lacked a careful photometric calibration as well as spectroscopic redshifts. Therefore, a deep radio survey with deep multicolor plates, calibrated photometry and spectroscopic redshifts was very much needed. This is the purpose of the current project, the « Leiden Berkeley Deep Survey » or LBDS, of which this is the first paper.

(*) Now at : Mount Wilson and Las Campanas Observatories, 813 Santa Barbara Street, Pasadena, CA 91101, U.S.A.

1.2 PURPOSE OF THE PROGRAM. — The ultimate purpose of the Westerbork Deep Surveys is a better understanding of the nature of faint radio galaxies and quasars and their cosmological (or population) evolution.

In recent years the emphasis has been on the determination of the epoch dependent radio luminosity function. Lacking spectroscopic redshifts, apparent magnitudes were transformed into distances using the standard candle assumption (de Ruiter, 1978; Katgert *et al.*, 1979). Although this is valid at the 3CR and 4C level for (giant) elliptical radio galaxies, and presumably also holds at intermediate flux density levels for such galaxies, it is certainly not valid *a priori* at fainter fluxes ($S_{1.4\mathrm{GHz}} \lesssim 10$ mJy), because increasing numbers of low luminosity ellipticals and even spiral galaxies are expected amongst the optical identifications of faint radio sources.

The use of broad band colors in the LBDS, however, will in many cases indicate the galaxy type and constrain the redshift, while emission lines or absorption features will provide unique answers to the questions of redshift and type. As a result, the cosmic epoch dependent RLF of various radio galaxy types can be determined directly. We therefore expect that the Leiden Berkeley Deep Survey will lead to a better understanding of the nature and (possible) cosmological evolution of various types of radio galaxies.

1.3 CHARACTERISTICS OF THE LEIDEN BERKELEY DEEP SURVEY. — We have made a deep 21 cm radio survey of fields in the selected areas SA57, SA68 and SA28 (hereafter referred to as Lynx) and an area in Hercules. Good seeing plates made with the Kitt Peak Mayall 4 m telescope are available in the passbands U ($\lambda = 3600$ Å), J ($\lambda = 4650$ Å), F ($\lambda = 6100$ Å) and N ($\lambda = 8000$ Å) (Kron, 1980; Koo, 1981). The object density on these plates is so high that the high positional accuracy of the WSRT 3 km array is needed for reliable optical identifications (Windhorst, Kron and Koo, 1984; hereafter Paper II). Available photoelectric calibration sequences allow accurate photographic photometry in four passbands (Kron, Koo and Windhorst, 1984; hereafter Paper III). For a substantial fraction of the identifications spectroscopic redshifts have been obtained with the KPNO 4 m Cryogenic Camera and the $2^{m}.7$ McDonald IDS (see Paper III).

In the current survey the 5 σ sensitivity of 0.60 mJy allows the break in the radio luminosity function (at $P^* \simeq 10^{25.0}$ WHz^{-1} for $H_0 = 50$ km/s/Mpc) to be seen out to redshifts of $z \sim 2.0$ ($q_0 = 0.5$). Thus the Leiden Berkeley Deep Survey is not radio flux limited for all radio galaxies with $P > P^*$, unless these are at very high redshift. Alternatively, we may expect that sources with $P < P^*$, like low luminosity ellipticals and spiral galaxies, will show up in substantial numbers, and could even be at cosmological distances. The contribution to the counts of such radio galaxies could be increasingly more important at fainter levels.

1.4 OUTLINE OF THE PAPER. — Section 2 describes the characteristics of the WSRT 3 km array, the observations and calibration of the nine LBDS fields. In section 3 we describe the production of the maps and the used clean-and-restore procedure. The noise and its uniformity are determined. In section 4 we obtain for each source candidate its observed parameters with a Gaussian source fitting routine. Statistical errors on the observed source parameters are derived empirically. Section 5 describes how the observed source parameters were transformed into intrinsic (model) parameters. Statistical corrections are given for systematic biasses in the source parameters introduced by noise. In section 6 we describe the selection criteria of the complete sample, and section 7 gives the source list. In section 8 angular size distributions and the median angular size-flux density relation are presented. In section 9 we derive the 1412 MHz source counts after correcting for population and resolution bias. A review of previous 1.4 GHz counts is given, in the context of which we discuss our counts.

2. Observation and calibration.

2.1 INSTRUMENT. — All observations were done with the 3 km Westerbork Synthesis Radio Telescope at 1412 MHz. The extension to 3 km maximum baseline has not changed its principles of operation, which can be found in Brouw (1971) and Högbom and Brouw (1974). Details of the new WSRT 3 km configuration and its operation are given by Willis and Kahlmann (1980). A description of the 5120 channel digital line backend (DLB), used for the current observations, is given by Bos *et al.* (1981).

Until autumn 1980 the system temperature of the receivers in the frontends was about 85-90 K. This yielded for 40 interferometers a noise of about 0.20 mJy in 1×12^{h}. After the installation of cooled frontends in the movable telescopes at the end of 1980 their system temperature improved to about 25-30 K. Combination with the 90 K frontends in the fixed telescopes resulted in an effective system temperature of about 50 K for the whole array. This improved the noise achieved in 1×12^{h} to about 0.12 mJy.

The first observations (SA57, SA68 and Hercules) were done in continuum with total bandwidth $\Delta\nu = 10$ MHz. This causes a bandwidth (or delay) smearing of at most 8 % at the − 7 dB attenuation radius ($r = 0°.464$), which manifests itself as a decrease of the source peak flux density S_p with the projected distance to the field centre, and a similar increase of its half power width in radial direction, so that in first order the total flux of the source is preserved (Willis and Kahlmann, 1980). Because complete samples of faint radio sources are defined in terms of peak flux density, a serious bias can be introduced in a synthesis radio survey if there is a substantial amount of bandwidth smearing. Although a delay smearing of at most 8 % is quite acceptable, we did the rest of the survey (namely the Lynx fields and SA68.2) with the new DLB line receiver, using 7 line channels of $\Delta\nu = 1.25$ MHz, separated by 1.25 MHz, while the middle channel was centred at 1412.0 MHz. This reduces the delay smearing to less than 0.1 % at the − 7 dB attenuation radius. For the whole survey the data sampling was at a rate of once every 10 seconds so that the time delay smearing is always smaller than the bandwidth smearing.

2.2 OBSERVATIONS. — Table Ia lists the characteristics of the 9 Leiden Berkeley fields and their WSRT observations, table Ib gives the quality of the observations.

For all fields the Westerbork pointing centre (equal to the fringe stopping centre) was chosen to coincide within 5′ with the 4 m plate centre. The selection of the fields was

purely done by optical criteria, like high galactic latitude (all fields have $b^{II} \gtrsim 35°$) and minimum HI column density. This gives a random selection of the extragalactic sky from the radio point of view.

All observations were 1×12^h in length and were done almost entirely during the night to minimize solar interference. Only the observations of SA68.1 and SA68.2 were done partially during daytime.

The baseline coverage ranged from the shortest baseline with increments of 72 m to the maximum baseline of 2700 m and is given in table Ia. The shortest baselines were either 72 m or 36 m, corresponding to spatial frequencies of 10′ to 20′, respectively. Mutual shadowing of the telescopes occurred only at the extreme hour angles in the observations of the low declination fields SA57 and SA68.1 and SA68.2. All affected hour angles were discarded.

On-line monitoring was done for system temperature and total power of each of the individual telescopes. All bad channels were traced this way, if not already realized beforehand, and their data were discarded. Short term interference spikes, caused mainly by solar flares, radar or a remote thunderstorm, were also deleted. Very short term interference spikes were already removed by the on-line routine that searches for interference. Interference on timescales of hours occurred only during sunrise in the observations of SA68.1 and SA68.2. In SA68.1 it did not affect the map, because this was noise limited anyway. In SA68.2, all HA ranges affected were discarded, yielding complete HA coverage after combining 2×12^h observations.

The dipoles of the fixed and movable telescopes were used in the crossed configuration. The four Stokes parameters, I, Q, U and V are formed following Weiler (1974). The linearly polarized (Q and U) and circularly polarized (or V) data were Fourier transformed simultaneously with the total intensity (I) data. Because only the strongest radio sources showed some visible linear polarization, we did not further analyse the Q- and U-maps. The amplitude and phase data in V were used to trace bad channels and interference. The Q- and U-data were also checked, since some interference turns out to be linearly polarized.

2.3 The calibration. — To determine the geometry of the array, regular baseline calibrations were done, by monitoring a calibration source for 12^h, for which the positions and fluxes are listed in table II. Typical errors in their absolute positions are $0^s.002$ in α and $0''.03$ in δ, derived from recent reobservations of 3C48, 3C147 and 3C286 by Elsmore (1982, unpublished). The resulting positions of the individual telescopes have an accuracy of 1-2 mm.

Before and after each 1×12^h survey observation, calibration sources were observed for $1\text{-}2^h$ to establish the actual instrumental amplitude gains and phase zeros for every interferometer. These parameters were determined according to the procedure described by Brouw (1971) and van Someren Greve (1974), using the known calibrator positions and fluxes. The accuracy of the instrumental phases was better than 5 degrees; the resulting dynamic range was better than 23 dB for the night-time observations, but $\lesssim 20$ dB for SA68.1 and SA68.2. The calibration also corrected clock errors down to 0.02 to 0.03 seconds of time, while frequency errors were corrected to $\pm$ 1 kHz accuracy. Adding these errors, absolute position uncertainties of order $0''.4$ are obtained for our observations, but sometimes $\sim 0''.2$ for an excellent calibration.

The 1412 MHz calibrator fluxes were tied to the scale of Baars *et al.* (1977). The quality of our amplitude gain calibrations was generally of order 2 %, but deteriorated to $\sim$ 5 % for SA68.1 and 2, so that the flux scale in the present survey is consistent with that of Baars *et al.* to within 3-4 %.

The fields SA68.2 and Lynx.1 needed self-calibration, because the strongest sources were about 800 σ. Both sources were identified with a blue stellar or compact object which makes it likely that the radio source is point-like. Phase self-calibration improved the dynamic range to 28 – 30 dB, residual phase errors being less than 3°. The result of the phase self-calibration is illustrated in figures 1b and 1c. Amplitude self-calibration did not yield a significant improvement in dynamic range.

In Lynx.4 it was known in advance that the extended source 4C45.17 would be in the field with $S_{1.4} \sim 1.6$ Jy so that severe dynamic range problems were expected. Therefore, Lynx.4 was observed in the redundancy mode (Noordam and de Bruyn, 1982). However, the standard calibration of Lynx.4 turned out to be very good (27 dB) so that the initial map was essentially noise limited. We therefore used this map in the subsequent analysis.

2.4 Primary beam. — The WSRT primary beam was measured recently at 21 cm by Bregman and de Waard (1982, private communication) out to large radial distances r from the pointing centre at 6 different position angles. The 1412 MHz primary beam is circular in shape and can be accurately represented by :

$$ATT\left(\frac{r}{\text{deg}}, \frac{\nu}{\text{GHz}}\right) = \cos^{-6}(61.191 \times \nu \times r) \qquad (1)$$

(Lugtenborg, 1982, private communication) and scales with frequency for $\nu \geqslant 1.4$ GHz. By definition, the attenuation factor $ATT \geqslant 1.0$.

The difference between this fit of the measured attenuation values at 1412 MHz and the exponential primary beam fit of Katgert (1975), is on average smaller than 0.3 % out to a radius of $0^\circ.55$ (– 10 dB radius at 21 cm). The advantage of formula (1) is that it is easily invertable, so that the weights in the source counts can be computed analytically (see Sect. 6).

3. Fourier transforms and post map reduction.

3.1 Production of the maps. — Both the continuum and line observations were Fourier transformed with the routine LINEMAP of Harten (1979) using the Fast Fourier Transform (FFT) as programmed by Brouw (1971). Before the FFT the (U, V)-data were first convolved to a rectangular grid using a prolate Bessel function, which reduces aliasing of the grating rings around a source in the field centre to less than 0.7 % of the peak (Lugtenborg, private communication). Then the data were weighted proportional to baseline length to compensate for the baseline dependent sampling density in the (U, V)-plane. In addition, the visibility data were tapered with a Gaussian weight as a function of baseline, being unity at the zero spacing and 0.25 at the longest baseline. This gives an elliptical

beam with half power widths 12″.5 × 12″.5 cosec δ and near-in side-lobes of at most − 4 % of the peak. Areas of 1°.75 × 1°.75 cosec δ around the pointing centre were mapped. This has the advantage that the 50′ grating rings of sources close to the field centre (and of the antenna pattern) are still completely within the map, hence minimizing aliasing.

In order to increase the sensitivity for sources with large angular sizes, low resolution maps were made with maximum baslines of 1440 m, by excluding the 20 interferometers with telescopes C and D from the data. The resulting « 1.5 km » maps have a resolution of 23″.1 × 23″.1 cosec δ. In all maps the sampling was at least 2.0 points per synthesized half power beamwidth in the direction of both α and δ, requiring the 3 km maps to be made of 1024^2 pixels. The 1.5 km maps were also made 1024^2 in size.

For the line observations in SA68.2 and Lynx.1, 2 and 3 seven channel maps and seven corresponding antenna patterns were made at *one fixed grid* per field. Individual channel maps were checked for frequency dependent effects. In Lynx.1 and SA68.2 the highest frequency channel had a much higher noise and was discarded. Both the channel maps and the corresponding antenna patterns were combined on a pixel-to-pixel basis with weights proportional to $\sigma_{\rm map}^{-2}$. The synthesized beam of the combined channel map is identical to that of a comparable continuum observation, but grating rings in the map as well as in the antenna pattern are slightly smeared out. The combined map has a sensitivity corresponding to the total bandwidth, but a delay smearing corresponding to the (smaller) bandwidth of the individual line channels. Since the theoretical antenna pattern and the actual point source response remain identical (for a perfect calibration), precise deconvolution can still be done afterwards.

3.2 Cleaning and restoration of the maps. — After the Fourier transform the maps contain series of elliptical grating rings around each source at distances of 10′ × 10′ cosec δ and multiples thereof. The resulting « dirty » maps look typically like figure 1a. It is clear that, due to grating ring confusion, such maps are inappropriate for any deep survey work. However, as long as the maps are noise limited, grating rings can be removed exactly by deconvolving the map with its antenna pattern using the clean algorithm (Högbom, 1974). After the cleaning has converged, the delta function source components were restored in the remaining noise map by convolving them with the clean beam (the central positive part of the antenna pattern) and adding them to the noise map. The resulting cleaned and restored map has no grating rings left, if it is noise limited (Fig. 1c compared to 1b).

Because the 60′ grating ring is not fully present in the antenna pattern it may cause troubles for very strong sources far away from the field centre. In order to get rid of these remote grating rings as well as their aliasing, we made for all fields a second generation 3 and 1.5 km maps, where before the FFT the (U, V)-responses of all source components stronger than 10 σ were subtracted from the data. After the subtraction of about 50-100 delta function components, the residual map shows only some grating ring leftovers at the $\lesssim 2\ \sigma$ level. These are easily removed by cleaning this residual map in the same way as described above, but now down to 4 σ, so that any grating rings left are less than 0.25 σ. The total list of source components found in the two clean runs is restored in the cleaned noise map that remained after the second run.

As a check of possible influences of the cleaning algorithm on the source parameters, we compared 30 sources found in a dirty map (not on grating rings) with the same sources in a map that was cleaned and restored after source components were subtracted from the (U, V)-data. Deviations in positions were on average 0″.05 ± 0″.35 (rms) and deviations in flux were on average less than 1 % ± 4 %.

3.3 Determination of the noise. — We determined the noise in each of the 3 and 1.5 km maps from the histogram of peak intensities in the central 512^2 pixels. Figure 2 shows this histogram for the cleaned and restored map of Lynx.2, of which a grey scale plot is shown in figure 3. The other noise histograms are similar. At the positive side an excess of points with respect to the Gaussian noise distribution is seen for $S_{\rm p} \gtrsim 3.5\ \sigma$, which is due to real sources. At the negative side the distribution is perfectly Gaussian in shape, the few deflections below − 4.5 σ being consistent with the expectation for a true Gaussian distribution. We are therefore confident that at the level of $S_{\rm p} \geqslant +5.0\ \sigma$ the noise limited maps will contain essentially no spurious sources. The values of σ for the cleaned 3 km and 1.5 km maps are listed in table Ib (in mJy/beam), and could be determined to about 2 % accuracy. The noise in the 1.5 km maps is on average 1.31 times that of the 3 km maps, due to the different baseline tapering. From table Ib and Ia it follows that the observed noise in the maps is consistent with the expected value.

The difference between the actual zero level in the cleaned map and the true zero level ($S_{\rm p} = 0$) is less than 0.015 × σ. We checked for variation in the noise over the maps by determining the noise in the 256^2 corners of the map and in the centre as well. Variations in the numerical value of σ were found to be less than 2.5 %. The resulting total uncertainty in the actual value of the noise is less than 3.5 %.

4. Source definition and observed source parameters.

4.1 Source definition. — In the absence of *a priori* optical information, the source definition depends purely on radio criteria and is therefore frequency and instrument dependent, as has been discussed by K75 and WOR.

We define a *source component* as one coherent collection of positive pixels without a relative minimum in its surface brightness distribution. Three different types of sources are considered :

(U). An unresolved source consists of one component that is, given its signal-to-noise ratio, not distinguishably larger than the beam.

(R). A resolved source consists of one component whose extent with respect to the beam is larger than some signal-to-noise dependent amount.

(E). A source is called extended if it is either clearly resolved into two components (the classical double) or if it is triple with all components aligned. Multi-component sources with other morphology are called complex.

In the case of extended sources WOR introduced a fixed upper limit definition of 50″ for the equivalent angular

size ψ_{EQ} which is defined as :

$$\psi_{EQ} = \psi\sqrt{1 - \cos^2\phi\cos^2\delta} \qquad (2)$$

where δ and ϕ are the declination of the source and the position angle of its true angular size ψ. This definition results in a redshift dependent selection of intrinsic diameters. Due to the higher source density in the LBDS the number of unrelated source components with $\psi_{EQ} \lesssim 50''$ could be larger than 10 %. Therefore, the optical identification information is used as an additional criterion. About 53 % of the mJy radio sources have reliable identifications (Paper II). For these a redshift independent definition of extended sources is given : an extended source candidate (with $\psi_{EQ} \leqslant 50''$) will *not* be considered to be one physical source, if at least one of the components, other than the central component of a triple source, has a reliable identification, unless low surface brightness emission connecting the components suggests the contrary.

4.2 Derivation of source parameters.

4.2.1 *Unresolved and resolved sources.* — Because the 21 cm WSRT 3 km beam is comparable to the median angular size ($\sim 10''$) of mJy radio sources, a large fraction of them is clearly resolved, so that a point source fitting routine cannot be used to derive observed source parameters. Instead we used a two dimensional elliptical Gaussian fitting routine (Brinks, 1980, private communication). This routine is more sophisticated than that of WOR, hence requiring a different Monte Carlo calibration (Sect. 5.1).

An iterative least squares Gaussian fit is made at the positions of a complete list of source candidates, using matrices of $(4 \times n)^2$ pixels, where n is the number of points per HPBW. Six independent free parameters are solved for in the fit, namely the source coordinates, its peak flux density S_p, observed Gaussian half power widths a and b and the position angle PA of the major axis a, defined relative to north over east. A least squares Gaussian fit to the restoring beam was also made, yielding the half power beamwidths a_{AP} and b_{AP} (see Table Ib) and the beam position angle, which never deviated more than 5° from zero. For a two-dimensional Gaussian beam the observed source half power widths a and b, at position angle PA, can be deconvolved analytically with the half power beamwidths a_{AP} and b_{AP}, yielding the deconvolved major and minor axes σ and τ, at position angle ϕ (Wild, 1970).

The normalized source area R and the total flux S_{TOT} are defined as :

$$S_{TOT} = S_p \times R = S_p \times \frac{a \times b}{a_{AP} \times b_{AP}}. \qquad (3)$$

The algorithm partially compensates for delay smearing in the continuum maps, since S_p is underestimated by ~ 5 %, while R is overestimated by ~ 2.5 %, so that systematic errors in the *total* flux do not exceed 2.5 %. Thus the elliptical Gaussian fitting routine generally recovers most of the flux that would have been lost with a point source fitting routine.

4.2.2 *Extended and complex sources.* — For clearly *extended* or *complex* sources the Gaussian fitting routine breaks down. Every recognizable source component is dealt with separately, even though the components may be so close that source blending affects the results.

The component position is the flux weighted average over a matrix of pixels that is symmetric around the peak. Its integrated flux is the sum of pixel intensities above the 0.5 σ contour, normalized to the volume of the restoring beam. Its peak flux density is obtained by interpolation in the matrix. The normalized source area R then simply follows from equation (3).

The parameters for the source as a whole are derived as follows : the most likely source position for a double source occurs between the midpoint and the centroid position, but closer to the midpoint. From the data of Katgert-Merkelijn *et al.* (1980) we find that the most probable position for the identification is at $2/3 \times$ (the midpoint) + $1/3 \times$ (the centroid). It is noteworthy that the correct identification of the very extended source in Lynx.4, 55W037 ($\psi \simeq 114''$, Fig. 10), would have been missed if instead of this position we had used the centroid position. The total number of *independent* beam areas, R_{TOT}, covered by the source as a whole, is simply the sum of the R's of each component. The effective peak flux density is defined as $S_p^{eff} = S_{TOT}/R_{TOT}$, and is used to determine their position error and weight in the source counts. The overall largest angular size ψ_{TOT} for extended or complex sources is derived in the conventional way. The smallest angular size χ is the maximum extent in the direction perpendicular to ψ_{TOT}.

4.3 Empirical determination of the statistical errors.

— To describe the position and flux error distribution a functional form of the individual parameter errors is adopted, whose coefficients are determined empirically. A good description of the individual position errors is given by (Robertson, 1980, private communication) :

$$\sigma_\alpha, \sigma_\delta = \sqrt{\left(C_p \cdot \left(\frac{S_p}{N}\right)^{-1} \cdot R\right)^2 + C_{\alpha,\delta}^2}. \qquad (4)$$

Here the first term is the signal-to-noise dependent position error with coefficient C_p, which is larger in declination by cosec δ due to the beam ellipticity. The number of uncorrelated beam areas of the source R is used as multiplier, yielding an error ellipse with size proportional to R. In the case of resolved sources this results in a larger search area for optical identifications than in the case of point sources of the same S_p/N. The second term is the absolute calibration error in position.

The individual relative error in the total flux is given by :

$$\frac{\sigma_{S_{TOT}}}{S_{TOT}} = \sqrt{\left(\frac{S_p}{N}\right)^{-2} + C_f^2 + \left(\frac{\partial \ln ATT(r)}{\partial r} \cdot \Delta r\right)^2}. \qquad (5)$$

The first term is the signal-to-noise dependent relative flux error, while the second term C_f is the (fractional) error in the absolute flux calibration. The third term is the relative flux error due to the pointing error (Δr) of the individual WSRT dishes. It scales with frequency and amounts to 2 % at 1.4 GHz at the $-$ 7 dB radius. The last terms in (4) and (5) dominate for strong sources.

In each set of overlapping fields we have 5-15 sources in common. For SA57 we had no other overlapping WSRT

observations, but we could compare our sources with the 17 sources found in a 1 × 12^h VLA map at 1465 MHz, provided by Owen and Thuan (1980, private communication). For Lynx.2 we could also compare our sources with those of Windhorst *et al.* (1984), obtained in a 2 × 6^h VLA C-array observation at 1462 MHz of the same field. These two observations had 55 sources in common. All fluxes were scaled to 1412 MHz.

For a perfect calibration, the position differences and the (flux ratios-1), normalized with respect to the combined errors in the two fields, should be Gaussian distributed with zero averages and unity dispersions. The latter requirement determines the empirical values of the error distribution coefficients C_p, C_α, C_δ, C_f and Δr.

Because for well calibrated observations the coefficients C_α and C_δ are small, we determine the more critical value of C_p first, which turns out to be 0.3-0.4 × HPBW$_\alpha$. Using this, the values of C_α and C_δ are found iteratively and turn out to be 0″.4 − 0″.5. The values of Δr turned out to be generally 20-30″, i.e. larger than the 10″ mechanical pointing error which is generally claimed for the individual WSRT antennae. The values of C_f are of order 5 %, which is somewhat large, because the consistency of the WSRT flux scale on different days is of order 2-3 %. All error coefficients are given in table Ib.

Some examples of the error distribution are shown in figures 4a and 4c for right ascension, figures 4b and 4d for declination and figures 4e and 4f for the total fluxes. Evident bad cases like double, extended or variable sources are drawn, but not included in the computations and for the remaining sources a Gaussian with unity dispersion is drawn. An impression of the quality of the absolute positions and the flux scale is obtained from table III. Comparing these data with the error distribution in figure 4 the following conclusions can be drawn :

1) the agreement between the VLA and WSRT positions in SA57 and Lynx.2 is excellent (sometimes better than 0″.25);

2) the average position difference between SA68.1 and SA68.2 is somewhat large and is due to a non-optimal calibration. The coordinate system of SA68.2 should be more reliable because it was defined by self-calibration on the optical position of the blue compact object 54W057;

3) the differences in declination in Lynx.3-2 and Lynx.1-4 are of acceptable magnitude, but systematic in direction. From the comparison with the VLA data we believe that the positions in Lynx.2 in any case are very good. The absolute coordinate system of the radio maps will be discussed in Paper II in the context of the optical astrometry;

4) the correspondence of the flux scales in all fields is of order 1-2 %, apart from that in SA68. The amplitude calibration of the two fields was of lower quality, but we do not know which field is closest to the scale of Baars *et al.* Neither of the two flux scales in SA68 was corrected for this difference.

5. Intrinsic source parameters.

5.1 THE RELATION BETWEEN OBSERVED AND INTRINSIC SOURCE PARAMETERS. — To obtain consistency in the description of extended (and complex) sources on the one hand and the (slightly) resolved sources on the other, we describe the latter in the framework of the unequal double source model. Figure 10 shows that this model describes the main characteristics of most of the extended sources quite well.

The *observed* source parameters derived from the Gaussian fitting routine and describing the observed surface brightness distribution are the peak flux density S_p, the deconvolved major axis σ, its position angle ϕ, and the normalized source area R (or, equivalently the fitted source major and minor axes a and b). The basic *noise-free* (hereafter called *intrinsic*) source parameters that we want to derive from the Gaussian fit parameters are the total flux S_{TOT}, the largest angular size ψ (i.e. the distance between the two point-like components), the fraction f of the total flux contained in the stronger component ($0.5 \leqslant f < 1$) and the true position angle ϕ of the line that connects both source components. The transformation between the observed and intrinsic source parameters must incorporate two effects : the strongly non-linear relations between these parameters, which would be obtained in the *noise-free* limit and the (non-linear) *effects of noise* on the Gaussian fitting parameters.

5.1.1 *The noise-free limit.* — In the case of infinite signal-to-noise the empirical relation between the intrinsic source parameters (S_{TOT}, ψ, f, ϕ) and the observed source parameters (S_p, R, σ, ϕ) simplifies because then by definition : $S_{TOT} = S_p \times R$. To study the relation between (ψ, f, ϕ) and (R, σ, ϕ) we injected artificial unequal double sources in a noise-free map at 8 different component separations ψ, 8 flux ratios f and 8 position angles ϕ_{proj} (obtained from $\mathrm{tg}\,\phi_{proj} = \mathrm{tg}\,\phi/\sin\delta$, where ϕ is the true position angle of the source on the sky). All artificial sources were analysed using the same Gaussian fitting routine as for the LBDS catalogue. The resulting relations that describe the transformation between observed and intrinsic source parameters are the functions $R(\psi_{EQ}, f)$, $\sigma(\psi, f)$ and $R(\sigma, \cos\phi_{proj})$ which are shown in figures 5a, 5b and 5c, respectively. The rightmost dashed line in figures 5a and 5b shows beyond which values of ψ the Gaussian fitting routine breaks down, because the source is resolved into two components.

Using the functions $R(\psi_{EQ}, f)$ and $\sigma(\psi, f)$ one can derive the intrinsic parameters (ψ, f) from any combination of (R, σ), given the declination and position angle of the source, which are needed to transform ψ_{EQ} into ψ according to equation (2). In order to do so we approximate these functions as :

$$R(\psi_{EQ}, f) = A + B\psi_{EQ} + C\psi_{EQ}^2 + D\psi_{EQ}^3 \qquad (6)$$

$$\sigma(\psi, f) = a + b\psi + c\psi^2 + d\psi^3 \qquad (7)$$

where the coefficients are each third order polynomials in f and are given in the Appendix. These relations can be inverted in such a way that every fitted parameter pair (R, σ) yields a unique set of intrinsic parameters (ψ, f). The numerical accuracy of this inversion is better than 0.06 × HPBW$_\alpha$ ~ 0″.75 in ψ and 0.025 in f.

Figure 5c shows that R and σ are not independent, but coupled *via* ϕ_{proj}, which is the deconvolution relation. Thus R and σ, as found from the Gaussian fit parameters, imply also a value of ϕ, when using the following represen-

tation of figure 5c :

$$R(\sigma, \phi_{\text{proj}}) = 1 + [\alpha + \beta\sigma + \gamma\sigma^2 + \delta\sigma^3]^2 \qquad (8)$$

where the coefficients are third order polynomials in $\cos \phi_{\text{proj}}$, given in the Appendix. Inversion of (8) yields another value of ϕ with a numerical accuracy of 1°.5. A better estimate of the true position angle could then be obtained by averaging the value of ϕ, derived from (8), with the value of ϕ, obtained from the analytical deconvolution in the Gaussian fitting routine. The uncertainty in ϕ was taken to be equal to half the difference between the two estimates. We added 5° in quadrature.

5.1.2 *The noisy reality.* — To investigate the effects of noise, artificial sources were inserted in the cleaned, noise limited map of Lynx.2 from which all real sources were removed. Sources were generated with east-west separations of 0.0, 0.5, ..., 3.5 gridpoints (0-22″), component flux ratios of 0.55, 0.65, 0.75 and 0.85, and with total fluxes of 4, 4.5, 5, 6, 7, 8, 9, 10, 15 and 20 σ (σ = 0.121 mJy/beam). This was repeated 32 times at different positions in the map for each realization.

Again all these sources were analysed in the same way as the LBDS catalogue. From the redistribution of the input parameter values it turns out that noise tends to overestimate the values of R, σ and S_p by some S_p/N-dependent amount, so that equations (6), (7) and (8) should be S_p/N-dependent too. In addition, the distribution functions resulting from a delta-function-shaped input are asymmetrical in R, S_p and σ with a skewness towards larger values. The noise affected parameters R_{OBS} and $(S_p/N)_{\text{OBS}}$ were corrected to obtain the most likely parameters R_{COR} and $(S_p/N)_{\text{COR}}$.

The corrections for noise induced overestimation of R_{OBS} and $(S_p/N)_{\text{OBS}}$ are :

$$R_{\text{COR}}/R_{\text{OBS}} = C_R((S_p/N)_{\text{OBS}}, R_{\text{OBS}}, \sigma_{\text{OBS}}) \qquad (9)$$

and

$$(S_p/N)_{\text{COR}}/(S_p/N)_{\text{OBS}} = C_{S_p}((S_p/N)_{\text{OBS}}, R_{\text{OBS}}, \sigma_{\text{OBS}}). \qquad (10)$$

The correction factors are in the range $0.70 \lesssim C_R \lesssim 1.15$ and $0.80 \lesssim C_{S_p} \lesssim 1.05$ while they are on average $\lesssim 1$, which shows that R and (S_p/N) are generally overestimated. These relations are necessary for $4 \lesssim S_p/N \lesssim 11$ and are applicable only for $0.8 \lesssim R \lesssim 2.8$. Their effect is that for a population with a wide range of R, S_p/N and σ the corrected values R_{COR} and $(S_p/N)_{\text{COR}}$ are unbiassed with respect to the values of the input population, while the numerical errors in C_R and C_{S_p} are 6 % and 4 % (rms), respectively.

To obtain angular sizes, we applied the inversion of relations (6), (7) and (8) to the observed source parameters (R_{OBS}, σ_{OBS}, ϕ). Only *after* the application of this inversion an empirical correction for noise is applied to ψ_{OBS} which yields ψ_{COR}, the best estimate of the true angular size. In the Appendix we give the correction function $\psi_{\text{COR}}(\psi_{\text{OBS}}, S_{\text{TOT}}/N)$. To first order ψ_{COR} is identical to ψ_{OBS} for high S_{TOT}/N. For lower S_{TOT}/N, however, ψ_{COR} becomes increasingly smaller than ψ_{OBS}, while the maximum correction for a 5 σ source is 0.25 HPBW_α. An angular size contingency table was used to derive errors in ψ_{COR} as a function of ψ_{OBS} and S_{TOT}/N, which are also given in the Appendix. The relative error in ψ_{COR} decreases monotonically with both ψ_{OBS} and S_{TOT}/N. For sources with $\psi_{\text{OBS}} \simeq 12''$ the relative error in ψ_{COR} amounts to 50 % for $S_{\text{TOT}}/N = 10$ and decreases monotonically to less than 1 % for $S_{\text{TOT}}/N = 1000$. We added 10 % in quadrature to this relative error. The f-values turned out to be poorly determined for faint sources ($S_p/N \lesssim 10$), so no attempt was made to correct the f-values. Only for strong resolved (and of course extended) sources the value of f is meaningful.

5.2 Resolution criterion and upper limits to ψ for unresolved sources. — For cosmological tests like angular size statistics one must have a well-defined statistical criterion for source resolution. The decision, whether a source is extended or not, necessarily has to be made from observed source parameters, whose estimates are unavoidably affected by noise. We decided to use ψ_{OBS} to distinguish between unresolved and resolved sources. From the angular size contingency table we determined values of ψ_{CRIT} as a function of S_{TOT}/N, in such a way that only 2.3 % of all *intrinsic* point sources will have $\psi_{\text{OBS}} > \psi_{\text{CRIT}}$, which is an effective 2 σ criterion. We could of course have chosen any confidence level for the definition of ψ_{CRIT}, but our rather severe 2 σ criterion is needed to obtain reliable angular size statistics. This criterion is uniform in the parameter ψ_{EQ}, so that *a source is called resolved if* :

$$\psi^{\text{EQ}}_{\text{OBS}} \geqslant \psi^{\text{EQ}}_{\text{CRIT}} =$$

$$= \text{HPBW}_\alpha \Big/ \left[0''.828 + 2''.49 \times {}^{10}\log^2 \left(\frac{S_{\text{TOT}}/N}{5.0}\right)\right]. \qquad (11)$$

Here $\psi^{\text{EQ}}_{\text{CRIT}}$ decreases monotonically with S_{TOT}/N and for $S_{\text{TOT}}/N \sim 9$ the resulting $\psi^{\text{EQ}}_{\text{CRIT}}$ equals the east-west beamsize.

Statistical 1 σ upper limits to ψ were obtained for unresolved sources from the angular size contingency table. The Appendix gives a functional form for these upper limits, which are a strong function of ψ_{OBS} and, given ψ_{OBS}, decrease monotonically with S_{TOT}/N. For a source with $\psi_{\text{OBS}} = 0$, the upper limit ranges from $\sim 9''$ for $S_{\text{TOT}}/N = 5$ to $\sim 1''$ for $S_{\text{TOT}}/N = 1000$. Especially for the stronger sources the 1 σ upper limits are useful.

5.3 Consistency of the method. — The reliability of the method is illustrated in figure 6 using source parameters determined independently in overlapping fields. (Filled thin circles mark parameters that have been determined directly for (components of) extended sources in Lynx).

Figure 6a shows a comparison of the largest angular sizes. For 21 sources an upper limit was indicated in one field, while ψ could be determined in the other field. Only for 3 sources the derived 1 σ upper limit is clearly smaller than the corresponding value of ψ in the other field. This shows that the derived 1 σ upper limits are meaningful. More importantly, we learn from figure 6a that the 22 resolved sources for which a value of ψ could be determined in *both* fields are close to the line $\psi_2 = \psi_1$.

Figure 6b shows a comparison of the intrinsic source position angles. The symbols are the same as in figure 6a. Most sources follow the line $\phi_2 = \phi_1$ within $\sim 30°$, with the exception of SA68. This shows that on average the algorithm produced unbiased intrinsic source position angles, albeit with rather large, but random errors.

Finally, figure 6c shows a comparison of the source component flux ratio f for those sources for which it was not undetermined in both fields. The points follow globally the line $f_2 = f_1$, but for the weaker sources the parameter f is not very well determined.

An independent check of the algorithm is made by comparing the intrinsic source parameters of one strong resolved source with those observed by other authors, at a different frequency and also with a different instrument. Available data are summarized in table IV for 3C9 (54W090) which was 0°.741 away from the field centre of SA68.1. Fluxes were transformed to 1412 MHz.

6. Sample selection and completeness.

6.1 THE SAMPLE SELECTION CRITERIA. — An overcomplete list of source candidates was made up using a point source finding routine, applying a peak signal-to-noise cut-off of 3.5 σ. The 3 km maps were primarily used to produce this list, while any additional low surface brightness sources in the 1.5 km maps, that were below the 3 km but above the 1.5 km map threshold, were included. In the actual catalogue of section 7 a cut-off in observed peak flux density is chosen at $S_p = 5.0\ \sigma$, because at this level the behaviour of the algorithm is well understood, and not more than one spurious source is expected for the whole survey. For $S_p < 5\ \sigma$ we expect about 8 spurious sources per map down to 4 σ, so we cannot define a reliable sample anymore. Data on sources with $4 < S_p/N < 5$ are also given in section 7, since most of these sources are real (and confirmed in the 50 cm maps of Paper IV). These sources are *not* to be used for statistical studies.

Because uncertainties in the primary beam, and hence in total sky flux, increase with r rather steeply at large r due to pointing errors (Eq. (5)), we will cut off the sample conservatively at the -7 dB radius ($r = 0°.464$, attenuation factor of 5.0). The used WSRT field then covers the same area as the Mayall 4 m plates which are used in Paper II.

6.2 THE SAMPLE COMPLETENESS. — Given the selection criteria discussed in the previous section, the LBDS sample will be complete only for certain ranges in S_{TOT}, ψ and f.

Due to the primary beam attenuation the sample is only complete in terms of map flux, because we have cut off the sample at $(S_p^{MAP})_{OBS} = 5.0\ \sigma$. The correction for this apparent incompleteness is simply a weight factor in the source counts and optical identification statistics. Assuming isotropy within the WSRT primary beam, every radio source is weighted inversely proportional to the area over which it could have been seen, before it dropped below the $S_p^{MAP} = 5.0\ \sigma$ threshold (Katgert *et al.*, 1973). If a source was detected in the overlapping part of two fields this weight was increased by about 9 % in order to compensate for the smaller area over which it would have been visible.

A more complicated factor of incompleteness is the resolution bias, i.e. the fact that a resolved source of certain sky flux S_{TOT}^{SKY} will drop below the 5 σ peak flux density cut-off more easily than a point source of the same S_{TOT}^{SKY}. Consequently, the sample completeness limit in S_{TOT}^{SKY} also depends on the source angular size and its component flux ratio. A discussion of the resolution bias in the 1.5 km Westerbork surveys has been given by Katgert (1976) and Oosterbaan (1978). The resolution bias not only depends on the beamsize, but also on the flux determining algorithm. Due to the 2 times smaller beam the resolution bias is expected to be more severe in the LBDS. On the other hand, we have used a flux determining algorithm that is more sensitive to extended structures and used the additional information from the 1.5 km maps, which will turn out to make us about as sensitive for sources with large angular size as the previous 1.5 km WSRT surveys.

Using the artificial sources generated in the Monte Carlo simulations, it was found that the 5.0 σ peak flux density cut-off implies the following completeness level in S_{TOT}/N :

$$\left(\frac{S_p^{MAP}}{N}\right)_{OBS} = 5.0 \quad \text{for} \quad \left(\frac{S_{TOT}^{MAP}}{N}\right) = $$
$$= 5.0 \exp\left[0.461 \times \left(\frac{1-f}{f}\right)^{0.838} \times \left(\frac{\psi_{EQ}}{HPBW_\alpha}\right)^2\right] \quad (12)$$

The sample completeness in S_{TOT}^{MAP}/N as a function of $\psi_{EQ}/HPBW_\alpha$ and f is given in figure 7, where on average the 1.5 and 3 km scales are related by : $\sigma_{1.5} = 1.31\ \sigma_3$ and $HPBW_\alpha(1.5\ km) = 1.88\ HPBW_\alpha(3\ km)$. The arrow at $\psi_{EQ} \simeq 34'' \simeq 1.5\ HPBW_\alpha(1.5\ km)$ shows where the Gaussian fitting routine breaks down for sources in the 1.5 km map. This is the effective completeness limit in ψ_{EQ} of the LBDS, although some sources are certainly detectable beyond this limit. The completeness in S_{TOT}^{MAP}/N as a function of ψ_{EQ} is shown for $f = 0.50$ and $f = 0.65$, where the latter represents the average completeness limit for the whole LBDS (see Sect. 6.3). For $f = 0.65$ the 3 km array is more sensitive out to $\psi_{EQ} \simeq 1.2\ HPBW_\alpha(3\ km) \simeq 15''$, where the 1.5 km takes over and is more sensitive out to $\psi_{EQ} \lesssim 1.5\ HPBW_\alpha(1.5\ km) \simeq 34''$, where in the 1.5 km maps the Gaussian fitting routine breaks down. Beyond $\psi_{EQ} \gtrsim 34''$ the sensitivity deteriorates with increasing f, because such sources will be included in the sample only if the faintest component also has a flux $\geqslant 5.0\ \sigma$. However, the fraction of sources with $\psi \gtrsim 34''$ and $f \geqslant 0.70$ is less than 5 %, because only 25 % of all sources has $f \gtrsim 0.70$ (Sect. 6.3), while only 15 % has $\psi_{EQ} \gtrsim 35''$ (Sect. 8). When compared with similar figures in K75 and WOR, figure 7 shows that the combination of the 3 and 1.5 km maps and our flux determining algorithm, make us about as sensitive as the previous 1.5 km WSRT surveys for sources with large ψ_{EQ} at comparable S_{TOT}^{MAP}/N.

The two curves in the left part of the diagram, labelled with $\psi_{CRIT}^{EQ}(3\ km)$ and $\psi_{CRIT}^{EQ}(1.5\ km)$ show the critical equivalent angular size ψ_{CRIT}^{EQ} as a function of S_{TOT}^{MAP}/N. At a given S_{TOT}^{MAP}/N sources with $\psi_{OBS}^{EQ} \geqslant \psi_{CRIT}^{EQ}$ are resolved according to our 2 σ criterion.

6.3 THE f-DISTRIBUTION. — For the statistical corrections for incompleteness (Sect. 6.4) we need the f-distribution, which was determined for both the complete sample of 26 extended and complex sources for which an f-value could be computed directly and for the subsample of 46 (out of 69) resolved sources, for which an f-value could be determined from R and σ (Sect. 5.1). The resulting f-distribution is shown in table V for our extended and resolved sources separately as well as for previous Westerbork Surveys and the 3CR. The integral and differential f-distribution are plotted for these surveys in figure 8.

Table V shows that the f-distribution for resolved sources in the LBDS is consistent with that of the extended sources, for which f was measured directly. The average f-value in the LBDS is 0.65, implying unequal components of flux ratio 1.78 to 1.

It is noteworthy that our f-distribution is quite similar to that of surveys with a 10-1000 times higher flux density limit. Depending somewhat on the radio source redshift distribution, this could mean that the probability of obtaining a certain f-value when producing a radio source, is strictly independent of its total radio power.

6.4 STATISTICAL CORRECTIONS FOR POPULATION AND RESOLUTION BIAS. — Oosterbaan (1978) showed that a correction for population and resolution bias can be calculated from a flux density contingency table. Given a source population with a realistic input distribution of total fluxes, angular sizes and f-values, such a table describes the redistribution of the real input fluxes over intervals of observed total flux. This redistribution does not have the shape of a δ-function due to the asymmetrical influence of noise and faint sources on the algorithm (population bias), and more importantly, due to the decreasing sensitivity for large angular sizes near the 5 σ peak flux density cut-off (resolution bias).

We constructed the flux density contingency table for our algorithm, using the 10240 artificial sources. Weighted with the f-distribution (Sect. 6.3) and the differential angular size distribution (Sect. 8.1), the contingency table was computed for the average slope of the source counts around 1 mJy ($\gamma \simeq 1.9$, $dN/dS \propto S^{-\gamma}$, Sect. 9). The results turn out not to be very sensitive to the value of γ, but are much more dependent on the angular size distribution. The normalized flux density contingency table is shown in table VI. Each row contains the distribution of sources over the input total flux for a given observed (and corrected) total flux. It is important that exactly the *same* analysis and selection criteria of the actual catalogue are also applied to the artificially generated sources. So the 5 σ cut-off in $(S_p^{MAP}/N)_{OBS}$ was applied to the flux density contingency table as well. The bottom row of the contingency table shows what fraction of all sources actually appear in the catalogue (see also the lower part of Fig. 9). Using the 5 σ cut-off in (S_p/N) the fraction of sources with total corrected flux S_{TOT}/N that appears in the catalogue is well described by :

$$\text{COMPLETENESS}\,(S_{TOT}/N) = \\ = 1 - \frac{57''.6}{\text{HPBW}_\alpha} \exp(-\,0.415\,S_{TOT}/N) \quad (13)$$

for HPBW_α in the range 12-25″. It is seen that below 9 σ the catalogue is becoming less than 90 % complete. At the 5 σ level only one out of three radio sources appears in the catalogue. This might seem disappointing, but as long as the incompleteness can be modeled precisely, it is in principle not worse than the incompleteness in sky flux due to primary beam attenuation (for which the correction per 5 σ source can amount to a factor 5-10 !).

The resolution correction is the number of sources that should have been observed in an interval of real input flux density $(S_{TOT}/N)_{IN}$, divided by the actual number of sources, seen in the corresponding interval of observed (and corrected) flux density $(S_{TOT}/N)_{COR}$. The resolution correction and the sample completeness are not each others reciprocals, because sources in a certain $(S_{TOT}/N)_{COR}$-bin have all kinds of $(S_{TOT}/N)_{IN}$ values due to the asymmetrical influence of noise at various signal-to-noise levels. The combined correction for resolution and population bias is shown in the upper panel of figure 9 and is represented well by :

$$C_{RES}(S_{TOT}/N) = 1 + \frac{175''}{\text{HPBW}_\alpha} \exp\left(\frac{-\,2.71\,S_{TOT}/N}{(S_p/N)_{CUT-OFF}}\right). \quad (14)$$

Here $(S_p/N)_{CUT-OFF}$ is the numerical value of the peak signal-to-noise cut-off of the sample. We calculated the contingency tables for $12.5 \leqslant \text{HPBW}_\alpha \leqslant 25''$ and $5.0 \leqslant (S_p/N)_{CUT-OFF} \leqslant 7.0$, where the resolution correction scales perfectly with HPBW_α and $(S_p/N)_{CUT-OFF}$. The statistical errors in the resolution correction are estimated to be a few percent at the $S_{TOT} \simeq 10\ \sigma$ level, increasing to about 10 % at the 5 σ level.

7. The source list.

The source lists for the Leiden Berkeley Deep Survey fields are given in tables VIIa and VIIb. Table VIIa contains the complete sample of 306 sources found with the selection criteria of section 6 (all sources with map peak signal-to-noise $S_p/N \geqslant 5$ and primary beam attenuation factor $ATT \leqslant 5$). Table VIIb gives all sources that are not in the complete sample (i.e. $S_p/N < 5$ or $ATT > 5$).

For sources seen in the overlapping part of two fields, average source parameters were derived with the inverse square of their errors as weights. If the source was unresolved in both fields, the smallest upper limit in ψ is listed (from the field where it had the highest S_p/N). If the source was observed to be resolved in only one of the two fields, then only the size information of this field is listed.

For every source the table contains the relevant observed source parameters as derived directly from the map, as well as intrinsic source parameters, corrected for noise overestimation. The tables are organized as follows :

Column 1 : the Westerbork name that consists of the Westerbork Survey number, which is 52 for SA57, 53 for Hercules, 54 for SA68 and 55 for Lynx, and a sequence number (in order of increasing RA). An asterisk (*) behind the Westerbork name indicates that for this source multiple components were found, which are listed directly below, and are labelled A, B, C, etc. A detectable central component is always labelled « C ». Generally A and B are the western — and easternmost components.

Columns 2, 3 : the right ascension and declination for the equinox 1950.0 and their errors.

Column 4 : the total flux density, S_{TOT}^{SKY}, corrected for primary beam attenuation and noise overestimation, as well as its error, both in mJy. This value is an unbiassed or best estimate of the total flux density.

Column 5 : resolution code : U = Unresolved, R = Resolved, E = Extended.

Column 6 : for unresolved sources a 1 σ upper limit to the source largest angular size ψ is given in arcsec. For resolved and extended sources the intrinsic largest angular size ψ and its error are given (both in arcsec).

Columns 7, 8, 9 : are given for resolved and extended sources only :

Column 7 : the position angle ϕ of the intrinsic largest angular size, in degrees, from north to east, as well as its error.

Column 8 : the deconvolved minor axis χ, in arcsec.

Column 9 : the component flux ratio f.

Column 10 : the observed total sky flux density, $(S_{\rm TOT}^{\rm SKY})_{\rm OBS}$, not corrected for noise overestimation, and its error, both in mJy.

Column 11 : the observed map peak signal-to-noise $S_{\rm p}/N$.

Column 12 : the observed normalized source area R.

Column 13 : the upper number is the attenuation factor ATT. The lower number is the corresponding weight that the source should have in the source counts or in optical identification statistics. This weight includes both incompleteness due to primary beam attenuation and resolution bias.

Column 14 : contains various notes :

- ∽ : the source was below the 5 σ peak flux density cut-off in the 3 km map, but above this level in the 1.5 km map.
- O : the source was seen in the overlapping area of two fields. For SA57 it means that it was also seen in the VLA map of Owen and Thuan.
- V : the total fluxes in the two overlapping fields differed by more than 3 times the combined flux error so that the source may be variable.
- H : the source has a low surface brightness halo as found by comparison of contour plots from the 1.5 and 3 km maps.
- T : head tail source, generally suggested by the position of the optical identification (see Paper II).
- B : a bridge of radio emission is visible between the components of an extended source.
- X : detected as an X-ray source by the Einstein Observatory (Katgert *et al.*, 1983).
- C : a contour plot of this source is given in figure 10.

Column 15 : alternative source names, from the following catalogues : the 3CR (Bennett, 1961), the 4C (Pilkington and Scott, 1965; Gower *et al.*, 1967), the B2 (Colla *et al.*, 1970, 1972), the Ohio survey (Dixon and Kraus, 1968; Fitch *et al.*, 1969; Brundage *et al.*, 1971) and the Westerbork Background Survey (Willis *et al.*, 1976).

8. The angular size distribution and $\theta_{\rm MED}(S)$ relation.

8.1 THE ANGULAR SIZE DISTRIBUTION. — With the 12″.5 east-west beam there are 95 sources out of the total complete sample of 306 radio sources, which are extended or resolved according to the 2 σ criterion. This fraction is of course dependent on declination, being 43 % for Hercules, 30 % for Lynx, 27 % for SA57 and 21 % for SA68.

Two different methods are used to derive the differential angular size distribution $g(\psi)$. First the integral $h(\psi)$ of the angular size distribution $g(\psi)$ is computed, following the method of Katgert (1976). This uses the known relation between the (total) map flux density $S_{\rm TOT}^{\rm MAP}$ and the « critical » angular size $\psi_{\rm CRIT}$, separating resolved and unresolved sources (Eq. (11)). The values of $h(\psi)$ are independent and are determined without knowing $g(\psi)$. These $h(\psi)$ points are plotted in figure 11a as filled circles. The point with the smallest ψ is derived from sources with the highest $S_{\rm TOT}^{\rm MAP}/N$, as is illustrated in table VIIIa. The maximum ψ for which $h(\psi)$ can be determined is $\sim 10''$ for $S_{\rm TOT}^{\rm MAP} \sim 13\ \sigma$. This method of computing $h(\psi)$ rests upon the assumption that one can determine various points of $h(\psi)$ at different flux levels, which is justified as long as the angular size distribution is not dependent on flux density. This holds roughly for the flux density range (1 mJy $\lesssim S_{1.4} \lesssim$ 1 Jy), as shown by Swarup (1975) at the brighter levels and verified for fainter fluxes *a posteriori* in section 8.3.

It is clear that we want to extend $g(\psi)$ to larger values of ψ. Beyond $\psi \gtrsim 10''$ we use another method, in which $h(\psi)$ is calculated as the integral over $g(\psi)$. If one cuts off the sample severely enough, Oosterbaan (1978) showed that $g(\psi)$ can be obtained from the catalogue in a reliable way. In order not to be biassed against sources with large values of ψ and f, we define a complete subsample of 74 sources by $S_{\rm p}^{\rm MAP} \geqslant 25\ \sigma$ and $ATT \leqslant 5.0$. As a result, even the faintest components of sources with $f \leqslant 0.85$ can be seen everywhere within the − 7 dB attenuation radius. Because the fraction of sources with $f > 0.85$ is only 8 %, this selection introduces essentially no bias in the sample. The sample contains only sources with $S_{\rm p}^{\rm SKY} \geqslant 5$ mJy and is complete in skyflux for $S_{\rm p}^{\rm SKY} \geqslant 25$ mJy. The resulting $g(\psi)$ and implied $h(\psi)$ are given in table VIIIb and figures 11b and 11a, where the points are plotted for 2″- or 10″-bins.

Good fits for both $h(\psi)$ and its derivative $g(\psi)$ are :

$$h(\psi) = \exp(-0.097 \pm 0.005)\,\psi \quad (15a)$$

and

$$g(\psi) = (0.097 \pm 0.005)\exp(-0.097 \pm 0.005)\,\psi \quad (15b)$$

where ψ is in arcsec. The fit for $h(\psi)$ might not be optimal for $\psi \sim 10''$, but is, given the limited statistics, a good representation of $h(\psi)$ over the whole range of ψ. It is also clear that the $h(\psi)$ for the LBDS is consistent with the integral angular size distributions derived in the previous 1.5 km Westerbork surveys, at least for $\psi \lesssim 18''$. The systematic difference for $\psi \gtrsim 18''$ between our $h(\psi)$ and that of Oosterbaan (1978) is considered to be significant, since the 1.5 km maps make the LBDS complete up to angular sizes of 34″ (arrow in Fig. 11b, see Sect. 6.2), and, due to the beam ellipticity, even beyond.

The BGS radio sources used by Oosterbaan to compute $h(\psi)$ were mainly in the flux density range 60 $\lesssim S_{1.4} \lesssim$ 1000 mJy, while our sample has its sources predominantly in the range 5 $\lesssim S_{1.4} \lesssim$ 100 mJy, by far most of the sources are actually fainter than 50 mJy. It is thus possible that radio sources with large angular sizes ($\psi \geqslant 20''$) occur more frequently amongst bright radio sources than amongst fainter ones.

8.2 THE ANGULAR SIZE DISTRIBUTION AS A FUNCTION OF FLUX DENSITY. — In the following we will only use the LBDS radio sources that are within the − 3 dB radius (attenuation $\leqslant 2.0$). Secondly, only those sources are chosen with $S_{\rm TOT}^{\rm MAP} \geqslant 20\ \sigma$, in order to have reliable information on ψ. However, to improve the statistics a deeper sample with $S_{\rm TOT}^{\rm MAP} \geqslant 10\ \sigma$ will be defined as well. The « 20 σ » sample will be complete for flux ratios $f \leqslant 0.8$, which includes more than 90 % of all radio sources. The « 10 σ » sample is complete up to $f \sim 0.66$, still including about 75 % of all radio sources (see Fig. 8*a*). We make the samples complete in *sky flux* by taking only those sources with $S_{\rm TOT}^{\rm SKY} \geqslant 2 \times 10\ \sigma$ or $2 \times 20\ \sigma$. Due to the low declination of SA68, its ψ-information is less reliable and more upper limits are seen in this field, so we excluded the radio sources in SA68. To extend the distribution to lower flux densities, we included the angular size information of the sources in Lynx.2 that were also observed by Windhorst *et al.* (1984) with the VLA C-array at 1462 MHz, and analysed in the same way as in the present paper. Fluxes were transformed to 1412 MHz.

The angular size distributions of the 20 σ sample are shown in the left three panels of figure 12. The 10 σ LBDS sample is complete for $S_{\rm TOT}^{\rm SKY} \geqslant 20\ \sigma \simeq 5$ mJy and the 10 σ VLA sample for $S_{\rm TOT}^{\rm MAP} \geqslant 0.90$ mJy, while their angular size distributions are shown in the middle three panels of figure 12. To improve the statistics we added the three distributions in the two flux ranges, after cutting off the samples at 1 mJy and 100 mJy. The resulting angular size distributions are shown in the two right hand panels of figure 12 for the flux density range 10-100 and 1-10 mJy.

The angular size distribution in the range 1-10 mJy is similar to the one for the whole survey (i.e. $g(\psi)$ in Fig. 11b), since most of the sources in the determination of $g(\psi)$ were in the range 5-15 mJy. The angular size distribution in the range 10-100 mJy shows a larger fraction of sources with $\psi \gtrsim 20''$, in agreement with Oosterbaan's angular size distribution, whose integral is shown in figure 11a. In order to decide whether the angular size distribution in the 10-100 mJy range is significantly different from that in the 1-10 mJy range, the hypothesis was tested that both come from the same population, characterized by equation (15b), using a χ^2-test. The angular size distribution for the 1-10 mJy range turns out to be perfectly consistent with equation (15b). In contrast, for the size distribution in the 10-100 mJy range this hypothesis is rejected at the 2 σ level, if we consider only sources with $\psi \leqslant 35''$, which sample is certainly complete. If we include also the sources with $\psi > 35''$, which may not be entirely complete, then it can be rejected at the 5 σ level.

8.3 THE MEDIAN ANGULAR SIZE-FLUX DENSITY RELATION. — From the data, presented in figure 12, we computed $\theta_{\rm MED}(S)$ and its errors following Swarup (1975). The results are listed in table IX, with the values of $\theta_{\rm MED}(S)$ from various other 21 cm surveys, covering different depths in flux. At bright flux density levels we plotted the GB-values of Bridle *et al.* (1972), as summarized by Ekers and Miley (1977). In the intermediate flux density range the recent 5C-measurements of Downes *et al.* (1981) and Fielden *et al.* (1983) are plotted. We also derived the $\theta_{\rm MED}(S)$ for the 2nd and 3rd WBK Survey and the BGS. At the highest flux levels the $\theta_{\rm MED}(S)$-points from various low frequency surveys are plotted, as summarized by Kapahi and Subrahmanya (1982). Most of these surveys were defined originally at 408 MHz. The 408 MHz fluxes were converted to 1412 MHz, using the median spectral index $\alpha_{\rm MED}$, which turns out to be a function of S_{408} (Gopal-Krishna and Steppe, 1982; Windhorst and Oppe, 1984) and adopted $\langle \alpha \rangle = 0.75$ for $S_{408} < 100$ mJy. The agreement between the points from several 1.4 GHz surveys (filled symbols in Fig. 13) and 408 MHz surveys (open symbols) is good, showing that data at both frequencies may be combined for the $\theta_{\rm MED}(S)$-relation.

The value of $\theta_{\rm MED}$ decreases from about 100″ at $S_{1.4} \sim 10$ Jy to 20″ around 1 Jy, below which it decreases asymptotically to 10″. This behaviour has long been known and has been modeled by various authors (see Kapahi and Subrahmanya (1982) for a review). The 21 cm surveys, including our new data, show that the values of the median angular size remain around $\sim 10''$ even down to 1 mJy. Omitting the two points with $S_{1.4} > 10$ Jy, a good fit through the $\theta_{\rm MED}(S)$-data in the flux density range 1 mJy $\lesssim S_{1.4} \lesssim 10$ Jy is :

$$\log\left(\frac{\theta_{\rm MED}}{\rm arcsec}\right) = 1.21 + 0.46 \log\left(\frac{S_{1.4}}{\rm Jy}\right) + 0.30 \log^2\left(\frac{S_{1.4}}{\rm Jy}\right) + 0.061 \log^3\left(\frac{S_{1.4}}{\rm Jy}\right). \quad (16)$$

Summarizing this section, we reach the following conclusions :

1. The angular size distribution $g(\psi)$ in the range $10 \lesssim S_{1.4} \lesssim 100$ mJy has relatively more sources of larger ψ than for $1 \leqslant S_{1.4} < 10$ mJy, Hence, below about 10 mJy a larger fraction of compact radio sources is seen.

2. The median angular size $\theta_{\rm MED}$ is almost independent of flux density for $1 \lesssim S_{1.4} \lesssim 200$ mJy, and stays around 10″.

The $\theta_{\rm MED}(S)$-relation has been modeled extensively by various authors down to about $S_{1.4} \gtrsim 30$ mJy (Kapahi, 1975; Katgert, 1977; Kapahi and Subrahmanya, 1982; Fielden *et al.*, 1983). Because the radio source redshift distribution is still largely unknown for radio sources with $S_{1.4} \lesssim 1$ Jy, and because it is not known *a priori* that there is no correlation between the radio source luminosity P and intrinsic linear size l, we will not model the observed $\theta_{\rm MED}(S)$-relation at the moment. Yet it seems safe to suggest that models with size evolution are preferred to account for the small $\theta_{\rm MED}$ in the 1-100 mJy range (see Kapahi and Subrahmanya, 1982), unless there exists a severe dependence of linear size on radio luminosity, especially for low P. The 1-10 mJy radio sources are probably of lower luminosity and at intermediate redshifts ($z \lesssim 0.5$) and could have small intrinsic linear sizes. Especially if they are lower luminosity ellipticals, spiral or Seyfert galaxies, rather than the luminous ellipticals and quasars, one expects that their linear sizes are smaller than assumed in the models that are used to predict $\theta_{\rm MED}(S)$.

9. The 1.4 GHz source counts.

9.1 HISTORY OF THE 21 cm SOURCE COUNTS. — During the last decade systematic radio source surveys have been made at 1.4 GHz with several instruments, covering over four decades in flux density. In figure 14 we summarize all

1.4 GHz surveys for which the original source count data were accessible in the literature. In a few surveys we combined their lowest two bins to improve the statistics to at least 20 objects per bin. Some of the highest flux bins are probably not complete and are placed between brackets in figure 14.

At bright flux levels ($S_{1.4} \gtrsim 100$ mJy) we mention the Greenbank and Ohio surveys. The brighter Greenbank surveys are the BDFL (Bridle *et al.*, 1972) and the GA, whose counts down to 0.5 Jy were summarized by Fomalont *et al.* (1974). Deeper surveys down to $S_{1.4} \sim 100$ mJy have been done with the 300 ft telescope by Maslowski (1973; the GB survey) and Machalski (1978; the GB2 Survey), and with the Ohio Survey Instalment V (Kraus, 1972). All these surveys were done with a large beam (HPBW $\sim 10'$), and were confusion limited especially for the source density at $S_{1.4} \sim 100$ mJy. Statistical corrections for confusion and for noise have been applied for the GB and GB2, but not for the Ohio V survey.

In the intermediate flux density range ($10 \lesssim S_{1.4} \lesssim 100$ mJy) the most important contributions come from various Westerbork surveys, all done before 1979 with a maximum baseline of 1.5 km. Due to the low source density within the WSRT primary beam for $S_{1.4} \gtrsim 10$ mJy, confusion in these surveys is negligible, but the 23″ beam starts to introduce a serious resolution bias, which is even more pronounced due to the flux determining algorithm. In table Xd we present the weighted average total count for the 1st, 2nd and 3rd WBK survey. Because the 3rd WBK survey was originally slightly overcorrected for the resolution bias, we applied Oosterbaan's resolution correction to the 3rd WBK sources, yielding a count consistent with that of the 1st and 2nd WBK survey, as well as with that of the BGS.

At low flux densities ($1 \lesssim S_{1.4} \lesssim 10$ mJy) we mention the source count of the combined One Mile Cambridge Surveys 5C5+6+7 (Pearson and Kus, 1978) and the Deep Westerbork count of Le Poole and Willis (reviewed by Willis *et al.*, 1977). The latter was done with the 1.5 km Westerbork array in three fields of which two were observed for 16×12^h each and one for 8×12^h, and reduced according to the procedure of the 1st and 2nd Westerbork survey. The original source count data were made available to us very kindly by Le Poole (private communication) and are summarized in table Xa. Figure 14 shows that the 5C and Deep Westerbork counts are in good agreement.

All above data show that if one takes proper account of confusion, noise and resolution corrections at the various flux levels, one can obtain a consistent picture of the 21 cm counts in the flux density range 1 mJy$\lesssim S \lesssim$10 Jy.

9.2 Derivation of the Leiden Berkeley Deep Survey counts. — The correction for population and resolution bias is crucial to obtain a reliable count for a survey with a beamsize of 12″. In section 6 this correction was derived from the flux density contingency table, based on our actual determination of $g(\psi)$ in section 8.1. As we showed in section 8, our $g(\psi)$ is consistent with that of Oosterbaan for $\psi \lesssim 20''$, and becomes about a factor of two lower for $\psi \gtrsim 20''$. If this difference were due to an unrecognized selection effect in the LBDS, our resolution correction from section 6 would be a slight *under*estimation. Apart from the resolution correction, each source was given a weight inversely proportional to its visibility area within the primary beam.

For the LBDS we chose flux density bins, each a factor $\sqrt{2}$ wide. The lowest bin boundary is not to be taken exactly at the 5 σ level of the deepest field, because otherwise a few sources with very large weight ($\gtrsim 10$) could dominate the counts in the lowest bins. The bin boundaries are chosen at $0.778 \times \sqrt{2}^n$ mJy, but the width is increased to a factor 2 for $S_{1.4} \gtrsim 10$ mJy, as well as for the faintest bin, and to a factor $2\sqrt{2}$ for $S_{1.4} \gtrsim 100$ mJy in order to improve the statistics. If the actual number of sources per bin is smaller than about 20, the uncertainty in the average weight can be dominated by discretization effects. In our counts this number generally exceeds 30 so such effects should average out.

Now, given the bin boundaries and the 5 σ mapflux cut-off level in each field, we only count a field in a bin if its 5 σ completeness limit is below the lower bin boundary. In this respect we treat the 3 km and 1.5 km maps separately, since they have different noise. The number of fields (NOF) that are complete in a particular bin is given in table Xb, c and d as well as the corresponding number of sources from the high resolution maps (NH) and the number of *additional* sources seen only in the low resolution maps (NL).

The count in each bin follows from the sum of source weights divided by the appropriate survey area. The area for one survey field is 2.063×10^{-4} steradian. The relative error in the count is determined by its sampling error :

$$\sqrt{\left(\sum_i WT_i^2\right) \Big/ \left(\sum_i WT_i\right)}. \qquad (17)$$

The average weight per bin can become slightly less than unity due to the way we treated sources in the overlapping areas. These sources were counted twice (once in each field), but with a weight of $\sim 0.55 \times$ the original weight that they had in each of the fields. The normalized differential count is :

$$\frac{n}{n_0} = \left(\frac{dN}{dS}\right) \Big/ \left(\frac{dN}{dS}\right)_0$$

where

$$\left(\frac{dN}{dS}\right)_0 = 150 \frac{(S_L^{-1.5} - S_U^{-1.5})}{(S_L - S_U)} \text{ ster}^{-1} \text{ Jy}^{-1} \qquad (18)$$

is the normalizing Euclidean count expected for a non-evolving population in a static universe and S_L and S_U are the lower and upper bin boundaries.

The results have been plotted in figure 14 at the expected average flux :

$$S_{AV} = \left[(1-\gamma)\left(\frac{S_L - S_U}{S_L^{1-\gamma} - S_U^{1-\gamma}}\right)\right]^{1/\gamma}. \qquad (19)$$

Note that only when the differential source count slope γ equals 2, which occurs for $S_{1.4} \sim 2$ mJy, the value of S_{AV} becomes equal to the geometrical mean. To calculate S_{AV} we used γ as a function of $S_{1.4}$, derived in the next section.

The integral count in the last column of table Xb, c and d was added to the density of bright radio sources ($S_{1.4} > 1.6$ Jy) of Maslowski (1977).

9.3 Discussion of the resulting LBDS counts. — Using the 5 σ source list (Table VIIa), based primarily upon the 3 km maps, we derived the 1412 MHz Leiden Berkeley Deep Survey count, which is listed in table Xb, and plotted as filled circles in figure 14. A second 5 σ source list was made up mainly from the 1.5 km maps, but taking for double and complex sources the more reliable 3 km data. The resulting 1.5 km 5 σ count is listed in table Xc and plotted as filled triangles (▼) in figure 14. A third source list was constructed from the 3 km maps, but now with a cut-off of $S_p^{MAP} = 7\ \sigma$. The resulting 7 σ counts are given in table Xd and plotted in figure 14 as filled triangles (▲). The 1.5 km 5 σ and 3 km 7 σ counts are not shown for $S_{1.4} \gtrsim 10$ mJy because here they are identical to the original 3 km 5 σ count, since essentially all sources have a weight equal to unity. The error bars of the 1.5 km 5 σ and 3 km 7 σ counts are not drawn everywhere to prevent overcrowding the picture. The agreement between the 1.5 km and 3 km 5 σ and 7 σ counts shows that the correction for population and resolution bias, which depends strongly on signal-to-noise and beamwidth respectively, was done properly.

For convenience we made a weighted least squares fit to the source counts in the range 1 mJy $\leqslant S_{1.4} \leqslant$ 10 Jy using a polynomial in log S. This fit includes all available data, with the exception of the uncorrected Ohio V counts and a few points placed between brackets in figure 14 due to reasons of survey incompleteness. Because the average flux density of a bin is defined by equation (19) one is allowed to do a least squares fit in the log-log plane :

$$\left(\frac{dN}{dS}\right) = 341 \times S^{-\gamma}\ \text{ster}^{-1}\ \text{Jy}^{-1}$$

with

$$\gamma = 2.63 + 0.349 \log S + 0.0405 \log^2 S \qquad (20)$$

where S is the 1412 MHz flux density in Jy. The exponent γ of the count reaches its Euclidean value of 2.5 for $S_{1.4} \simeq 420$ mJy, and decreases gradually to about 2.3 at 100 mJy, 2.1 at 10 mJy and 1.9 at 1 mJy. The presented fit (20) may not be optimal below 100 mJy. For instance, around and just below 10 mJy the actual value of γ might be smaller than given by (20), resulting in a steeper normalized count while γ could well be increasing gradually for $S_{1.4} \lesssim 3$ mJy, resulting in a flattening of the normalized count. This will be studied in more detail in deeper follow-up surveys of the Lynx.2 area with the VLA (Windhorst *et al.*, 1984) and the WSRT (Oort and Windhorst, 1984).

It is seen from figure 14 that the LBDS source count is also consistent with those of previous surveys even up to a flux of 1000 mJy. This shows that the purely optically selected LBDS fields are a random part of the radio sky, yielding even in the highest two bins about the expected number of sources.

In figure 14 the total LBDS counts in the range $10 \lesssim S_{1.4} \lesssim 100$ mJy seems to be somewhat below those of the combined WBK surveys and BGS, although only marginally significant. The reason for this is that in the range $S \geqslant 7$ mJy the total Lynx count is a factor 1.5 lower than the combined count of the other five areas. However, for $S_{1.4} \leqslant 7$ mJy the Lynx counts look normal, not distinguishable from the other surveys. In a χ^2-test of the number of expected sources per bin, the source distributions for $S_{1.4} \leqslant 7$ mJy in Lynx and in the other areas do not differ at more than the 0.7 σ level. However, in the range $7 \leqslant S_{1.4} \leqslant 200$ mJy the Lynx source distribution differs from that of the comparison areas at the 2 σ level. The apparent lack of 10-100 mJy sources in Lynx reminds us that most synthesis radio surveys cover only a few square degrees on the sky, often with all fields located in the same area so that local anisotropies could play a role. Anisotropies on scales of a few to a few dozen square degrees have been reported by several auhors (see e.g. Maslowski, 1973, 1977; Katgert *et al.*, 1973), but have also been questioned by others (e.g. Gillespie, 1975; Willis *et al.*, 1977). If these anisotropies are real, they should be visible in the redshift distribution. We therefore consider it of great importance to measure the redshift distribution of the LBDS radio galaxies (see Paper III).

Appendix.

Here we give the precise numerical expressions for the relations between the observed and intrinsic source parameters, as well as for the functions that correct the observed source parameters in a statistical sense for noise induced overestimation (described in Sect. 5). Their functional form will be similar (but may be not identical) for other comparable flux determining algorithms. If we express ψ_{EQ}, ψ and σ in units of HPBW$_\alpha$ (= 12″.5 in our case), equations (6), (7) and (8) are expressed as follows :

equation (6) : $R(\psi_{EQ}, f) = A_f + B_f \psi_{EQ} + C_f \psi_{EQ}^2 + D_f \psi_{EQ}^3$ with :

$$\begin{aligned}
A_f &= +0.9351 + 0.2678\, f - 0.3366\, f^2 + 0.1342\, f^3 \quad (f \geqslant 0.50)\\
B_f &= +13.825 - 68.013\, f + 109.99\, f^2 - 59.175\, f^3 \quad (f \leqslant 0.70)\\
&\quad -9.725 + 32.363\, f - 36.500\, f^2 + 13.900\, f^3 \quad (f > 0.70)\\
C_f &= -38.234 + 190.31\, f - 307.97\, f^2 + 165.78\, f^3 \quad (f \leqslant 0.70)\\
&\quad +26.125 - 86.547\, f + 100.22\, f^2 - 39.922\, f^3 \quad (f > 0.70)\\
D_f &= +21.875 - 107.68\, f + 177.83\, f^2 - 99.043\, f^3 \quad (f \leqslant 0.70)\\
&\quad -12.188 + 46.113\, f - 60.078\, f^2 + 26{,}250\, f^3 \quad (f > 0.70)
\end{aligned}$$

equation (7) : $\sigma(\psi, f) \times \mathrm{HPBW}_\alpha = a_f + b_f\,\psi + c_f\,\psi^2 + d_f\,\psi^3$ with :

$$\begin{aligned}
a_f &= +1.8192 - 7.7773\,f + 10.451\,f^2 - 4.4582\,f^3 \quad (f \geqslant 0.50)\\
b_f &= -164.94 + 758.72\,f - 1089.9\,f^2 + 523.91\,f^3 \quad (f \leqslant 0.70)\\
&\quad +650.35 - 2328.1\,f + 2821.9\,f^2 - 1141.8\,f^3 \quad (f > 0.70)\\
c_f &= +156.45 - 581.67\,f + 761.69\,f^2 - 352.67\,f^3 \quad (f \leqslant 0.70)\\
&\quad -653.86 + 2391.9\,f - 2870.0\,f^2 + 1129.4\,f^3 \quad (f > 0.70)\\
d_f &= -35.215 + 110.82\,f - 100.55\,f^2 + 18.756\,f^3 \quad (f \leqslant 0.70)\\
&\quad +248.05 - 867.97\,f + 993.55\,f^2 - 372.66\,f^3 \quad (f > 0.70)
\end{aligned}$$

equation (8) : $R(\sigma, \cos\phi_{\mathrm{proj}}) = 1 + [\alpha_c + \beta_c\,\sigma + \gamma_c\,\sigma^2 + \delta_c\,\sigma^3]^2$ with, if we define $c = \cos(\phi_{\mathrm{proj}})$:

$$\begin{aligned}
\alpha_c &= +1.5626 \times 10^{-2} + 6.1881 \times 10^{-3}\,c - 6.381 \times 10^{-3}\,c^2 + 5.5694 \times 10^{-5}\,c^3 \quad (c \geqslant 0.0)\\
\beta_c &= +0.70008 - 0.18914\,c - 0.36149\,c^2 + 0.33978\,c^3 \quad (c \geqslant 0.0)\\
\gamma_c &= -0.08295 + 0.09295\,c + 0.09101\,c^2 - 0.14156\,c^3 \quad (c \geqslant 0.0)\\
\delta_c &= +3.0146 \times 10^{-3} - 1.8557 \times 10^{-3}\,c - 0.04658\,c^2 + 0.05118\,c^3 \quad (c \leqslant 0.65)\\
&\quad +3.2158 \times 10^{-2} - 0.13777\,c + 0.16464\,c^2 - 0.05806\,c^3 \quad (c > 0.65)\,.
\end{aligned}$$

If we express σ in units of HPBW_α, and if we define :

$$\Sigma^2 = (\sigma - 1)^2 \times (1 - \cos^2\phi\,\cos^2\delta)$$

then the average corrections for noise induced overestimation are :

equation (9) : $$\left(\frac{R_{\mathrm{COR}}}{R_{\mathrm{OBS}}}\right) = C_R\left(\left(\frac{S_\mathrm{p}}{N}\right)_{\mathrm{OBS}}, R_{\mathrm{OBS}}, \sigma_{\mathrm{OBS}}\right) = 0.6850 + 0.02413\left(\frac{S_\mathrm{p}}{N}\right)_{\mathrm{OBS}} + 0.05482\,R_{\mathrm{OBS}} + 0.08688\,\Sigma^2$$

equation (10) : $$\frac{(S_\mathrm{p}/N)_{\mathrm{COR}}}{(S_\mathrm{p}/N)_{\mathrm{OBS}}} = C_{S_\mathrm{p}}\left(\left(\frac{S_\mathrm{p}}{N}\right)_{\mathrm{OBS}}, R_{\mathrm{OBS}}, \sigma_{\mathrm{OBS}}\right) = 0.9232 + 0.00798\left(\frac{S_\mathrm{p}}{N}\right)_{\mathrm{OBS}} - 0.01190\,R_{\mathrm{OBS}} - 0.01784\,\Sigma^2\,.$$

Both equations are only valid for :

$$4.0 \lesssim \left(\frac{S_\mathrm{p}}{N}\right)_{\mathrm{OBS}} \lesssim 11.0 \quad \text{and} \quad 0.8 \lesssim R_{\mathrm{OBS}} \lesssim 2.8$$

$$\text{and} \quad R_{\mathrm{OBS}} \lesssim -0.20(S_\mathrm{p}/N)_{\mathrm{OBS}} + 3.4 \quad \text{and} \quad \left|\sigma_{\mathrm{OBS}} - \frac{58\,R_{\mathrm{OBS}}}{(S_\mathrm{p}/N)_{\mathrm{OBS}}\,\mathrm{HPBW}_\alpha}\right| \lesssim 0.5\,.$$

Otherwise we assume $C_R = C_{S_\mathrm{p}} = 1.0$.

If we express ψ in units of HPBW_α, and the inverse total signal-to-signal ratio as $\Sigma = (S_{\mathrm{TOT}}/N)^{-1}$, the most likely value of ψ, corrected for noise overestimation, becomes :

$$\psi_{\mathrm{COR}}(\psi_{\mathrm{OBS}}, \Sigma) = (0.7743\,\Sigma - 33.14\,\Sigma^2 + 84.44\,\Sigma^3) + (1 - 2.809\,\Sigma + 34.67\,\Sigma^2 - 74.72\,\Sigma^3)\,\psi_{\mathrm{OBS}}$$

where ψ_{OBS} is found from (6), (7) and (8) using R_{OBS}, $(S_\mathrm{p}/N)_{\mathrm{OBS}}$ and σ. In that case its 1 σ error can be given as relative error :

$$\left(\frac{\sigma_{\psi\mathrm{COR}}}{\psi_{\mathrm{COR}}}\right)(\psi_{\mathrm{OBS}}, \Sigma) = (-0.0099 + 5.698\,\Sigma - 109.1\,\Sigma^2 + 341.3\,\Sigma^3) + (0.0008 + 7.441\,\Sigma)\,\psi_{\mathrm{OBS}}^{-1}$$

and the 16 % upper limit in ψ is given for unresolved sources as :

$$\psi_{\mathrm{UL}}(\psi_{\mathrm{OBS}}, \Sigma) = 1.531\,\Sigma^{0.468} + (0.4355 + 42.73(0.2 - \Sigma)^{2.10})\,\psi_{\mathrm{OBS}}^2\,,$$

where ψ_{OBS} and ψ_{UL} are also expressed in units of HPBW_α.

Acknowledgements.

The high quality observations of this paper were obtained in a period in which many changes took place in the Westerbork hardware and software systems. We especially want to thank the Westerbork Telescope group for their careful installation and operation of the 3 km extension, the DLB, the digital delay and digital steering system, and the computer group for their help in the (sometimes non-standard) calibration.

We thank Klaas Lugtenborg for his continuous fulfilment of our ever increasing demands to extend the Westerbork software. Eli Brinks provided us with his elliptical Gaussian fitting routine and René Walterbos instructed us in the art of self-calibration. Rudolf Le Poole gave useful feedback in various stages of the data reduction and kindly allowed us to use his source counts. Harry van der Laan encouraged us in the project with his continuous interest. Marc Oort assisted us in the final stage of the wordprocessing.

We also thank Lena Cijntje, Wanda van Grieken, Liesbeth van der Poel and Petra Steehouwer for a careful typing of the manuscript, Sjaak Ober for drawing the pictures and Wim Brokaar for making the photographs.

The Westerbork Radio Observatory is operated by the Netherlands Foundation for Radio Astronomy with the financial support of the Netherlands Organization for the Advancement of Pure Research (ZWO).

RAW wishes to thank ASTRON/ZWO for financial support (grant 19-23-009).

References

Baars, J. W. N., Genzel, R., Pauliny-Toth, I. I. K., Witzel, A. : 1977, *Astron. Astrophys.* **61,** 99.
Bennett, A. S. : 1961, *Mem. R. Astron. Soc.* **68,** 163.
Bos, A., Raimond, E., van Someren Greve, H. W. : 1981, *Astron. Astrophys.* **98,** 251.
Bridle, A. H., Davis, M. M., Fomalont, E. B., Lequeux, J. : 1972, *Astron. J.* **77,** 405.
Brouw, W. N. : 1971, Ph. D. Thesis, University of Leiden.
Brundage, R. K., Dixon, R. S., Ehman, J. R., Kraus, J. D. : 1971, *Astron. J.* **76,** 777.
Colla, G., Fanti, C., Fanti, R., Ficarra, A., Formiggini, L., Gandolfi, E., Grueff, G., Lari, C., Padrielli, L., Roffi, G., Tomasi, P., Vigotti, M. : 1970, *Astron. Astrophys. Suppl. Ser.* **1,** 281.
Colla, G., Fanti, C., Fanti, R., Ficarra, A., Formiggini, L., Gandolfi, E., Lari, C., Marano, B., Padrielli, L., Tomasi, P. : 1972, *Astron. Astrophys. Suppl. Ser.* **7,** 1.
Dixon, R. S., Kraus, J. D. : 1968, *Astron. J.* **73,** 381.
Downes, A. J. B., Longair, M. S., Perryman, M. A. C. : 1981, *Mon. Not. R. Astron. Soc.* **197,** 593.
Ekers, R. D., Miley, G. K. : 1977, in « Radio Astronomy and Cosmology », *IAU Symp.* No. 74, D. L. Jauncey, ed. (Reidel, Dordrecht), p. 109.
Fielden, J., Downes, A. J. B., Allington-Smith, J. R., Benn, C. R., Longair, M. S., Perryman, M. A. C. : 1983, *Mon. Not. R. Astron. Soc.*, in press.
Fitch, L. T., Dixon, R. S., Kraus, J. D. : 1969, *Astron. J.* **74,** 612.
Fomalont, E. B., Bridle, A. H., Davis, M. M. : 1974, *Astron. Astrophys.* **36,** 273.
Gillespie, A. R. : 1975, *Mon. Not. R. Astron. Soc.* **170,** 541.
Gopal-Krishna, Steppe, H. : 1982, *Astron. Astrophys.* **113,** 150.
Gower, J. F. R., Scott, P. F., Wills, D. : 1967, *Mem. R. Astron. Soc.* **71,** 49.
Harten, R. H. : 1979, Internal Technical Report of the Netherlands Foundation for Radio Astronomy, No. 151.
Högbom, J. A. : 1974, *Astron. Astrophys. Suppl. Ser.* **15,** 417.
Högbom, J. A., Brouw, W. N. : 1974, *Astron. Astrophys.* **33,** 289.
Kapahi, V. K., Subrahmanya, C. R. : 1982, in « Extragalactic Radio Sources », *IAU Symp.* No. 97, D. S. Heeschen and C. M. Wade, eds. (Reidel, Dordrecht) p. 401.
Katgert, P., Katgert-Merkelijn, J. K., Le Poole, R. S., van der Laan, H. : 1973, *Astron. Astrophys.* **23,** 171.
Katgert, J. K., Spinrad, H. : 1974, *Astron. Astrophys.* **35,** 393.
Katgert, P. : 1975, *Astron. Astrophys.* **38,** 87 (K75).
Katgert, P. : 1976, *Astron. Astrophys.* **49,** 221.
Katgert, P. : 1977, Ph. D. Thesis, University of Leiden.
Katgert, P., de Bruyn, A. G., Willis, A. G. : 1979, *Astron. Astrophys. Suppl. Ser.* **36,** 213.
Katgert, P., de Ruiter, H. R. and van der Laan, H. : 1979, *Nature* **280,** 20.
Katgert-Merkelijn, J., Lari, C., Padrielli, L. : 1980, *Astron. Astrophys. Suppl. Ser.* **40,** 91.
Katgert, P., Thuan, T. X., Windhorst, R. A. : 1983, *Astrophys. J.* **275,** 1.
Koo, D. C. : 1981, Ph. D. Thesis, University of California, Berkeley.
Kron, R. G. : 1980, *Astrophys. J. Suppl. Ser.* **43,** 305.
Kron, R. G., Koo, D. C., Windhorst, R. A. : 1984, *Astron. Astrophys. Suppl. Ser.*, submitted (Paper III).
Kraus, J. D. : 1972, *Nature Phys. Sci.* **236,** 4.
Machalski, J. : 1978, *Astron. Astrophys.* **65,** 157.
Mackay, C. D. : 1971, *Mon. Not. R. Astron. Soc.* **154,** 209.
Maslowski, J. : 1973, *Astron. Astrophys.* **26,** 343.
Maslowski, J. : 1977, in *IAU Symp.* No. 74, p. 47 (*op. cit.*).
Miley, G. K., Hartsuyker, A. P. : 1978, *Astron. Astrophys. Suppl. Ser.* **34,** 129.
Noordam, J. E., de Bruyn, A. G. : 1982, *Nature* **299,** 597.
Oort, M. J. A., Windhorst, R. A. : 1984, *Astron. Astrophys.*, submitted.
Oosterbaan, C. E. : 1978, *Astron. Astrophys.* **69,** 235.
Pearson, T. J., Kus, A. J. : 1978, *Mon. Not. R. Astron. Soc.* **182,** 273.
Pilkington, J. D. H., Scott, P. F. : 1965, *Mem. R. Astron. Soc.* **69,** 183.
De Ruiter, H. R., Willis, A. G., Arp, H. C. : 1977, *Astron. Astrophys. Suppl. Ser.* **28,** 211.
De Ruiter, H. R. : 1978, Ph. D. Thesis, University of Leiden.
Van Someren Greve, H. W. : 1974, *Astron. Astrophys. Suppl. Ser.* **15,** 343.
Swarup, G. : 1975, *Mon. Not. R. Astron. Soc.* **172,** 501.
Swarup, G., Sinha, R. P., Saikia, D. J. : 1982, *Mon. Not. R. Astron. Soc.* **201,** 393.

WEILER, K. W. : 1974, *Astron. Astrophys.* **26,** 403.
WILD, J. P. : 1970, *Austr. J. Phys.* **23,** 113.
WILLIS, A. G., OOSTERBAAN, C. E., DE RUITER, H. R. : 1976, *Astron. Astrophys. Suppl. Ser.* **25,** 453 (WOR).
WILLIS, A. G., DE RUITER, H. R. : 1977, *Astron. Astrophys. Suppl. Ser.* **29,** 103.
WILLIS, A. G., OOSTERBAAN, C. E., LE POOLE, R. S., DE RUITER, H. R., STROM, R. G., VALENTIJN, E. A., KATGERT, P., KATGERT-MERKELIJN, J. K. : 1977, in *IAU Symp.* No. 74, p. 39 (*op. cit.*).
WILLIS, A. G., KAHLMANN, H. C. : 1980, *Westerbork Synthesis Radio Telescope Users Manual* (Netherlands Foundation for Radio Astronomy).
WINDHORST, R. A., MILEY, G. K., OWEN, F. N., KRON, R. G., KOO, D. C. : 1984, *Astrophys. J.,* in press (Paper V).
WINDHORST, R. A., KRON, R. G., KOO, D. C. : 1984, *Astron. Astrophys. Suppl. Ser.* This issue (Paper II).
WINDHORST, R. A., OPPE, J. : 1984, *Astron. Astrophys. Suppl. Ser.,* submitted (Paper IV).

Astronomy and Astrophysics n° 1 October 1984. — 2

TABLE Ia. — *Characteristics of the observed Leiden Berkeley Deep Survey fields.*

Field name	RA(1950) H M S	DEC(1950) ° ' "	l^{II} °	b^{II} °	Obs. date (YYDDD)	No of IF	Missing teles-copes	Base lines (m)	Band width (MHz)	T_{sys} (K)
SA57	13 06 15	+29 39 04	64.732	+85.593	80108	40	-	36(72)2700	1x10.0	89
Her.1	17 18 58	+49 58 00	76.629	+34.819	80187	40	-	36(72)2700	1x10.0	83
Her.2	17 15 33	+50 17 00	76.992	+35.377	80188	40	-	36(72)2700	1x10.0	91
SA68.1	00 14 53	+15 36 48	111.091	-46.198	80212	32	5,6	72(72)2592	1x10.0	92
SA68.2	00 14 30	+16 14 00	111.130	-45.572	80207 +81005	32	5,6	72(72)2592	6x1.25	73
Lynx.1	08 38 00	+44 59 00	175.727	+37.795	81011	27	0,D	72(72)2520	6x1.25	56
Lynx.2	08 41 48	+44 47 00	176.019	+38.459	81012	36	0	72(72)2592	7x1.25	46
Lynx.3	08 45 30	+44 36 00	176.284	+39.110	81013	36	0	72(72)2592	7x1.25	52
Lynx.4	08 34 12	+45 08 38	175.480	+37.134	81014	36	0	72(72)2592	1x 5.0	60

TABLE Ib. — *Quality of the 1412 MHz observations.*

Field name	... 3 km maps ... σ_{map} (mJy)	HPBW(α)x(δ) (") (")	... 1.5 km maps ... σ_{map} (mJy)	HPBW(α)x(δ) (") (")	... Error distribution coefficients ... $C_p/HPBW_\alpha$	C_α (")	C_δ (")	C_f (%)	Δr (°)
SA57	0.218	12.1x24.5	0.263	22.1x44.9	0.34	0.43	0.46	5.5	0.010
Her.1	0.199	12.0x15.8	0.273	22.7x29.7	0.30	0.40	0.45	5.5	0.010
Her.2	0.218	12.0x15.8	0.294	22.7x29.5	0.30	0.40	0.45	5.5	0.010
SA68.1	0.248	12.5x46.6	0.334	21.5x79.9	0.40	0.40	0.68	5.5	0.005
SA68.2	0.216	12.6x51.3	0.318	21.6x77.5	0.40	0.40	0.68	5.5	0.005
Lynx.1	0.189	14.9x21.2	0.219	24.4x34.6	0.32	0.48	0.44	4.5	0.007
Lynx.2	0.121	12.4x17.6	0.158	24.4x34.7	0.37	0.58	0.49	4.5	0.009
Lynx.3	0.138	12.4x17.6	0.170	24.3x34.3	0.37	0.58	0.49	4.5	0.009
Lynx.4	0.278	12.5x17.6	0.383	24.5x34.6	0.32	0.48	0.44	4.5	0.007

TABLE II. — *Positions and fluxes of calibration sources.*

NAME	α(1950.0)	δ(1950.0)	$S_{1412\ MHz}$/Jy
3C 48	$01^H\ 34^M\ 49^S.826$	+32° 54' 20".52	15.96
3C147	05 38 43.506	+49 49 42.83	21.94
3C286	13 28 49.654	+30 45 58.70	14.77(*1)
3C390.1	14 58 56.644	+71 52 11.15	7.97(*2)
3C380	18 28 13.516	+48 42 40.87	14.35(*3)

(*1) Polarized, only total flux is listed.
(*2) Variable, only used for position (phase) calibration.
(*3) Slightly resolved at 12".5 beam, only used as a secondary calibrator.

TABLE III. — *Systematic errors in positions and fluxes.*

Overlapping fields	$\langle\Delta\alpha\rangle$ ±m.e. (n)	$\langle\Delta\delta\rangle$ ±m.e. (n)	$\langle S_{TOT_1}/S_{TOT_2}\rangle$ ±m.e. (n)
SA57. VLA-WSRT	+0".25 ±0.25 (17)	-0".10 ±0.35 (17)	0.988 ±0.053 (10)
Her.1-2	-0.45 ±0.41 (13)	+0.39 ±0.36 (13)	0.998 ±0.054 (10)
SA68.1-2	+0.61 ±0.23 (10)	+1.31 ±0.95 (10)	1.067 ±0.038 (9)
Lynx.3-2	+0.20 ±0.52 (13)	-0.84 ±0.55 (13)	0.993 ±0.064 (10)
Lynx.2-1	-0.48 ±0.21 (5)	-0.28 ±0.79 (5)	0.931 ±0.039 (4)
Lynx.1-4	+0.27 ±0.32 (17)	-0.49 ±0.28 (17)	0.991 ±0.049 (13)
Lynx.2 VLA-WSRT	+0.01 ±0.29 (55)	+0.06 ±0.17 (55)	0.983 ±0.031 (52)

1984A&AS...58....1W

TABLE IV. — *Comparison of intrinsic source parameters of 3C 9.*

Reference	Instrument	$S_{1.4}$ (mJy)	ϕ (")	PA (°)	χ (")	f	Sp/N
This paper	3 km WSRT (21 cm)	2124 ±233	12.0 ±2.4	143 ±37	0.0	0.74	52
Miley and Hartsuijker (1978)	1.5km WSRT (6 cm)	1930 ±100	8.3 ±2.0	137 ±15	0.0	0.70	~ 400
Swarup et al (1982)	VLA (6 cm) (A-Array)	2240	12.5	146	3.0	0.76	~ 350

TABLE V. — *The f-distribution.*

f	LBDS Extended Sources	LBDS Resolved Sources	LBDS Total	3rd WBK Katgert (1976)	BGS Oosterbaan (1978)	3CR Mackay (1971)	Adopted
1.4 GHz limit:			0.6 mJy	6.25 mJy	7.5 mJy	3500 mJy	
0.50–0.59	0.46 (12)	0.46 (20)	0.46 (32)	0.50 (6)	0.49 (18)	0.49 (21)	0.48 (77)
0.60–0.69	0.31 (7)	0.29 (11)	0.30 (18)	0.25 (3)	0.35 (13)	0.30 (13)	0.30 (47)
0.70–0.79	0.17 (5)	0.19 (10)	0.18 (15)	0.17 (2)	0.10 (4)	0.07 (3)	0.14 (24)
0.80–0.89	0.06 (2)	0.03 (2)	0.04 (4)	0.08 (1)	0.06 (2)	0.14 (6)	0.07 (13)
0.90–1.00	0.00 (0)	0.03 (2)	0.02 (0)	0.00 (0)	0.00 (0)	0.00 (0)	0.01 (2)
Total	(26)	(45)	(71)	(12)	(37)	(43)	(163)

TABLE VI. — *The flux density contingency table.*

$(\frac{S^{MAP}_{TOT}}{\sigma})_{IN}$:	4σ	4.5σ	5σ	6σ	7σ	8σ	9σ	10σ	15σ	20σ
relative input:	0.238	0.193	0.160	0.115	0.087	0.069	0.056	0.046	0.022	0.014
$(\frac{S^{MAP}_{TOT}}{\sigma})_{COR}$ 3	0.029	0.010	0.016	–	–	–	–	–	–	–
4	0.036	0.044	0.043	0.037	0.002	0.002	–	–	–	–
5	0.067	0.120	0.160	0.159	0.065	0.020	0.003	0.001	–	–
6	0.017	0.051	0.073	0.260	0.227	0.085	0.027	0.007	–	–
7	0.008	0.013	0.041	0.145	0.231	0.212	0.114	0.031	–	–
8	–	0.005	0.013	0.038	0.149	0.262	0.228	0.109	–	–
9	–	–	0.003	0.014	0.054	0.172	0.246	0.181	0.002	–
10	–	–	–	0.009	0.016	0.055	0.180	0.259	0.003	–
11	–	–	–	0.001	0.006	0.026	0.069	0.191	0.009	–
12	–	–	–	–	0.001	0.005	0.020	0.094	0.016	–
13	–	–	–	–	–	0.002	0.007	0.033	0.088	0.001
14	–	–	–	–	–	0.001	0.003	0.011	0.245	0.002
15	–	–	–	–	–	–	–	0.002	0.280	0.004
16	–	–	–	–	–	–	–	–	0.217	0.010
17	–	–	–	–	–	–	–	–	0.078	0.039
18	–	–	–	–	–	–	–	–	0.041	0.141
19	–	–	–	–	–	–	–	–	0.015	0.169
20	–	–	–	–	–	–	–	–	0.003	0.305
21	–	–	–	–	–	–	–	–	–	0.183
22	–	–	–	–	–	–	–	–	–	0.076
23	–	–	–	–	–	–	–	–	–	0.037
24	–	–	–	–	–	–	–	–	–	0.022
25	–	–	–	–	–	–	–	–	–	0.011
fraction in catalogue	0.157	0.243	0.349	0.663	0.751	0.842	0.897	0.919	0.997	1.000

This table describes the redistribution of real input flux densities over intervals of observed flux densities, due to the asymmetrical influence of noise and of the angular size distribution on the algorithm. The fractions in each bin give the number of sources that actually appear in the catalogue after applying the 5σ cut-off in map peak flux density.

TABLE VIIa. — *Source list for the complete 1 412 MHz sample.*

NAME	RA(1950.0) H M S	DEC(1950.0) ° ′ ″	S1412 (MJY)	RES	PSI (″)	PHI (°)	CHI (″)	F	SSKY (MJY)	SP/N	R	ATTEN #EIGHT	NOTES	OTHER NAMES
52W005	13 4 27.14 0.03	29 31 18.0 1.6	7.75 1.23	U	<13.6				8.35 1.33	7.42	1.49	3.45 1.00		
52W007	13 4 59.55 0.03	29 17 15.4 0.5	46.4 4.5	R	12.5 2.9	160 6	4.6	0.74	46.6 4.5	38.20	1.20	4.66 1.00	O	1305+29W1A
52W008	13 5 0.65 0.04	29 18 27.7 0.6	20.5 2.1	R	16.5 4.6	162 19	0.0	0.82	20.5 2.1	19.81	1.16	4.08 1.00		1305+29W1B
52W012	13 5 23.81 0.04	29 19 1.9 0.7	10.0 1.0	U	<10.5				10.0 1.0	15.60	1.02	2.88 1.00		
52W013	13 5 26.29 0.05	29 41 46.9 1.1	2.88 0.36	U	<17.4				2.98 0.37	9.10	1.20	1.26 1.06	O X	
52W014	13 5 27.17 0.05	29 18 40.0 1.1	7.11 0.96	U	<22.0				7.30 0.98	9.27	1.26	2.87 1.03		
52W017	13 5 42.05 0.04	29 35 42.0 0.8	4.09 0.38	U	<22.1				4.09 0.38	14.00	1.19	1.13 1.37	O	
52W018	13 5 53.36 0.06	29 41 40.1 1.3	1.88 0.27	U	<17.3				2.05 0.30	7.54	1.18	1.06 3.86	O	
52W020	13 5 57.56 0.05	30 0 3.2 1.2	3.06 0.49	U	< 7.6				3.15 0.50	7.14	0.82	2.48 2.17		
52W022	13 6 10.68 0.04	29 50 21.9 0.7	4.16 0.37	U	< 4.8				4.16 0.37	15.25	0.98	1.28 1.17	O	
52W023	13 6 11.47 0.06	29 42 34.2 1.4	1.25 0.23	U	< 7.7				1.27 0.23	5.67	1.00	1.05 17.93		
52W025	13 6 15.69 0.04	29 59 7.4 0.6	10.6 0.9	U	<15.2				10.6 0.9	19.79	1.10	2.22 1.00	O	
52W026	13 6 18.71 0.05	29 13 24.6 1.1	7.65 1.11	U	<14.2				8.08 1.19	8.65	1.12	3.84 1.11		
52W027	13 6 18.89 0.05	29 11 27.0 1.1	8.61 1.33	U	<11.1				9.26 1.43	8.14	1.07	4.86 1.20		
52W029	13 6 21.34 0.03	29 14 17.3 0.5	104.8 9.0	R	6.0 1.0	168 13	0.0	0.58	104.8 9.0	135.22	1.02	3.50 1.00	OV	B2 1306+29
52W032e	13 6 43.21 0.08	29 55 15.8 2.1	6.58 0.85	E	19.3	91	0.0	0.72	6.58 0.85	7.88	2.13	1.80 1.50	C	
A	13 6 42.58 0.04	29 55 15.9 0.9	4.73 0.53						4.73 0.53	11.21	1.08	1.79	O	
B	13 6 44.07 0.08	29 55 15.7 1.9	1.84 0.43						1.84 0.43	4.45	1.05	1.81		
52W033	13 6 45.03 0.05	29 58 55.8 1.1	3.46 0.57	U	< 6.9				3.73 0.58	7.35	0.98	2.38 1.70		
52W034	13 6 45.68 0.09	29 30 3.2 2.4	1.93 0.32	U	<14.9				1.98 0.33	6.47	0.92	1.27 4.10	# M7	
52W035	13 6 46.93 0.05	29 42 17.4 1.0	2.10 0.27	U	< 8.4				2.14 0.28	8.68	1.01	1.12 2.65	O	
52W037	13 6 53.37 0.04	29 38 1.9 0.7	4.77 0.39	U	< 9.5				4.77 0.39	17.66	1.08	1.14 1.14	O	
52W038	13 6 55.86 0.05	29 22 47.7 1.1	7.25 0.82	R	11.7 4.7	139 31	0.0	0.58	7.25 0.82	11.34	1.49	1.97 1.07	O TC	
52W039	13 7 1.34 0.07	30 2 7.0 1.5	3.56 0.76	U	< 8.5				3.70 0.79	5.14	0.91	3.02 2.87		
52W041	13 7 4.26 0.08	29 26 7.4 1.4	1.73 0.32	U	< 8.4				1.80 0.34	5.73	0.83	1.74 5.17		
52W042e	13 7 11.37 0.04	29 34 30.9 0.8	35.9 1.5	E	53.0	144	5.1	0.74	35.9 1.5	37.77	3.13	1.39 1.00	BC	
A	13 7 10.38 0.03	29 34 48.8 0.5	26.5 1.7						26.5 1.7	75.77	1.17	1.37	O	1307+29W1
B	13 7 12.75 0.05	29 34 5.8 1.1	9.18 0.84						9.18 0.84	15.09	1.96	1.42	O	
52W044	13 7 14.50 0.08	29 41 26.2 1.5	10.2 1.0	R	25.1 4.6	151 30	0.0	0.56	10.2 1.0	13.36	2.51	1.40 1.20	O C	
52W046	13 7 32.60 0.07	29 48 27.4 1.6	2.12 0.44	U	< 8.3				2.21 0.46	5.11	0.95	2.08 4.59		
52W047	13 7 43.23 0.03	29 42 15.7 0.5	38.1 2.8	U	< 2.2				38.1 2.8	87.31	0.95	2.11 1.00	OV	
52W049	13 7 53.84 0.04	29 28 23.1 0.7	21.3 2.1	R	21.5 4.6	166 15	0.0	0.70	21.3 2.1	20.47	1.49	3.21 1.00		
52W050	13 8 6.42 0.05	29 50 55.9 1.0	8.10 1.19	U	< 6.4				8.18 1.20	8.66	0.97	4.46 1.18		
52W051	13 8 9.06 0.04	29 45 13.1 0.7	10.9 1.2	U	< 5.1				10.9 1.2	13.93	0.95	3.78 1.01		
53W002	17 12 59.71 0.04	50 18 51.7 0.5	50.1 4.3	R	6.6 1.8	94 7	0.6	0.56	50.1 4.3	57.18	1.18	3.40 1.00		
53W004	17 13 21.41 0.04	50 13 45.8 0.5	54.6 4.2	R	6.1 1.3	78 13	4.1	0.50	54.6 4.2	87.89	1.15	2.47 1.00		
53W005	17 13 22.34 0.12	50 31 43.4 1.4	7.58 1.27	U	<16.6				8.34 1.39	7.02	1.07	3.77 1.19	#	
53W006	17 13 39.13 0.09	50 9 8.2 1.0	2.41 0.49	U	< 9.8				2.65 0.54	5.28	1.06	2.18 3.59		
53W008	17 13 47.94 0.04	49 57 35.9 0.5	306.6 26.9	R	6.5 0.7	58 15	2.1	0.54	306.6 26.9	319.72	1.14	3.85 1.00		OT+523.3
53W009	17 13 48.90 0.04	50 24 49.2 0.5	92.7 6.7	R	20.0 2.1	36 31	5.7	0.50	92.7 6.7	82.46	2.66	1.04 1.00	C	
53W010	17 13 50.30 0.06	50 13 36.8 0.8	8.12 0.84	R	11.0 4.5	100 11	2.7	0.50	8.12 0.84	12.76	1.69	1.73 1.08		
53W011	17 13 50.44 0.08	49 59 4.3 1.0	3.48 0.69	U	< 8.8				3.61 0.71	5.61	0.89	3.35 2.52		
53W012	17 13 53.52 0.05	50 3 46.4 0.5	47.6 3.8	R	16.4 2.3	49 41	6.7	0.50	47.6 3.8	40.40	2.31	2.34 1.00	C	
53W013	17 13 58.55 0.09	49 57 12.7 1.2	3.70 0.80	U	<10.5				4.38 0.95	5.01	1.13	3.53 2.62		
53W014	17 14 2.27 0.07	50 3 46.0 0.9	5.28 0.72	U	<15.7				5.48 0.75	8.72	1.34	2.15 1.24		
53W015	17 14 8.58 0.04	50 16 29.7 0.5	184.6 11.8	R	16.1 1.6	126 24	5.2	0.59	184.6 11.8	293.89	2.03	1.42 1.00	C	

NAME	RA(1950.0) H M S	DEC(1950.0) ° ′ ″	S1412 (MJY)	RES	PSI (″)	PHI (°)	CHI (″)	F	SSKY (MJY)	SP/N	R	ATTEN #EIGHT	NOTES	OTHER NAMES
53W019	17 14 32.60 0.08	50 33 25.2 2.6	6.81 0.87	R	11.8 5.2	139 36	6.3	0.61	6.87 0.88	9.52	1.62	2.04 1.17		
53W020	17 14 34.19 0.05	50 28 14.5 0.6	6.74 0.59	R	7.3 4.3	45 19	0.0	0.56	6.74 0.59	17.27	1.18	1.51 1.08		
53W021	17 14 50.05 0.05	50 23 54.3 0.6	4.71 0.41	U	< 9.9				4.71 0.41	16.04	1.12	1.20 1.18		
53W022e	17 14 54.61 0.09	50 27 31.1 1.2	11.8 1.0	E	21.8	67	5.8	0.58	11.8 1.0	13.15	3.09	1.33 1.26	C	
A	17 14 53.70 0.07	50 27 26.7 0.8	4.91 0.54						4.91 0.54	10.91	1.55	1.33		
B	17 14 55.80 0.06	50 27 35.2 0.6	6.86 0.62						6.86 0.62	15.42	1.54	1.33		
53W023	17 14 56.89 0.04	50 8 47.1 0.5	109.9 6.3	R	9.3 1.0	65 17	3.9	0.50	108.7 6.5	301.39	1.35	1.22 1.00	O	
53W024	17 14 58.47 0.04	50 0 0.4 0.5	10.3 0.8	U	< 7.3				10.3 0.8	24.58	1.02	1.00 1.00		
53W025	17 15 7.93 0.08	50 20 10.0 0.9	1.14 0.22	U	< 8.7				1.18 0.22	5.73	0.90	1.05 16.09		
53W026	17 15 12.11 0.04	49 50 23.3 0.5	21.1 2.0	R	7.2 4.0	138 25	2.7	0.76	21.7 2.2	20.22	1.12	1.48 1.00	O M	
53W027e	17 15 12.37 0.19	50 27 9.4 2.4	9.25 1.10	E	26.8	127	10.2	0.51	8.25 1.10	7.71	3.95	1.24 2.35	BC	
A	17 15 10.80 0.06	50 27 8.0 0.8	2.87 0.36						2.87 0.36	8.96	1.18	1.25		
C	17 15 12.95 0.10	50 27 15.0 1.2	2.45 0.42						2.45 0.42	6.27	1.44	1.25		
B	17 15 13.03 0.07	50 26 51.8 0.9	2.93 0.40						2.93 0.40	8.17	1.34	1.23		
53W029	17 15 14.62 0.04	50 23 33.8 0.5	22.2 1.3	U	< 2.2				22.2 1.3	95.79	0.96	1.10 1.00		
53W030	17 15 27.90 0.06	50 12 49.0 0.7	1.41 0.20	U	< 7.8				1.44 0.20	7.85	0.81	1.03 4.68		
53W031	17 15 30.62 0.03	49 59 54.4 0.4	110.5 6.9	R	6.1 0.7	111 6	1.2	0.74	114.9 7.9	281.24	1.06	1.77 1.00	O	
53W032e	17 15 30.94 0.40	49 52 2.0 4.9	10.5 2.1	E	22.4	155	0.0	0.50	10.5 2.1	5.08	2.66	3.55 1.24	C	
A	17 15 30.45 0.10	49 52 12.1 1.3	5.21 1.09						5.21 1.09	5.23	1.31	3.49		
B	17 15 31.42 0.11	49 51 51.7 1.4	5.27 1.16						5.27 1.16	4.93	1.35	3.62		
53W034e	17 15 38.66 0.21	50 3 49.1 2.6	10.9 1.4	E	40.2	38	35.9	0.62	10.9 1.4	8.10	4.42	1.48 1.88	TC	
C	17 15 37.48 0.05	50 3 34.5 0.6	4.98 0.48						4.98 0.48	13.97	1.15	1.42		
A	17 15 40.04 0.14	50 4 6.3 1.7	3.02 0.60						3.02 0.60	5.33	1.88	1.38		
B	17 15 42.03 0.09	50 3 43.5 1.0	2.97 0.47						2.97 0.47	6.96	1.38	1.41		
53W035	17 15 41.06 0.08	50 21 49.7 0.6	4.39 0.40	R	7.3 4.4	133 43	3.6	0.50	4.39 0.40	13.86	1.38	1.05 1.46		
53W036	17 15 42.28 0.05	50 32 12.4 0.6	3.18 0.35	U	< 6.5				3.18 0.35	11.19	0.83	1.57 1.38		
53W037	17 15 44.97 0.04	50 22 25.5 0.5	6.60 0.45	R	5.1 3.3	66 24	3.3	0.50	6.60 0.45	25.59	1.11	1.06 1.00		
53W039	17 15 47.52 0.06	50 28 41.8 0.7	3.43 0.39	U	<11.4				3.44 0.39	10.32	1.16	1.31 1.59		
53W041	17 16 3.17 0.05	49 52 24.5 0.5	9.42 0.93	U	< 9.5				9.72 1.22	10.92	1.14	3.58 1.02	O	
53W042	17 16 6.00 0.05	49 51 34.1 0.6	6.55 0.82	U	< 8.1				5.15 0.98	5.97	0.99	4.08 1.72	OV	
53W043	17 16 15.06 0.05	50 22 0.3 0.6	2.67 0.28	U	< 6.1				2.67 0.28	11.37	0.94	1.14 1.70		
53W044	17 16 21.56 0.06	50 6 13.1 0.8	1.75 0.26	U	< 8.5				1.83 0.28	6.28	0.85	1.41 2.14	O	
53W045	17 16 26.63 0.08	50 18 51.9 0.9	1.46 0.26	U	< 9.0				1.57 0.28	6.06	1.03	1.19 1.77		
53W046	17 16 38.18 0.03	50 10 56.1 0.4	63.1 3.2	R	2.1 0.5	143 37	0.0	0.76	63.6 3.9	220.07	1.00	1.32 1.16	O	
53W047	17 16 53.47 0.04	50 25 49.2 0.5	23.9 1.6	R	4.6 1.6	94 7	0.0	0.50	24.5 1.7	60.82	1.15	1.60 1.00	O	
53W048	17 16 56.88 0.06	50 27 5.3 0.7	11.5 1.1	R	11.0 3.7	90 5	5.9	0.50	11.5 1.1	16.02	1.90	1.73 1.00		MC
53W049	17 16 57.27 0.05	50 36 18.6 0.5	95.1 8.0	R	20.4 2.3	78 13	3.1	0.61	95.1 8.0	53.06	2.70	3.05 1.00		C
53W051	17 17 14.23 0.03	49 51 35.6 0.5	141.6 8.3	R	19.6 1.6	30 21	5.9	0.57	142.8 10.1	162.33	2.36	1.88 1.00	O	C
53W052	17 17 18.74 0.04	50 1 55.7 0.4	8.61 0.56	U	< 8.2				7.95 0.65	22.23	1.06	1.69 1.10	O	
53W054e	17 17 32.38 0.13	49 49 2.4 1.6	6.89 0.92	E	35.1	50	0.0	0.57	6.89 0.92	7.81	2.62	1.69 1.60		C
A	17 17 31.05 0.08	49 48 51.5 0.9	3.91 0.55						3.91 0.55	8.21	1.38	1.73		
B	17 17 33.82 0.07	49 49 14.1 0.9	3.00 0.45						3.00 0.45	7.36	1.23	1.66		
53W057	17 17 51.80 0.20	49 48 41.6 2.5	2.93 0.57	U	<24.8				3.37 0.65	5.46	1.54	1.47 3.65	# M7	
53W058	17 18 3.63 0.09	50 0 47.4 1.1	1.39 0.26	U	<11.3				1.63 0.31	5.56	1.25	1.17 2.87		
53W059	17 18 5.08 0.03	50 3 20.3 0.4	18.7 1.0	R	4.8 1.4	97 9	2.2	0.51	19.4 1.2	74.17	1.08	1.21 1.08	O	
53W060	17 18 8.24 0.06	49 31 42.9 0.7	9.97 1.38	U	< 8.4				9.87 1.41	9.25	1.12	4.77 1.06		

TABLE VIIa *(continued).*

NAME	RA(1950.0) H M S	DEC(1950.0) ° ′ ″	S1412 (MJY)	RES	PSI (″)	PHI (°)	CHI (″)	F	SSKY (MJY)	SP/N	R	ATTEN #EIGHT	NOTES	OTHER NAMES
53W061	17 18 11.26 0.09	49 46 58.7 1.1	2.56 0.40	R	12.3 5.4	72 6	0.0	0.73	2.81 0.44	6.94	1.44	1.41 2.52		
53W062	17 18 16.51 0.11	50 2 4.3 1.3	1.74 0.32	U	<17.7				1.94 0.36	5.70	1.52	1.12 7.33		
53W065	17 18 24.61 0.04	50 0 37.0 0.5	5.25 0.36	U	< 4.1				5.25 0.36	27.13	0.91	1.07 1.00		
53W066	17 18 27.65 0.05	50 4 3.1 0.5	4.07 0.32	U	< 4.7				4.07 0.32	18.53	0.98	1.12 1.12		
53W067	17 18 36.53 0.03	50 13 54.6 0.4	23.2 1.4	R	10.4 2.0	101 12	5.4	0.50	24.5 1.7	47.22	1.55	1.68 1.00	O	
53W068	17 18 43.32 0.06	49 39 6.1 0.8	3.89 0.52	U	< 9.8				4.07 0.55	8.85	1.13	2.04 1.33		
53W069	17 18 46.45 0.05	49 47 47.2 0.5	3.73 0.33	U	< 5.1				3.73 0.33	15.52	0.98	1.23 1.19		
53W070	17 18 51.17 0.07	50 9 1.8 0.8	2.58 0.33	U	< 9.7				2.58 0.35	8.80	1.21	1.26 2.03		
53W071	17 18 57.01 0.09	50 20 10.3 1.1	2.78 0.56	U	< 9.5				3.19 0.64	5.43	1.10	2.48 2.75		
53W072	17 19 15.37 0.10	50 25 33.9 1.3	6.56 1.34	U	<13.7				7.53 1.53	5.52	1.40	4.90 1.39		
53W075	17 19 26.37 0.04	49 46 42.2 0.5	96.1 6.0	U	< 1.2				96.1 6.0	375.44	0.97	1.33 1.00		
53W076	17 19 39.88 0.08	49 42 53.7 1.0	1.42 0.29	U	< 9.4				1.48 0.30	5.20	0.84	1.71 6.69		
53W077	17 19 44.40 0.10	49 51 23.7 1.3	7.78 0.83	R	16.8 4.2	82 9	6.3	0.50	7.78 0.83	11.35	2.85	1.21 1.54	C	
53W078	17 20 3.27 0.13	50 6 22.8 1.6	1.99 0.36	U	<16.1				2.06 0.37	5.93	0.90	1.42 4.33	* H7	
53W079	17 20 8.02 0.04	50 13 22.7 0.5	13.2 1.1	R	8.4 3.3	39 16	1.3	0.88	13.2 1.1	30.59	1.06	2.04 1.00		
53W080	17 20 22.11 0.04	49 58 26.8 0.5	27.6 1.8	R	11.0 1.7	35 26	3.4	0.72	27.6 1.8	77.29	1.26	1.42 1.00		
53W081	17 20 22.56 0.04	50 0 47.9 0.5	12.2 0.8	U	< 3.2				12.2 0.8	45.08	0.94	1.45 1.00		
53W082	17 20 22.84 0.07	50 11 16.3 0.9	1.99 0.36	U	< 8.7				2.06 0.37	6.11	0.83	2.04 3.47		
53W083	17 20 33.96 0.05	50 5 28.1 0.6	5.09 0.47	U	< 5.3				5.09 0.47	15.77	0.90	1.77 1.01		
53W085	17 20 37.07 0.05	49 57 23.4 0.6	4.31 0.42	U	< 5.5				4.31 0.42	14.31	0.92	1.64 1.05		
53W086	17 20 41.84 0.10	49 56 22.7 1.2	0.95 0.70	R	11.2 5.3	124 34	13.0	0.50	5.15 0.73	8.04	1.85	1.73 1.53	H	
53W087	17 20 44.19 0.06	50 11 31.3 0.7	5.85 0.76	U	< 9.4				5.91 0.77	9.61	1.20	2.57 1.04	H7	
53W088	17 20 44.26 0.04	50 14 42.1 0.5	14.9 1.4	U	< 6.0				14.9 1.4	23.17	1.02	3.16 1.00		
53W089	17 20 46.15 0.09	50 9 48.6 1.1	2.48 0.50	U	<13.1				2.88 0.58	5.38	1.12	2.40 3.10		
53W090	17 21 8.54 0.08	49 59 30.8 1.0	2.06 0.43	U	< 9.3				2.14 0.44	5.20	0.86	2.41 4.13		
53W091	17 21 17.80 0.04	50 8 47.5 0.5	22.1 2.0	U	< 3.7				22.1 2.0	32.20	0.98	3.53 1.00		
54W003	0 12 51.09 0.03	16 10 42.0 1.4	10.5 0.9	U	< 4.6				10.5 0.9	16.50	0.92	3.20 1.00		
54W007	0 13 14.51 0.02	16 2 14.5 0.7	63.6 3.4	U	< 1.8				64.2 3.9	112.58	0.99	2.54 1.00	O X	
54W008	0 13 16.26 0.18	15 48 25.8 13.6	12.1 2.4	U	<99.0				13.6 2.9	5.38	1.89	4.00 1.10	* H7	
54W009*	0 13 20.50 0.11	15 58 15.5 5.6	5.99 1.18	E	22.5	130	0.0	0.60	5.99 1.18	5.34	1.80	2.88 1.52	XC	
A	0 13 19.94 0.05	15 58 22.3 3.3	3.57 0.61						3.57 0.61	6.26	0.91	2.89		
B	0 13 21.13 0.07	15 58 7.8 4.7	2.43 0.57						2.43 0.57	4.40	0.89	2.88		
54W011	0 13 23.98 0.04	15 34 42.7 2.8	5.42 0.72	U	<22.0				5.77 0.77	8.47	1.09	2.52 1.26		
54W013	0 13 39.70 0.06	16 11 27.6 3.8	1.51 0.29	U	< 8.2				1.59 0.31	5.42	1.01	1.34 7.93		
54W014	0 13 40.11 0.04	15 34 40.4 1.9	5.47 0.56	U	< 5.5				5.47 0.56	12.01	1.00	1.85 1.10		
54W015	0 13 46.00 0.02	16 11 9.7 0.7	68.8 3.6	R	7.1 0.8	155 25	0.0	0.56	69.9 4.0	256.94	1.00	1.26 1.00	O	
54W016	0 13 47.15 0.06	16 32 52.9 3.9	6.17 0.87	U	<23.0				6.52 0.92	7.82	1.53	2.51 1.20		
54W017*	0 13 49.16 0.15	15 41 48.8 8.0	10.8 1.5	E	23.8	44	23.3	0.57	10.8 1.5	7.43	3.51	1.66 1.71	C	
A	0 13 48.57 0.08	15 41 39.8 6.0	4.65 0.80						4.65 0.80	6.21	1.80	1.67		
B	0 13 49.70 0.06	15 41 57.0 4.1	6.10 0.79						6.10 0.79	8.71	1.71	1.66		
54W018	0 13 50.13 0.06	15 53 26.8 3.8	3.22 0.62	U	< 7.6				3.33 0.64	5.51	1.00	2.81 2.68		
54W019	0 13 50.99 0.02	15 56 22.5 1.5	6.59 0.49	U	< 4.9				6.42 0.48	14.84	0.91	2.20 1.20	O	
54W020	0 13 51.29 0.05	16 23 45.5 3.2	1.71 0.29	U	< 7.4				1.76 0.29	6.36	0.90	1.42 4.65		
54W021	0 13 52.41 0.04	16 4 22.9 2.5	2.23 0.30	U	< 6.5				2.26 0.30	8.38	0.89	1.40 2.36		
54W022	0 13 54.87 0.04	16 28 48.1 2.5	3.25 0.42	U	<11.3				3.43 0.45	8.61	1.05	1.76 1.64		
54W023	0 13 58.44 0.03	15 31 4.3 1.2	10.7 0.8	U	<37.1				10.7 0.8	24.09	1.20	1.49 1.00		

NAME	RA(1950.0) H M S	DEC(1950.0) ° ′ ″	S1412 (MJY)	RES	PSI (″)	PHI (°)	CHI (″)	F	SSKY (MJY)	SP/N	R	ATTEN #EIGHT	NOTES	OTHER NAMES
54W024	0 14 0.28 0.08	15 30 38.0 4.1	1.63 0.33	U	< 8.7				1.70 0.34	5.21	0.89	1.47 8.42		
54W028	0 14 6.08 0.02	15 51 52.6 0.6	53.3 2.4	R	15.3 1.5	44 8	4.0	0.65	55.4 3.4	81.91	1.35	2.01 1.10	O	
54W031	0 14 15.11 0.06	15 31 57.2 4.4	2.03 0.36	U	<26.2				2.31 0.40	6.04	1.26	1.23 5.43		
54W033	0 14 19.77 0.03	15 30 29.2 1.0	9.03 0.60	U	<11.4				9.03 0.60	28.59	1.04	1.22 1.00		
54W034	0 14 20.71 0.04	16 6 57.2 2.5	2.10 0.27	U	<18.0				2.22 0.28	8.74	1.06	1.11 2.64		
54W036	0 14 26.24 0.04	15 22 51.1 2.1	5.72 0.56	U	<55.6				5.72 0.56	12.58	1.16	1.58 1.16		
54W038	0 14 28.43 0.03	15 53 58.0 1.4	5.25 0.40	U	< 5.5				5.11 0.55	11.14	0.96	2.22 1.20	O	
54W039	0 14 29.27 0.03	15 26 34.4 1.6	8.32 0.65	R	25.8 5.5	170 11	0.0	0.68	8.39 0.65	19.20	1.35	1.30 1.00		
54W040	0 14 29.35 0.06	16 22 19.1 4.5	1.90 0.32	U	<18.2				2.14 0.36	6.25	1.39	1.14 5.29		
54W043	0 14 33.01 0.03	16 23 45.9 1.5	3.66 0.32	U	< 4.8				3.66 0.32	14.74	0.96	1.20 1.26		
54W045	0 14 41.35 0.08	16 37 42.1 5.5	4.74 0.94	U	<19.2				5.44 1.08	5.33	1.50	3.16 1.80		
54W046	0 14 44.79 0.02	15 42 30.9 0.8	16.8 0.9	U	< 2.5				17.1 1.0	65.03	0.99	1.07 1.00	O	
54W048	0 14 55.55 0.03	16 32 19.6 1.6	5.37 0.50	U	< 5.2				5.37 0.50	14.01	0.85	2.09 1.03		
54W049	0 14 59.29 0.07	16 38 49.1 4.4	5.68 1.04	U	<27.8				6.45 1.18	5.84	1.31	3.90 1.51		
54W050	0 15 0.42 0.03	15 12 47.5 1.2	17.6 1.4	U	<24.8				17.6 1.4	21.29	1.03	3.23 1.00		
54W051	0 15 2.81 0.03	15 41 39.3 1.5	3.54 0.30	U	< 5.2				3.54 0.30	15.55	0.87	1.06 1.33		
54W052	0 15 5.70 0.02	15 54 27.0 0.8	10.4 0.6	U	< 4.3				11.8 0.9	24.11	1.05	1.88 1.10	OV	
54W053	0 15 6.19 0.04	15 30 49.6 1.9	2.82 0.29	U	< 5.9				2.82 0.29	11.83	0.88	1.09 1.73		
54W054*	0 15 6.51 0.06	16 9 54.3 2.7	7.75 0.57	E	43.3	142	0.0	0.70	7.75 0.57	9.97	3.03	1.20 1.78	C	
A	0 15 4.65 0.04	16 10 20.2 1.8	3.26 0.32						3.26 0.32	12.30	1.05	1.17		
C	0 15 8.51 0.03	16 9 54.3 1.7	3.10 0.30						3.10 0.30	12.53	0.96	1.20		
B	0 15 8.67 0.06	16 9 23.3 4.0	1.40 0.28						1.40 0.28	5.17	1.02	1.23		
54W057	0 15 9.53 0.03	16 34 37.2 0.7	476.6 29.6	R	8.8 0.9	156 25	0.0	0.55	476.6 29.6	750.64	1.05	2.81 1.08		4C16.01
54W058	0 15 14.51 0.04	15 23 9.1 2.6	3.73 0.45	U	<26.2				3.85 0.47	9.32	1.10	1.51 1.61		
54W059	0 15 16.60 0.04	15 39 34.6 2.8	1.75 0.25	U	< 7.3				1.78 0.26	7.57	0.88	1.08 4.46		
54W060*	0 15 21.84 0.12	15 45 0.1 6.1	5.69 0.80	E	41.9	125	0.0	0.71	5.69 0.80	7.14	2.58	1.25 2.63		
A	0 15 20.49 0.05	15 45 13.8 3.5	1.66 0.29						1.66 0.29	5.96	0.90	1.25		
B	0 15 22.87 0.15	15 44 49.7 11.2	4.04 0.74						4.04 0.74	5.78	1.67	1.25	*	
54W061	0 15 24.57 0.03	15 25 18.1 0.8	19.7 1.2	U	< 5.4				19.7 1.2	53.97	1.02	1.44 1.00		
54W063	0 15 30.05 0.08	15 56 23.0 5.7	4.50 0.87	U	<33.8				5.11 0.99	5.43	1.51	3.52 2.03		
54W065	0 15 31.82 0.04	16 19 14.8 2.4	2.55 0.33	U	< 6.5				2.58 0.34	8.50	0.87	1.62 2.03		
54W066	0 15 33.68 0.06	15 47 1.0 4.1	3.30 0.51	U	< 9.1				3.52 0.54	5.06	0.84	1.47 6.91		
54W067	0 15 34.92 0.03	16 20 53.2 0.7	66.6 3.6	U	< 1.5				66.6 3.6	176.12	0.99	1.76 1.00		
54W068*	0 15 34.97 0.08	16 32 52.3 4.0	24.6 2.4	E	33.4	36	17.7	0.60	24.6 2.4	11.84	2.86	3.37 1.00	C	
A	0 15 34.34 0.03	16 32 39.8 1.5	14.8 1.3						14.8 1.3	17.27	1.21	3.28		
B	0 15 35.62 0.06	16 33 4.8 4.2	9.70 1.38						9.70 1.38	7.85	1.65	3.48		
54W069	0 15 39.53 0.04	16 26 59.0 2.0	5.23 0.59	U	< 5.6				5.20 0.59	10.53	0.94	2.43 1.08		
54W070	0 15 41.17 0.03	15 57 4.3 2.0	5.33 0.54	U	< 6.4				5.38 0.69	8.88	0.87	3.23 1.52	O	
54W071	0 15 41.64 0.07	16 29 35.1 5.1	5.41 0.95	U	<68.6				6.04 1.06	6.11	1.55	2.95 1.44		
54W072	0 15 42.42 0.06	16 26 45.8 4.1	2.77 0.55	U	<20.7				3.09 0.62	5.26	1.08	3.53 3.27		
54W073	0 15 49.04 0.05	15 23 42.8 3.4	2.70 0.45	U	< 8.0				2.80 0.47	6.36	0.88	2.01 3.01	K	
54W074	0 15 50.02 0.06	16 1 28.7 4.6	4.61 0.80	U	< 6.7				5.21 0.91	6.14	1.36	2.88 1.62		
54W075	0 15 52.06 0.05	15 49 5.5 3.1	2.72 0.43	U	< 7.9				2.79 0.44	6.77	0.83	2.00 2.80		
54W078	0 15 53.98 0.06	15 14 5.9 4.7	10.4 1.7	R	20.5 4.1	147 33	0.0	0.72	11.2 1.8	6.80	1.47	4.52 1.10	TC	
54W079	0 15 56.16 0.02	16 4 3.9 0.5	254.4 12.0	R	6.4 0.6	117 22	0.0	0.63	265.2 16.6	399.39	1.07	2.88 1.00	O	
54W081	0 16 1.88 0.03	15 41 51.3 0.9	15.0 1.0	U	< 3.4				15.0 1.0	36.23	0.93	1.80 1.00		

TABLE VIIa *(continued)*.

NAME	RA(1950.0) H M S	DEC(1950.0) D ' "	S1412 (MJY)	RES	PSI (")	PHI (D)	CHI (")	F	SSKY (MJY)	SP/N	R	ATTEN WEIGHT	NOTES	OTHER NAMES
54W084*	0 16 6.19 0.06	15 45 25.3 3.0	28.6 1.9	E	15.6	70	18.2	0.52	28.6 1.0	17,76	3.03	2.14 1.00	C	
A	0 16 5.68 0.04	15 45 22.5 2.0	13.7 1.1						13.7 1.1	17.12	1.53	2.12		
B	0 16 6.69 0.04	15 45 28.0 1.8	14.8 1.2						14.8 1.2	18.41	1.50	2.16		
54W088	0 16 35.06 0.03	15 35 40.1 1.6	11.6 1.1	U	< 5.2				11.6 1.1	14.79	0.93	3.42 1.01		
55W007	8 32 5.77 0.06	45 5 50.1 0.7	8.47 0.92	U	< 6.2				8.47 0.92	11.77	0.94	2.76 1.04		
55W010*	8 32 49.46 0.09	45 7 46.8 1.0	32.8 1.6	E	39.4	0	7.7	0.78	32.8 1.6	20.20	3.85	1.51 1.00	TC	
A	8 32 49.15 0.16	45 7 7.4 2.4	7.33 1.20						7.33 1.20	6.49	2.67	1.52		
B	8 32 49.46 0.05	45 7 46.8 0.5	25.5 1.5						25.5 1.5	51.27	1.18	1.51		
55W011	8 33 6.42 0.06	45 5 37.9 0.8	3.07 0.40	U	<10.3				3.19 0.41	8.43	1.03	1.32 2.22		
55W012	8 33 6.68 0.08	45 16 36.2 1.1	4.14 0.36	U	<13.9				4.40 0.60	8.03	1.36	1.45 1.93		
55W013	8 33 7.85 0.05	45 12 22.6 0.5	22.1 1.2	R	6.7 2.0	4 6	0.5	0.94	22.1 1.2	59.60	1.02	1.31 1.00		
55W014	8 33 15.62 0.08	45 20 13.0 1.1	1.89 0.35	U	< 9.6				1.96 0.37	5.58	0.81	1.55 6.45		
55W015	8 33 18.86 0.05	45 32 50.4 0.6	16.2 1.6	U	< 5.4				16.2 1.6	15.48	0.98	3.84 1.00		
55W016	8 33 20.13 0.06	45 16 46.5 0.8	5.92 0.57	R	8.3 5.1	64 6	0.0	0.55	5.92 0.57	12.23	1.31	1.32 1.34		
55W017	8 33 22.08 0.06	45 23 12.6 0.7	7.68 0.76	U	<11.5				7.68 0.76	12.47	1.28	1.73 1.09		
55W018	8 33 31.82 0.05	44 42 49.5 0.5	34.6 3.1	U	< 9.8				34.6 3.1	25.10	1.09	4.53 1.00		
55W019	8 33 41.84 0.05	45 12 44.1 0.6	4.16 0.37	U	< 7.7				4.16 0.37	13.34	1.03	1.09 1.48		
55W020	8 33 42.04 0.12	45 20 23.5 1.7	2.37 0.40	U	<15.2				2.72 0.56	5.03	1.43	1.36 1.00		
55W022	8 33 44.65 0.05	45 17 22.0 0.5	64.4 3.3	R	19.9 2.1	25 11	0.0	0.62	64.4 3.3	100.26	1.92	1.20 1.00	C	
55W023	8 33 48.30 0.12	45 18 11.2 1.8	4.07 0.65	R	11.5 5.6	77 14	5.9	0.50	4.37 0.70	6.54	1.97	1.22 3.31		
55W024	8 33 49.36 0.05	45 11 57.7 0.6	4.85 0.37	U	< 7.4				4.85 0.37	16.24	1.02	1.05 1.29		
55W025	8 33 52.80 0.07	45 8 47.5 0.9	2.17 0.30	U	<10.0				2.31 0.32	7.74	1.05	1.02 4.04		
55W027	8 33 55.68 0.08	45 9 1.7 1.0	1.83 0.29	U	< 8.0				2.03 0.32	6.64	1.08	1.02 7.14		
55W032	8 34 6.70 0.10	45 5 47.9 1.4	2.46 0.40	U	<17.3				2.73 0.44	6.42	1.49	1.02 6.23		
55W033	8 34 7.92 0.20	45 2 48.3 2.9	4.65 0.85	R	24.6 5.9	32 33	2.6	0.51	4.85 0.88	5.68	2.85	1.08 7.42	H	
55W034	8 34 8.94 0.09	45 35 50.0 1.2	4.19 0.90	U	<10.8				4.38 0.94	5.04	0.70	4.43 3.47		
55W036	8 34 15.55 0.05	45 15 47.2 0.5	6.29 0.42	U	< 4.6				6.29 0.42	21.67	0.95	1.09 1.03		
55W037*	8 34 27.34 0.04	45 0 54.4 0.4	1519.2 43.2	E	114.2	10	12.9	0.54	1507.6 46.6	610.43	7.72	1.15 1.00	0 9C	4C45.17
A	8 34 26.44 0.04	44 59 55.8 0.4	792.5 24.3						792.3 24.3	607.95	3.51	1.18	0	
B	8 34 28.19 0.04	45 1 48.5 0.4	816.7 36.3						804.9 38.3	612.49	4.21	1.12	0	
55W039	8 34 32.16 0.04	44 45 16.7 0.5	35.2 2.5	R	7.4 2.9	123 5	0.0	0.90	34.2 2.6	36.92	1.04	3.18 1.00	0	
55W041	8 34 46.72 0.08	44 58 53.5 1.0	2.02 0.35	U	< 8.6				2.09 0.36	6.07	0.94	1.31 5.59		
55W042	8 34 51.41 0.06	45 32 43.6 0.7	12.3 1.4	U	< 9.9				12.3 1.4	11.43	1.11	3.48 1.02		
55W043	8 35 14.48 0.06	44 57 36.9 0.8	8.27 0.73	R	8.8 4.9	96 8	4.0	0.50	8.12 0.76	12.61	1.42	1.63 1.13	0	
55W044	8 35 16.54 0.05	44 58 57.5 0.5	15.8 1.0	R	11.7 3.5	101 12	8.3	0.50	15.8 1.2	20.94	1.73	1.56 1.00	0	
55W046	8 35 23.94 0.07	45 32 9.0 0.9	9.91 1.47	U	<10.4				10.7 1.6	7.97	1.15	4.19 1.15	H?	
55W048	8 35 30.05 0.04	44 49 24.3 0.4	26.3 1.6	U	< 6.1				27.2 2.1	29.97	1.03	3.18 1.00	0	
55W049	8 35 35.86 0.07	44 50 52.3 0.9	4.52 0.63	U	<10.1				4.89 0.91	5.91	1.00	4.39 2.27	0	
55W051	8 35 43.08 0.06	45 10 47.5 0.8	3.53 0.46	U	< 7.4				3.58 0.46	8.63	0.90	1.67 1.82		
55W053*	8 35 45.30 0.05	45 14 46.2 1.7	40.4 2.0	E	23.8	70	7.0	0.50	40.3 2.0	27.55	2.89	1.82 1.00	0 C	
A	8 35 44.25 0.04	45 14 42.1 1.4	20.2 1.4						20.6 1.4	29.03	1.42	1.79	0	
B	8 35 46.35 0.04	45 14 50.4 0.4	20.3 1.2						19.7 1.4	26.12	1.47	1.84	0	
55W054	8 35 46.08 0.09	44 54 34.2 1.2	2.64 0.53	U	<10.5				2.74 0.55	5.25	0.71	2.63 4.61		
55W056	8 35 59.27 0.05	45 18 48.1 0.6	6.74 0.66	U	< 6.5				6.80 0.80	10.36	0.95	2.48 1.07	0	
55W058	8 36 18.50 0.12	45 0 39.5 1.7	4.25 0.65	R	14.6 6.7	70 21	0.0	0.60	4.51 0.69	7.05	1.79	1.89 1.61	C	
55W061	8 36 26.88 0.10	44 47 46.9 1.4	2.06 0.42	U	<14.4				2.33 0.47	5.16	1.09	2.20 3.40		

NAME	RA(1950.0) H M S	DEC(1950.0) D ' "	S1412 (MJY)	RES	PSI (")	PHI (D)	CHI (")	F	SSKY (MJY)	SP/N	R	ATTEN WEIGHT	NOTES	OTHER NAMES
55W063	8 36 36.82 0.06	44 55 29.7 0.4	24.5 1.2	R	7.6 1.6	98 5	0.8	0.72	23.3 1.3	72.35	1.10	1.46 1.00	0	
55W065	8 36 42.73 0.09	44 44 13.8 1.3	2.72 0.46	U	<13.4				3.11 0.53	6.32	1.17	2.23 2.05		
55W066	8 36 52.25 0.04	45 16 18.0 0.4	24.7 1.5	R	10.4 2.5	22 8	0.0	0.66	23.0 1.6	44.89	1.13	2.41 1.00	OV	
55W067	8 36 52.95 0.04	45 10 29.3 0.5	9.82 0.63	R	8.1 4.0	144 9	0.1	0.54	9.77 0.67	27.12	1.12	1.70 1.00	0	
55W068	8 37 3.95 0.07	45 15 24.9 0.9	3.56 0.47	U	<13.1				3.76 0.49	8.69	1.11	2.04 1.34		
55W069	8 37 10.07 0.07	45 7 5.5 0.8	2.57 0.30	U	<12.8				2.61 0.30	9.74	1.08	1.32 1.72		
55W070*	8 37 12.44 0.12	44 42 8.8 1.6	11.2 1.1	E	37.5	153	0.0	0.77	11.2 1.1	10.74	2.68	2.04 1.07	TC	
A	8 37 11.78 0.06	44 42 22.4 0.7	8.37 0.74						8.37 0.74	15.56	1.43	1.99		
B	8 37 13.40 0.11	44 41 49.1 1.6	2.50 0.51						2.50 0.51	5.20	1.25	2.05		
55W075	8 37 26.75 0.04	44 50 40.6 0.3	187.3 8.8	U	< 1.0				182.6 9.1	795.86	1.00	1.22 1.00	OV	0J+463
55W077	8 37 30.58 0.05	44 45 18.8 0.5	8.75 0.55	U	< 4.6				8.75 0.55	31.79	0.96	1.52 1.00		
55W080	8 37 38.10 0.05	45 1 8.7 0.5	9.66 0.51	R	23.5 4.4	18 18	22.2	0.50	9.66 0.51	38.88	1.27	1.04 1.00		
55W082*	8 37 42.49 0.05	45 1 33.1 0.5	74.3 2.3	E	53.6	94	5.3	0.69	73.4 2.3	93.14	4.06	1.03 1.00	BC	
A	8 37 40.16 0.05	45 1 34.4 0.4	51.1 2.4						50.7 2.4	147.18	1.76	1.04	0	
B	8 37 45.20 0.05	45 1 30.5 0.5	23.2 1.1						23.0 1.1	51.72	2.30	1.02	0	
55W083	8 37 46.48 0.05	44 53 13.8 0.6	4.78 0.32	U	<10.9				4.78 0.32	21.24	1.11	1.08 1.05		
55W085	8 38 2.55 0.09	45 5 39.5 1.2	1.14 0.21	U	<13.3				1.18 0.21	5.76	1.00	1.09 10.46		
55W086	8 38 4.34 0.09	44 44 21.3 1.2	2.17 0.34	U	<15.9				2.41 0.37	6.88	1.22	1.52 2.56		
55W088	8 38 9.59 0.10	44 42 17.2 1.3	1.36 0.28	U	<11.7				1.41 0.29	5.11	0.84	1.74 5.98		
55W089	8 38 9.76 0.10	44 59 31.3 1.4	1.29 0.21	U	<13.0				1.40 0.24	6.06	1.21	1.91 10.27		
55W092	8 38 13.46 0.08	45 6 54.0 1.1	2.48 0.31	U	<17.6				2.57 0.32	8.74	1.37	1.24 2.47		
55W093	8 38 17.85 0.09	44 48 52.2 1.2	1.46 0.24	U	<12.4				1.63 0.27	6.39	1.09	1.24 4.62		
55W097	8 38 30.20 0.09	44 54 1.8 1.2	0.91 0.17	U	<11.4				0.95 0.18	5.56	0.82	1.11 15.09		
55W099	8 38 32.29 0.09	45 21 19.1 1.2	2.82 0.51	U	<10.6				2.95 0.53	6.03	0.89	2.91 2.19		
55W102	8 38 46.89 0.05	45 4 52.8 0.5	9.66 0.54	U	< 7.8				9.66 0.54	40.04	1.05	1.22 1.00		
55W103	8 38 47.76 0.05	45 23 15.8 0.4	135.0 10.3	R	12.1 1.5	49 10	1.8	0.54	135.0 10.3	139.68	1.33	3.85 1.00		0J+463.1
55W104	8 38 48.40 0.06	45 11 23.6 0.6	6.04 0.49	R	7.9 5.2	89 5	6.7	0.50	6.04 0.49	16.68	1.24	1.55 1.00		
55W105	8 38 48.70 0.08	45 21 31.5 1.0	3.94 0.64	U	< 9.5				4.04 0.65	6.92	0.95	3.24 1.46		
55W109	8 39 19.74 0.07	45 16 27.0 0.9	8.11 0.91	R	10.8 6.2	115 5	0.0	0.50	8.11 0.91	11.29	1.39	2.74 1.00		
55W110*	8 39 28.34 0.07	44 44 58.9 1.0	24.8 1.3	E	47.9	122	3.6	0.69	24.6 1.8	16.90	3.39	3.54 1.10	0 C	
A	8 39 26.45 0.05	44 45 14.5 0.6	5.67 0.46						5.63 0.65	10.68	1.19	3.66	0	
C	8 39 28.34 0.05	44 44 58.9 0.5	6.28 0.46						6.19 0.59	14.14	1.00	3.54	0	
B	8 39 30.24 0.04	44 44 49.5 0.4	12.8 0.7						12.6 1.0	25.32	1.20	3.42	0	
55W111	8 39 26.57 0.08	45 14 10.5 1.1	6.30 0.81	R	14.3 6.7	67 5	0.0	0.70	6.44 0.83	9.06	1.46	2.58 1.05		
55W112	8 39 42.15 0.04	45 6 43.0 0.4	15.0 0.8	R	10.8 3.6	121 6	0.0	0.91	16.1 1.1	37.85	1.05	2.14 1.00	0	
55W116	8 40 16.52 0.09	44 50 15.4 1.2	0.96 0.18	U	< 9.3				1.00 0.18	5.68	0.85	1.70 5.01		
55W118	8 40 23.14 0.10	44 46 45.1 1.4	1.00 0.19	U	<12.5				1.14 0.22	5.47	1.11	1.56 9.21		
55W119	8 40 23.62 0.07	45 1 31.5 0.9	1.39 0.19	U	< 9.3				1.33 0.21	6.97	0.68	2.33 2.94	OV	
55W120	8 40 29.21 0.08	44 35 21.5 1.0	1.79 0.25	U	< 9.5				1.94 0.28	7.63	1.08	1.95 1.78		
55W121	8 40 40.23 0.09	44 42 11.1 1.2	1.04 0.17	U	< 9.5				1.17 0.19	6.32	1.09	1.39 4.09		
55W122	8 40 48.19 0.10	44 42 4.1 1.4	0.72 0.15	U	< 9.4				0.75 0.15	5.03	0.94	1.31 12.05		
55W123	8 40 50.64 0.06	44 45 51.3 0.7	1.71 0.16	U	< 6.0				1.71 0.16	12.69	0.91	1.23 1.42		
55W124	8 40 50.96 0.06	44 49 44.6 0.5	5.21 0.29	U	< 6.4				5.21 0.29	34.50	1.01	1.23 1.00		
55W125	8 40 52.20 0.06	44 22 10.1 0.5	21.4 1.6	R	8.3 3.0	12 13	0.0	0.71	21.4 1.6	35.29	1.10	4.51 1.00		
55W126	8 40 56.03 0.09	45 8 57.2 1.1	1.93 0.33	U	< 8.8				2.01 0.34	6.30	0.86	3.05 2.18	V	
55W127	8 41 3.45 0.07	44 54 1.8 0.8	1.31 0.14	U	< 6.9				1.33 0.15	10.11	0.88	1.23 1.91	V	

TABLE VIIa *(continued).*

NAME	RA(1950.0) H M S	DEC(1950.0) ° ′ ″	S1412 (MJY)	RES	PSI (″)	PHI (°)	CHI (″)	F	SSKY (MJY)	SP/N	R	ATTEN WEIGHT	NOTES	OTHER NAMES
55W128	8 41 8.65 0.08	45 1 9.4 1.0	3.25 0.33	R	9.4 5.0	50 40	5.4	0.50	3.25 0.33	11.43	1.47	1.60 1.22	H	
55W129	8 41 8.66 0.10	44 40 36.7 1.3	0.57 0.11	U	<10.0				0.59 0.11	5.37	0.76	1.20 16.15	V	
55W131	8 41 11.64 0.10	44 56 54.9 1.3	0.80 0.15	U	< 8.9				0.83 0.16	5.46	0.96	1.29 8.32		
55W132	8 41 12.77 0.15	45 1 26.0 2.1	1.39 0.28	U	<11.4				1.61 0.32	5.17	1.62	1.59 3.92		
55W133	8 41 13.72 0.06	44 36 54.5 0.7	2.26 0.19	U	< 5.5				2.26 0.19	15.21	0.92	1.32 1.15		
55W135	8 41 17.71 0.06	44 32 31.3 0.7	2.38 0.23	U	< 5.9				2.38 0.23	12.18	0.99	1.62 1.18	V	
55W136	8 41 21.42 0.09	44 43 18.4 1.1	0.77 0.13	U	< 8.3				0.80 0.13	6.36	0.96	1.08 7.55		
55W137	8 41 22.88 0.07	44 55 31.9 0.7	1.60 0.15	U	< 6.1				1.60 0.15	12.02	0.93	1.18 1.54		
55W138	8 41 30.35 0.07	44 57 17.0 0.7	1.69 0.16	U	< 6.1				1.69 0.16	12.18	0.92	1.23 1.47		
55W141	8 41 39.57 0.10	44 39 10.0 1.3	0.75 0.14	U	<10.8				0.82 0.15	5.63	1.05	1.14 10.38		
55W142	8 41 41.55 0.09	44 55 3.9 1.2	0.66 0.12	U	< 9.1				0.68 0.12	5.87	0.85	1.13 10.96		
55W143	8 41 42.05 0.07	44 36 39.5 0.8	3.01 0.26	R	7.9 4.5	116 27	0.0	0.50	3.01 0.26	14.35	1.38	1.25 1.24	H	
55W144	8 41 53.98 0.09	45 12 11.7 1.2	2.68 0.46	U	<10.1				3.04 0.52	6.33	1.12	3.53 1.59	H?	
55W146	8 41 58.86 0.07	45 13 56.6 0.8	4.70 0.61	U	< 6.8				4.72 0.61	9.29	0.97	4.33 1.11		
55W147	8 41 59.77 0.07	45 1 20.8 0.8	1.78 0.19	U	< 6.5				1.80 0.19	10.86	0.92	1.48 1.44		
55W149	8 42 2.84 0.06	45 6 22.6 0.6	6.98 0.50	R	8.5 3.8	163 18	0.0	0.56	6.98 0.50	23.79	1.16	2.08 1.00		
55W150	8 42 5.35 0.10	45 1 34.1 1.3	0.84 0.16	U	< 9.3				0.87 0.17	5.38	0.88	1.51 6.83		
55W153	8 42 8.33 0.14	45 7 12.0 2.0	1.94 0.39	R	11.9 5.7	72 7	13.5	0.69	2.24 0.45	5.25	1.56	2.25 2.34	H	
55W154	8 42 17.30 0.06	44 51 10.2 0.6	11.7 0.6	R	15.0 2.2	99 10	4.3	0.57	11.7 0.6	43.26	2.05	1.08 1.00	C	
55W155	8 42 23.52 0.07	44 36 10.4 0.8	1.90 0.21	U	<14.3				1.95 0.21	10.60	1.10	1.37 1.50		
55W156	8 42 27.14 0.07	44 50 48.7 0.8	4.13 0.30	R	10.2 3.7	90 5	0.0	0.50	4.13 0.30	18.54	1.63	1.18 1.12		
55W157	8 42 40.48 0.08	44 56 50.2 1.1	1.23 0.16	U	<10.5				1.36 0.20	7.34	1.08	1.41 2.72		
55W158	8 42 40.90 0.09	44 41 51.5 1.3	0.69 0.13	U	< 9.4				0.71 0.13	5.52	0.84	1.26 10.36	V	
55W159	8 42 42.64 0.06	45 2 26.6 0.5	5.99 0.39	U	< 4.1				5.99 0.39	29.16	0.90	1.88 1.00		
55W160	8 42 44.81 0.09	44 47 48.9 1.2	0.85 0.15	U	< 9.6				0.88 0.15	5.92	1.00	1.22 6.75		
55W161*	8 43 1.59 0.40	44 41 6.6 6.0	3.20 0.73	E	48.9	112	2.9	0.58	3.20 0.73	5.10	3.45	1.50 3.54	RC	
A	8 42 59.49 0.09	44 41 15.4 1.2	1.23 0.20						1.23 0.20	6.45	1.07	1.47		
C	8 43 1.34 0.12	44 41 9.2 1.7	0.82 0.20						0.82 0.20	4.21	1.07	1.50		
B	8 43 3.76 0.13	44 40 57.4 1.9	1.15 0.25						1.15 0.25	4.71	1.30	1.54		
55W163	8 43 5.29 0.07	44 28 45.8 1.0	1.97 0.27	U	< 8.8				1.88 0.34	5.91	0.90	2.92 2.98	O	
55W164	8 43 7.91 0.10	44 45 7.2 1.4	0.67 0.14	U	<10.3				0.70 0.14	5.05	0.76	1.49 10.82		
55W165*	8 43 16.63 0.09	44 52 43.1 1.2	17.6 1.3	E	37.9	80	9.8	0.54	17.7 1.3	23.18	3.83	1.64 1.00	O BC	
A	8 43 16.84 0.08	44 52 37.8 1.1	8.04 0.64						8.27 0.64	17.64	2.40	1.61	O	
B	8 43 16.36 0.08	44 52 46.3 0.6	9.52 0.55						9.48 0.59	32.43	1.44	1.68	O	
55W166	8 43 12.71 0.06	44 41 53.5 0.8	2.40 0.23	U	<12.6				2.49 0.27	10.38	1.20	1.65 1.30	O H	
55W167	8 43 20.54 0.07	45 8 34.9 0.7	5.82 0.63	U	< 6.2				5.82 0.63	12.18	0.89	4.41 1.04		
55W169	8 43 35.51 0.05	44 43 33.1 0.6	2.90 0.25	U	<10.5				3.18 0.33	11.45	1.08	2.11 1.41	O	
55W171	8 43 43.36 0.05	44 33 46.7 0.7	2.89 0.25	U	< 6.8				2.58 0.29	10.37	0.88	2.06 1.25	O	
55W172	8 43 52.03 0.07	44 49 0.1 1.9	9.22 0.66	R	18.6 3.3	171 5	0.0	0.56	8.21 0.83	12.42	2.05	2.65 1.10	O TC	
55W173	8 43 57.37 0.05	44 49 46.2 0.6	3.57 0.27	U	< 6.5				3.51 0.38	11.26	0.88	2.92 1.15	O	
55W174	8 44 8.70 0.06	44 19 30.4 0.7	4.58 0.46	U	< 5.8				4.58 0.46	12.62	0.98	2.68 1.02		
55W175	8 44 10.65 0.05	44 15 13.3 0.5	42.9 2.8	U	< 2.4				42.7 2.9	85.71	0.97	3.73 1.00	O	
55W177	8 44 18.03 0.05	44 14 33.4 0.5	30.6 2.1	U	< 2.8				30.6 2.1	61.85	0.98	3.68 1.00		
55W178	8 44 21.15 0.11	44 45 52.4 1.5	1.24 0.23	U	<12.8				1.44 0.27	5.50	1.19	1.60 4.52	H?	
55W179	8 44 21.72 0.05	44 37 14.9 0.5	4.98 0.29	U	< 4.0				5.13 0.31	28.44	0.98	1.33 1.00	O	
55W180	8 44 25.94 0.07	44 23 35.3 0.9	5.14 0.47	R	14.0 4.9	116 5	0.0	0.70	5.14 0.47	13.71	1.53	1.77 1.02		

NAME	RA(1950.0) H M S	DEC(1950.0) ° ′ ″	S1412 (MJY)	RES	PSI (″)	PHI (°)	CHI (″)	F	SSKY (MJY)	SP/N	R	ATTEN WEIGHT	NOTES	OTHER NAMES
55W182	8 44 34.58 0.05	44 23 16.7 0.5	10.3 0.6	U	< 3.2				10.3 0.6	44.63	0.99	1.69 1.00		
55W183	8 44 37.78 0.14	44 44 9.1 2.0	1.33 0.26	U	<13.8				1.53 0.30	5.29	1.58	1.33 5.62	H?	
55W184	8 44 39.51 0.11	44 39 35.0 1.6	1.07 0.20	U	<16.8				1.24 0.23	5.71	1.32	1.19 6.84		
55W187*	8 44 54.95 0.09	44 24 27.6 1.2	19.3 1.2	E	36.8	54	12.5	0.57	19.3 1.2	24.20	4.09	1.42 1.00	C	
A	8 44 53.63 0.06	44 24 17.2 0.7	11.1 0.7						11.1 0.7	26.83	2.09	1.44		
B	8 44 56.39 0.07	44 24 39.0 0.8	8.25 0.57						8.25 0.57	21.47	2.00	1.39		
55W188	8 45 2.93 0.05	44 51 34.6 0.5	12.1 0.7	U	< 4.6				12.3 0.7	53.11	1.02	1.65 1.00	O	
55W189	8 45 12.16 0.16	44 10 29.6 2.4	4.64 0.73	U	<21.3				4.84 0.84	6.30	1.13	4.00 1.25	R H	
55W190	8 45 14.14 0.05	44 40 46.8 0.5	11.0 0.5	U	< 2.5				11.0 0.5	78.60	0.96	1.06 1.00		
55W191	8 45 16.61 0.06	44 13 3.3 0.5	14.0 1.0	U	< 3.7				14.0 1.0	34.38	0.98	3.01 1.00		
55W192	8 45 23.20 0.05	44 25 54.4 0.5	9.46 0.49	U	< 2.9				9.46 0.49	56.21	0.99	1.24 1.00		
55W195	8 45 34.17 0.07	44 17 37.9 0.8	2.86 0.33	U	< 9.4				2.88 0.33	10.09	1.04	1.99 1.20		
55W196	8 45 38.55 0.10	44 10 11.2 1.3	2.79 0.55	U	< 9.0				2.90 0.58	5.37	0.96	4.07 2.13		
55W197	8 45 38.63 0.07	44 26 40.6 0.8	1.63 0.17	U	< 6.5				1.64 0.17	10.75	0.92	1.20 1.75		
55W198	8 45 40.42 0.09	44 39 8.4 1.2	0.58 0.10	U	< 9.8				0.60 0.11	5.91	0.72	1.02 19.90		
55W199	8 45 42.96 0.06	44 32 27.2 0.6	3.36 0.23	R	6.1 4.0	100 11	5.3	0.50	3.36 0.23	19.86	1.18	1.04 1.12		
55W200	8 45 43.89 0.08	44 13 36.4 1.1	4.64 0.58	U	<11.2				4.74 0.59	9.21	1.31	2.85 1.02		
55W201	8 45 44.88 0.09	44 31 24.6 1.1	1.59 0.20	U	<11.3				1.66 0.21	8.59	1.32	1.06 2.63		
55W202	8 45 45.16 0.09	44 37 3.4 1.1	0.76 0.12	U	< 8.6				0.78 0.13	6.30	0.89	1.02 18.71		
55W203	8 45 47.92 0.05	45 1 17.0 0.5	187.6 12.7	U	< 1.2				187.6 12.7	390.84	0.96	3.64 1.00		0J+475
55W204	8 45 51.63 0.09	44 38 36.7 1.2	0.71 0.12	U	< 9.0				0.73 0.13	5.90	0.87	1.04 14.48		
55W205	8 45 53.22 0.11	44 22 33.9 1.6	1.12 0.22	U	<12.5				1.31 0.26	5.20	1.23	1.49 6.02		
55W209*	8 46 5.12 0.11	44 39 32.4 1.4	17.2 1.0	E	36.8	22	6.7	0.73	17.2 1.0	28.30	4.01	1.10 1.00	RC	
A	8 46 4.37 0.12	44 39 12.8 1.6	4.65 0.46						4.65 0.46	11.37	2.72	1.09		
B	8 46 5.68 0.06	44 39 46.9 0.5	12.6 0.6						12.6 0.6	63.94	1.29	1.11		
55W210	8 46 12.54 0.08	44 32 40.3 1.1	2.58 0.28	R	9.5 5.1	69 21	9.4	0.50	2.58 0.27	10.46	1.56	1.15 1.77		
55W211*	8 46 16.40 0.06	44 34 13.4 0.5	58.8 2.9	E	29.4	160	5.3	0.87	58.8 2.9	123.81	3.00	1.15 1.00	BC	
A	8 46 16.05 0.05	44 34 23.8 0.5	51.1 2.4						51.1 2.4	281.41	1.15	1.15		
B	8 46 16.99 0.06	44 33 56.2 0.7	7.64 0.47						7.64 0.47	25.91	1.85	1.16		
55W215	8 46 25.98 0.14	44 32 38.8 2.0	1.36 0.26	R	13.6 5.3	73 5	0.0	0.69	1.54 0.29	5.45	1.65	1.24 5.89	H	
55W219	8 47 8.30 0.06	44 40 21.2 0.7	3.47 0.33	U	< 6.6				3.47 0.33	13.10	1.02	1.88 1.02		
55W220	8 47 9.86 0.08	44 20 29.6 1.1	6.02 0.35	U	< 9.2				2.09 0.34	6.74	0.72	3.15 2.37		
55W222*	8 47 14.51 0.26	44 19 57.9 3.9	4.70 0.93	E	23.3	60	16.2	0.55	4.70 0.93	5.05	1.57	3.49 1.38	R C	
A	8 47 13.36 0.16	44 19 49.9 2.3	2.10 0.61						2.10 0.61	3.56	1.23	3.47		
B	8 47 15.22 0.14	44 20 1.9 2.0	2.60 0.63						2.60 0.63	4.26	1.26	3.51		
55W224*	8 47 29.98 0.06	44 48 59.9 0.6	33.8 2.0	E	31.1	53	7.5	0.85	33.8 2.0	32.36	2.17	3.50 1.00	C	
A	8 47 28.55 0.08	44 48 48.3 0.9	5.03 0.63						5.03 0.63	9.37	1.15	3.38		
B	8 47 30.87 0.06	44 49 7.2 0.5	29.2 2.0						29.2 2.0	58.45	1.02	3.57		
55W225	8 47 34.49 0.05	44 35 26.5 0.5	34.5 2.2	R	6.0 1.4	125 35	0.0	0.50	34.5 2.2	82.99	1.13	2.68 1.00		
55W226	8 47 35.83 0.07	44 34 38.8 0.8	6.35 0.63	U	< 9.6				6.35 0.63	12.93	1.30	2.75 1.00		
55W228	8 47 43.50 0.07	44 21 52.9 0.9	6.05 0.78	U	< 6.9				6.12 0.79	9.38	0.95	5.09 1.12		

TABLE VIIb. — *Radio source* not *in the complete sample.*

NAME	RA(1950.0) H M S	DEC(1950.0) ° ′ ″	S1412 (MJY)	RES	PSI (″)	PHI (°)	CHI (″)	F	SSKY (MJY)	SP/N	R	ATTEN WEIGHT	NOTES	OTHER NAMES
52W001	13 4 8.08 0.04	29 32 52.4 0.8	17.4 2.1	U	< 9.7				17.4 2.1	13.75	1.10	5.27 0.00		1304+29W1
52W002	13 4 8.58 0.07	29 47 5.3 1.8	17.0 2.7	R	21.3 5.1	2 5	7.6	0.62	17.5 2.7	8.11	1.80	5.50 0.00		1304+29W2
52W003	13 4 17.29 0.15	30 9 41.3 3.7	55.6 13.9	U	<30.2				66.1 16.6	5.02	1.23	40.83 0.00	*	
52W004	13 4 19.29 0.09	29 57 37.8 2.3	8.99 2.19	U	<14.1				10.8 2.6	4.57	1.36	7.96 0.00		
52W006	13 4 56.88 0.07	29 42 34.6 1.7	1.71 0.38	U	< 8.6				1.78 0.40	4.73	0.96	1.80 0.00		
52W009	13 5 12.64 0.09	29 20 45.1 2.2	2.84 0.67	U	<12.9				3.41 0.80	4.51	1.22	2.84 0.00		
52W010	13 5 13.92 0.13	29 37 44.5 3.4	1.24 0.28	U	<19.2				1.30 0.30	4.52	0.77	1.41 0.00	*	
52W011	13 5 26.13 0.08	30 1 33.6 1.9	3.54 0.82	U	<12.7				4.18 0.97	4.64	1.13	3.66 0.00		
52W015	13 5 34.89 0.09	29 46 59.4 2.3	1.26 0.30	U	<12.8				1.50 0.36	4.25	1.24	1.30 0.00		
52W016	13 5 35.69 0.09	29 24 24.7 2.2	2.19 0.47	U	<20.8				2.56 0.55	4.92	1.36	1.76 0.00	OV	
52W019	13 5 57.51 0.09	29 22 17.0 2.3	1.94 0.45	U	<15.3				2.30 0.54	4.50	1.31	1.78 0.00		
52W021	13 6 9.05 0.04	30 13 5.6 0.6	55.9 7.2	U	<12.1				55.9 7.2	18.77	1.08	12.59 0.00		82 1306+30
52W024	13 6 14.99 0.05	30 7 10.0 0.9	11.1 1.5	U	< 7.1				11.1 1.5	9.74	1.01	5.16 0.00		
52W028	13 6 19.69 0.06	29 10 17.1 1.4	7.31 1.39	U	< 8.8				7.90 1.50	6.13	1.05	5.65 0.00		
52W030	13 6 26.05 0.12	29 35 25.2 3.2	1.22 0.26	U	<16.8				1.27 0.27	4.80	0.97	1.04 0.00	*	
52W031	13 6 27.76 0.14	29 45 7.1 3.6	1.01 0.25	U	<18.8				1.06 0.26	4.18	0.89	1.09 0.00	*	
52W036	13 6 50.15 0.07	29 40 26.9 1.7	1.03 0.22	U	< 8.8				1.07 0.23	4.73	0.92	1.12 0.00		
52W040	13 7 3.90 0.14	29 10 9.7 3.7	0.88 1.80	U	<19.0				7.20 1.90	4.18	0.87	7.64 0.00	*	
52W043	13 7 11.74 0.07	29 35 44.6 1.8	1.23 0.29	U	< 8.8				1.30 0.30	4.40	0.98	1.37 0.00	O	
52W045	13 7 25.28 0.08	30 5 12.7 2.0	7.34 1.72	U	<13.1				8.77 2.05	4.75	1.19	7.09 0.00		
52W048	13 7 48.76 0.08	30 3 57.7 1.9	12.9 2.9	U	<19.6				14.5 3.1	5.42	1.33	9.18 0.00		
52W052	13 8 20.87 0.15	29 39 50.9 4.0	6.45 1.45	U	<30.9				7.68 1.73	4.89	1.28	4.69 0.00	*	
52W053	13 8 39.42 0.12	29 50 33.6 3.1	15.2 3.5	U	<24.8				17.0 3.7	5.34	1.08	11.25 0.00	*	
52W054	13 8 40.49 0.04	29 27 3.3 0.8	32.8 4.6	U	< 5.3				32.8 4.6	12.95	0.96	12.15 0.00		
52W055	13 8 53.67 0.04	29 29 38.8 0.8	46.9 7.1	U	<10.1				46.9 7.1	12.00	1.04	17.18 0.00		
52W056	13 8 53.86 0.07	29 32 1.2 1.8	34.4 6.6	R	17.4 4.5	157 23	0.0	0.65	36.8 7.0	6.87	1.57	15.60 0.00		
52W057	13 9 0.47 0.04	29 31 0.2 0.9	66.3 10.4	U	<21.1				66.3 10.4	11.94	1.20	21.31 0.00		
52W058	13 9 1.60 0.07	29 57 3.2 1.7	43.4 11.7	U	< 8.7				45.3 12.2	4.53	0.99	46.19 0.00		
53W001	17 12 56.40 0.05	49 56 35.8 0.6	33.6 4.4	U	< 8.7				33.6 4.4	14.70	1.10	9.49 0.00		
53W003	17 13 2.08 0.15	50 21 34.0 1.9	3.19 0.71	U	<20.1				3.37 0.74	4.90	0.69	3.39 0.00	*	
53W007	17 13 41.66 0.18	50 1 39.1 2.2	3.62 0.91	U	<21.3				3.91 0.94	4.22	1.03	3.05 0.00	*	
53W016	17 14 9.63 0.17	49 59 16.2 2.1	2.48 0.61	U	<20.3				2.62 0.64	4.33	0.77	2.68 0.00	*	
53W017	17 14 21.17 0.05	50 47 28.2 0.6	33.4 4.4	U	<10.1				33.4 4.4	13.98	1.12	9.78 0.00		
53W018	17 14 30.93 0.10	49 41 54.7 1.2	122.3 19.5	R	15.8 4.4	112 23	9.6	0.50	118.8 18.9	10.88	2.54	19.73 0.00		C
53W028	17 15 13.38 0.09	50 39 45.3 1.1	2.05 0.60	U	< 9.4				2.77 0.63	4.75	0.93	2.89 0.00		
53W033	17 15 37.11 0.05	49 46 28.5 0.5	21.3 2.1	U	< 4.9				20.4 2.3	17.31	0.99	5.46 0.00	O	
53W038*	17 15 45.99 0.25	50 46 59.8 3.1	17.3 4.1	E	23.2	148	4.8	0.54	17.3 4.1	4.31	2.80	6.59 0.00		
A	17 15 45.33 0.12	50 47 1.9 1.5	8.04 2.08						8.04 2.08	4.21	1.30	6.74		
B	17 15 46.62 0.14	50 46 41.3 1.6	2.60 2.30						2.60 2.30	4.40	1.50	6.45		
53W040	17 15 48.25 0.09	50 3 1.5 1.1	1.25 0.27	U	< 9.8				1.30 0.29	4.77	0.85	1.48 0.00		
53W050	17 17 10.92 0.16	49 39 4.8 2.0	4.02 0.99	U	<18.5				4.22 1.01	4.48	0.90	3.82 0.00	*	
53W053*	17 17 23.88 0.08	50 50 6.6 1.0	194.2 19.1	E	22.3	169	5.2	0.68	194.2 19.1	14.25	2.58	24.23 0.00		C 0T+528
A	17 17 23.60 0.05	50 50 16.4 0.6	133.0 19.6						133.0 19.6	18.18	1.35	24.89		
B	17 17 24.05 0.06	50 49 54.5 0.7	62.6 10.5						62.6 10.5	9.95	1.23	23.45		
53W055	17 17 34.47 0.16	50 42 53.2 1.9	14.9 3.7	R	14.2 5.0	147 25	5.1	0.62	16.9 4.2	4.50	1.83	9.41 0.00		
53W056	17 17 42.96 0.16	50 13 54.6 1.9	3.03 0.68	U	<17.6				3.19 0.72	4.73	0.95	2.40 0.00	*	

NAME	RA(1950.0) H M S	DEC(1950.0) ° ′ ″	S1412 (MJY)	RES	PSI (″)	PHI (°)	CHI (″)	F	SSKY (MJY)	SP/N	R	ATTEN WEIGHT	NOTES	OTHER NAMES
53W063	17 18 17.18 0.09	49 29 19.3 1.1	5.82 1.31	U	<11.6				6.63 1.49	4.94	1.09	6.15 0.00		
53W064	17 18 18.98 0.10	50 16 0.6 1.2	3.11 0.77	U	<10.4				3.26 0.81	4.33	0.81	4.25 0.00		
53W073	17 19 16.80 0.11	49 38 40.4 1.4	2.00 0.47	U	<11.1				2.42 0.56	4.52	1.26	2.13 0.00		
53W074	17 19 21.08 0.12	50 22 40.4 1.4	3.64 0.85	U	<17.2				4.36 1.01	4.63	1.34	3.55 0.00		
53W084	17 20 34.97 0.09	49 51 19.6 1.0	1.58 0.33	U	< 9.1				1.64 0.35	4.99	0.94	1.76 0.00		
53W092	17 22 7.80 0.04	50 0 4.5 0.5	76.0 8.1	R	13.6 2.8	130 14	2.0	0.75	76.0 8.1	39.53	1.33	7.25 0.00		
54W001	0 12 35.00 0.05	16 34 22.2 2.9	18.2 3.0	U	< 6.9				18.6 3.1	6.90	0.95	13.12 0.00		
54W002	0 12 44.19 0.04	15 56 18.0 1.8	34.6 3.0	R	25.7 5.5	174 8	2.3	0.67	34.2 3.2	15.85	1.30	7.69 0.00	O	
54W004	0 12 52.45 0.06	15 16 44.4 4.4	16.8 3.7	U	< 8.9				17.5 3.8	4.89	0.92	15.76 0.00		
54W005*	0 12 52.68 0.12	16 33 29.2 6.3	26.6 4.3	E	20.0	129	7.6	0.57	26.6 4.3	6.77	2.58	7.06 0.00		C
A	0 12 52.12 0.07	16 33 35.9 4.8	11.4 2.2						11.4 2.2	5.46	1.33	7.25		
B	0 12 53.19 0.05	16 33 23.2 3.1	15.2 2.1						15.2 2.1	8.15	1.25	6.90		
54W006	0 13 4.92 0.03	16 44 1.4 1.1	79.9 7.4	U	< 4.1				79.9 7.4	22.14	0.88	19.04 0.00		
54W010	0 13 23.09 0.06	15 1 39.6 4.8	65.2 15.1	U	<10.3				71.3 16.5	4.73	1.05	58.06 0.00		
54W012	0 13 26.89 0.06	15 55 59.3 3.9	6.28 1.25	U	< 8.4				6.51 1.30	5.33	0.94	5.25 0.00		
54W025	0 14 1.42 0.03	15 10 31.4 1.2	43.7 3.5	R	23.1 4.9	177 6	5.6	0.76	44.7 3.5	26.50	1.16	5.86 0.00		
54W026	0 14 3.69 0.07	16 44 2.9 4.5	7.24 1.61	U	<19.7				8.32 1.84	4.76	1.10	7.38 0.00		
54W027	0 14 4.20 0.06	15 34 35.2 4.4	1.42 0.38	U	< 8.9				1.47 0.32	4.84	0.93	1.32 0.00		
54W029	0 14 9.89 0.12	16 37 58.0 8.7	4.10 0.95	U	<17.6				4.29 0.99	4.50	0.89	3.36 0.00	*	
54W030	0 14 12.31 0.03	16 41 46.7 1.5	14.8 1.4	U	< 4.9				14.8 1.4	14.16	0.94	5.16 0.00		
54W032	0 14 16.36 0.06	16 42 12.4 4.1	8.75 1.50	U	<44.6				9.84 1.68	6.37	1.33	5.36 0.00		
54W035	0 14 25.10 0.06	16 17 47.0 4.2	1.01 0.22	U	< 8.2				1.05 0.23	4.77	0.99	1.03 0.00		
54W037	0 14 27.18 0.07	16 43 23.2 4.9	4.62 1.19	U	< 9.2				4.84 1.25	4.03	0.91	6.13 0.00		
54W041	0 14 31.17 0.12	15 44 26.4 9.3	9.56 2.02	U	<64.7				11.2 2.4	5.00	1.13	6.27 0.00	*	
54W042	0 14 31.77 0.06	15 55 48.2 4.4	2.08 0.46	U	< 9.3				2.17 0.49	4.64	0.88	2.15 0.00		
54W044	0 14 38.10 0.06	15 49 59.7 4.3	1.71 0.36	U	<11.0				1.81 0.38	4.98	1.02	1.44 0.00		
54W047	0 14 53.04 0.06	16 23 19.6 4.1	1.28 0.27	U	< 8.5				1.34 0.28	4.91	1.01	1.25 0.00		
54W055	0 15 8.68 0.06	16 20 31.9 4.1	1.11 0.24	U	< 8.6				1.16 0.24	4.93	0.85	1.28 0.00		
54W056	0 15 8.79 0.17	15 37 28.6 13.6	2.33 0.53	U	<15.3				2.93 0.61	4.94	1.72	1.03 0.00	*	
54W062	0 15 25.23 0.06	16 23 3.3 4.2	1.71 0.36	U	<12.8				1.85 0.38	5.00	1.04	1.65 0.00		
54W064	0 15 31.45 0.10	15 2 27.2 7.5	23.1 5.6	U	<22.6				27.4 6.6	4.37	1.52	16.59 0.00		
54W076	0 15 52.75 0.07	15 58 51.5 5.3	3.52 0.80	U	<18.7				4.18 0.95	4.57	1.19	3.56 0.00		
54W077	0 15 53.81 0.11	16 26 40.1 8.3	4.45 0.97	U	<16.4				4.63 1.01	4.78	0.98	3.13 0.00	*	
54W080	0 15 59.90 0.07	16 21 12.9 4.5	2.05 0.48	U	< 9.4				2.15 0.50	4.42	0.79	2.83 0.00		
54W082	0 16 2.69 0.13	15 32 26.8 10.5	2.94 0.65	U	<26.3				3.53 0.78	4.68	1.25	1.80 0.00	*	
54W083	0 16 3.70 0.08	15 53 44.6 4.3	3.71 0.80	U	<22.8				3.91 0.84	4.86	1.01	3.21 0.00		
54W085	0 16 14.56 0.07	16 12 25.3 4.7	2.85 0.68	U	< 9.0				2.99 0.71	4.35	0.88	3.62 0.00		
54W086	0 16 26.76 0.05	16 37 21.0 3.3	33.7 5.9	U	<25.7				37.1 5.9	7.23	1.21	19.64 0.00		
54W087	0 16 32.36 0.19	16 13 0.7 10.2	13.6 3.5	U	<45.4				15.9 3.5	4.73	1.67	6.32 0.00	*	
54W089	0 16 52.98 0.04	15 39 16.8 2.0	13.4 1.5	U	< 6.2				13.4 1.5	11.24	0.83	5.88 0.00		
54W090	0 17 50.12 0.05	15 24 14.9 0.8	2124.4 233.2	R	12.0 2.4	143 37	0.0	0.74	2124.4 233.2	51.05	1.16	142.34 0.00		3C 9
55W001	8 30 14.43 0.10	45 27 30.9 1.4	248.4 73.5	U	<11.5				265.7 78.5	4.39	1.02	212.36 0.00		0J+452
55W002	8 31 4.51 0.07	45 26 48.6 0.9	41.4 7.8	U	< 8.2				42.8 7.9	7.25	0.87	24.27 0.00		
55W003	8 31 35.04 0.10	44 56 34.2 1.5	7.03 1.85	U	<10.5				7.37 1.94	4.05	0.93	7.03 0.00		
55W004	8 31 46.78 0.10	45 41 45.0 1.4	65.2 18.6	U	<10.3				68.3 19.5	4.11	0.97	61.75 0.00		
55W005	8 31 52.44 0.10	45 20 21.2 1.2	1.89 1.22	U	<12.5				5.13 1.33	4.07	1.00	4.53 0.00		

TABLE VIIb *(continued).*

NAME	RA(1950.0) H M S	DEC(1950.0) ° ′ ″	S1412 (MJY)	RES	PSI (″)	PHI (°)	CHI (″)	F	SSKY (MJY)	SP/N	R	ATTEN #EIGHT	NOTES	OTHER NAMES
55W006	8 31 59.28 0.11	45 15 59.1 1.5	3.06 0.79	U	<11.0				3.22 0.85	4.04	0.86	3.35 0.00		
55W008	8 32 39.80 0.10	45 0 15.7 1.5	1.86 0.46	U	<10.8				1.95 0.49	4.13	0.87	1.96 0.00		
55W009	8 32 40.71 0.11	44 54 3.5 1.5	2.84 0.72	U	<11.9				3.09 0.79	4.07	1.04	2.62 0.00		
55W021	8 33 43.72 0.17	44 53 29.0 2.4	2.83 0.63	U	<18.7				2.99 0.66	4.67	1.00	1.67 0.00	*	
55W026	8 33 55.52 0.11	45 19 54.7 1.5	1.49 0.35	U	<13.1				1.76 0.41	4.38	1.13	1.28 0.00		
55W028	8 33 56.46 0.10	45 3 15.1 1.5	1.20 0.29	U	<11.2				1.30 0.32	4.20	1.03	1.08 0.00		
55W029	8 34 1.11 0.18	45 3 44.1 2.6	2.73 0.61	R	23.0 4.3	11 12	0.0	0.50	2.83 0.63	4.61	2.08	1.06 0.00		
55W030	8 34 3.05 0.11	45 47 44.7 1.5	36.9 9.8	U	<12.0				42.9 11.4	4.31	1.11	32.18 0.00		
55W031	8 34 3.68 0.12	45 6 3.0 1.7	1.41 0.32	U	<17.6				1.65 0.38	4.47	1.30	1.02 0.00		
55W035	8 34 10.01 0.11	45 5 39.6 1.6	1.52 0.33	U	<19.9				1.76 0.38	4.73	1.31	1.02 0.00		
55W038	8 34 29.20 0.08	44 31 56.9 0.5	238.2 26.7	R	7.2 2.8	140 34	4.3	0.50	247.5 29.6	34.23	1.16	23.40 0.00	0	
55W040	8 34 36.08 0.18	45 2 23.4 2.6	2.64 0.62	R	16.9 4.9	30 30	0.0	0.50	2.65 0.62	4.34	1.95	1.13 0.00		
55W045	8 35 21.16 0.15	45 35 25.4 2.2	10.2 2.2	U	<18.5				10.6 2.3	5.11	0.92	5.91 0.00	*	
55W047	8 35 25.34 0.09	45 5 39.5 1.3	1.47 0.33	U	<10.3				1.54 0.34	4.61	0.85	1.41 0.00		
55W050	8 35 37.92 0.10	44 55 30.6 1.4	2.59 0.62	U	<11.6				2.72 0.66	4.31	1.00	2.26 0.00		
55W052	8 35 44.30 0.13	45 12 53.2 1.8	2.06 0.52	U	<15.4				2.47 0.62	4.10	1.25	1.73 0.00		
55W055	8 35 54.71 0.10	44 49 38.6 1.4	4.97 1.19	U	<11.1				5.24 1.26	4.40	1.01	4.24 0.00		
55W057	8 36 12.97 0.10	45 23 59.4 1.4	3.76 0.94	U	<10.9				3.95 0.99	4.21	0.84	4.02 0.00		
55W059	8 36 21.30 0.10	45 22 35.5 1.4	4.03 1.01	U	<10.8				4.24 1.06	4.21	0.85	4.25 0.00		
55W060	8 36 26.39 0.25	45 11 58.8 3.7	3.11 0.73	U	<30.3				3.68 0.86	4.44	1.57	6.41 0.00	*	
55W062	8 36 33.68 0.13	45 4 24.6 1.8	1.30 0.31	U	<15.6				1.38 0.33	4.00	1.10	1.67 0.00		
55W064•	8 36 40.42 0.34	44 31 32.5 5.0	23.0 2.0	E	35.8	73	0.0	0.53	23.0 2.0	4.46	3.58	7.89 0.00		C
A	8 36 38.83 0.22	44 31 27.2 3.3	12.0 3.2						12.0 3.2	4.05	2.01	7.81		
B	8 36 42.03 0.15	44 31 37.9 2.2	10.6 2.4						10.6 2.4	4.86	1.57	7.34		
55W071	8 37 14.05 0.16	44 39 46.7 2.4	2.29 0.56	U	<16.4				2.75 0.66	4.10	1.49	2.38 0.00		
55W072	8 37 16.40 0.15	45 9 11.9 2.2	1.42 0.33	U	<16.0				1.69 0.39	4.44	1.47	1.37 0.00		
55W073	8 37 17.81 0.10	45 11 33.0 1.4	1.27 0.26	U	<11.3				1.33 0.28	4.99	0.93	1.51 0.00		
55W074	8 37 18.03 0.17	44 54 9.2 2.5	1.18 0.30	U	<22.6				1.37 0.35	4.05	1.54	1.16 0.00		
55W076	8 37 29.22 0.06	44 27 30.5 0.8	19.0 2.6	U	<10.7				19.0 2.6	10.18	1.10	8.93 0.00		
55W078	8 37 33.98 0.11	44 36 16.4 1.6	1.90 0.46	U	<12.9				1.99 0.49	4.26	0.84	2.95 0.00		
55W079	8 37 37.19 0.13	44 47 46.3 1.9	1.31 0.29	U	<14.7				1.57 0.34	4.73	1.34	1.31 0.00		
55W081	8 37 43.11 0.11	45 9 7.7 1.5	0.86 0.20	U	<12.5				0.89 0.21	4.35	0.87	1.24 0.00		
55W084	8 37 52.76 0.05	45 27 18.8 0.8	48.2 4.2	R	9.4 3.0	105 11	0.0	0.59	48.9 4.2	39.42	1.22	5.28 0.00		C
55W087	8 38 9.06 0.16	45 29 21.2 2.3	496.3 139.0	U	<20.4				531.5 148.0	5.03	1.03	268.70 0.00	*	
55W090	8 38 9.93 0.14	44 58 33.0 2.0	0.75 0.19	U	<17.5				0.92 0.23	4.00	1.21	1.01 0.00		
55W091	8 38 10.74 0.15	44 40 1.0 2.3	2.06 0.50	U	<21.3				2.39 0.56	4.25	1.45	2.05 0.00		
55W094	8 38 27.02 0.10	45 32 23.4 1.4	10.7 2.4	U	<13.5				11.8 2.7	4.94	1.07	11.91 0.00		
55W095	8 38 27.41 0.17	44 52 42.7 2.5	1.46 0.33	U	<28.9				1.65 0.38	4.49	1.73	1.13 0.00		
55W096	8 38 27.80 0.11	45 3 59.7 1.5	0.95 0.20	U	<13.1				1.05 0.23	4.76	1.06	1.10 0.00		
55W098	8 38 32.09 0.12	45 21 47.7 1.6	280.7 89.A	U	<10.6				304.4 94.3	4.20	0.87	683.43 0.00		
55W100	8 38 41.46 0.11	44 55 25.2 1.6	0.88 0.21	U	<15.1				0.94 0.22	4.31	1.02	1.14 0.00		
55W101	8 38 44.43 0.19	44 28 16.3 2.8	13.4 3.2	R	22.4 5.4	23 23	0.0	0.50	14.4 3.5	4.54	1.96	8.60 0.00		
55W106	8 38 49.73 0.08	45 36 30.8 0.7	75.6 11.5	U	<12.9				75.6 11.5	11.89	1.12	30.15 0.00		
55W107	8 39 0.55 0.33	45 25 19.5 4.9	11.5 3.0	R	22.1 6.4	127 37	17.4	0.50	12.6 3.3	4.06	3.07	5.36 0.00		
55W108	8 39 1.16 0.21	45 8 8.2 3.0	1.89 0.48	R	21.3 5.4	169 12	0.0	0.50	2.09 0.53	4.02	1.86	1.47 0.00		
55W113	8 39 1.75 0.04	45 18 47.9 0.6	20.5 1.9	R	10.5 4.6	63 27	7.0	0.50	26.0 2.5	20.37	1.34	5.05 0.00	0	

NAME	RA(1950.0) H M S	DEC(1950.0) ° ′ ″	S1412 (MJY)	RES	PSI (″)	PHI (°)	CHI (″)	F	SSKY (MJY)	SP/N	R	ATTEN #EIGHT	NOTES	OTHER NAMES
55W114	8 40 9.26 0.10	44 57 30.3 1.4	1.15 0.25	U	< 9.7				1.20 0.26	4.87	0.90	2.26 0.00		
55W115	8 40 14.91 0.27	44 56 10.8 4.0	1.55 0.36	U	<30.7				1.87 0.44	4.38	1.35	2.00 0.00	*	
55W117	8 40 17.56 0.12	45 23 18.2 1.8	10.4 2.6	U	<15.0				12.4 3.1	4.34	1.15	13.21 0.00		
55W130	8 41 9.01 0.10	44 17 5.4 1.5	4.42 0.96	U	<10.2				4.75 1.04	4.93	1.03	7.72 0.00		
55W134	8 41 15.36 0.12	44 50 45.5 1.6	0.49 0.12	U	<10.2				0.52 0.13	4.20	0.93	1.09 0.00		
55W139	8 41 35.55 0.11	44 43 47.8 1.5	0.51 0.11	U	< 9.9				0.53 0.12	4.70	0.90	1.03 0.00		
55W140	8 41 39.55 0.11	44 52 1.5 1.5	0.43 0.10	U	<10.7				0.46 0.11	4.41	0.81	1.05 0.00		
55W145	8 41 58.13 0.11	45 20 46.1 1.6	5.06 1.25	U	<10.4				5.31 1.32	4.33	0.88	11.45 0.00		
55W148	8 42 0.04 0.16	45 8 37.6 2.4	1.36 0.36	U	<14.7				1.85 0.46	4.12	1.48	2.50 0.00		
55W151	8 42 6.31 0.09	44 18 27.0 1.2	4.55 0.77	U	<11.1				5.06 0.86	6.58	1.09	5.84 0.00		
55W152	8 42 7.70 0.14	45 9 40.4 1.9	2.16 0.45	U	<15.9				2.46 0.52	4.98	1.46	2.80 0.00		H?
55W162	8 43 5.02 0.04	44 16 24.0 0.4	46.3 3.0	U	< 3.7				45.0 4.0	34.01	0.96	9.98 0.00	0	
55W168	8 43 33.55 0.13	44 29 49.0 1.8	1.45 0.35	U	<13.3				1.75 0.42	4.29	1.16	2.57 0.00		
55W170	8 43 40.99 0.11	44 39 36.3 1.6	1.20 0.28	U	<10.0				1.25 0.29	4.39	0.93	2.52 0.00		
55W176	8 44 12.69 0.11	45 4 30.0 1.5	4.97 1.14	U	<10.6				5.47 1.26	4.65	1.05	8.11 0.00		
55W181	8 44 31.00 0.15	45 5 24.8 2.1	8.51 1.73	U	<18.0				9.62 1.95	5.38	1.71	7.61 0.00		H?
55W185	8 44 42.84 0.23	44 37 40.1 3.4	0.89 0.20	U	<28.7				1.08 0.24	4.57	1.21	1.15 0.00	*	
55W186	8 44 51.47 0.11	44 59 24.1 1.5	1.66 0.39	U	<10.3				1.74 0.41	4.40	0.89	3.23 0.00		
55W193	8 45 25.91 0.11	45 6 55.3 1.5	4.79 1.04	U	<10.7				5.51 1.21	4.98	1.12	7.28 0.00		H?
55W194	8 45 29.04 0.14	44 47 2.1 2.0	0.75 0.18	U	<12.9				0.92 0.22	4.19	1.28	1.25 0.00		
55W206	8 45 54.22 0.14	44 11 4.8 2.1	2.26 0.57	U	<13.5				2.77 0.70	4.12	1.28	3.81 0.00		
55W207	8 45 57.89 0.12	45 1 20.2 1.6	2.12 0.52	U	<10.7				2.27 0.55	4.27	1.02	3.77 0.00		
55W208	8 46 0.18 0.22	44 22 48.4 3.3	1.07 0.25	U	<25.6				1.24 0.29	4.38	1.10	1.51 0.00	*	
55W212	8 46 21.82 0.06	44 9 20.7 0.6	12.4 1.2	U	< 7.5				12.4 1.2	16.19	1.02	5.44 0.00		
55W213	8 46 22.34 0.14	44 32 59.8 2.0	0.75 0.18	U	<14.5				0.90 0.22	4.26	1.27	1.21 0.00		
55W214	8 46 24.38 0.11	44 47 40.7 1.5	0.76 0.17	U	<10.5				0.80 0.18	4.49	0.83	1.54 0.00		
55W216	8 46 57.76 0.17	45 0 25.5 2.4	4.71 1.13	U	<15.4				5.40 1.29	4.40	1.60	5.58 0.00		
55W217	8 46 58.08 0.06	44 11 22.6 0.6	16.5 1.5	U	< 6.8				16.5 1.5	18.82	1.02	6.20 0.00		
55W218	8 47 5.20 0.11	45 6 35.5 1.4	7.81 1.80	U	< 9.9				8.16 1.88	4.74	0.89	14.01 0.00		
55W221	8 47 12.00 0.10	44 59 41.8 1.4	3.31 0.71	U	<10.1				3.47 0.74	5.00	0.80	6.27 0.00		
55W223	8 47 21.76 0.11	44 22 36.3 1.5	2.01 0.48	U	<11.8				2.18 0.49	4.64	1.04	3.27 0.00		
55W227	8 47 38.83 0.09	44 16 47.8 1.2	1.95 1.37	U	<21.5				9.53 1.38	8.07	1.31	6.54 0.00		
55W229	8 48 10.13 0.05	44 31 11.7 0.5	62.6 4.8	R	5.4 1.5	122 32	4.3	0.50	62.6 4.8	71.20	1.10	5.80 0.00		
55W230	8 48 35.96 0.10	44 32 24.8 1.3	10.4 1.9	U	<12.2				11.8 2.1	6.37	1.21	11.18 0.00		
55W231	8 48 42.83 0.09	44 32 35.8 1.2	10.1 1.9	U	< 8.7				10.4 1.9	6.18	0.89	13.75 0.00		

1984A&AS...58....1W

TABLE VIIIa. — *The integral angular size distribution $h(\psi)$.*

ψ_{CRIT} (")	h(ψ)	n	S_{TOT}^{MAP} (mJy)
0			∞
	0.79±0.18	19	
2			29.90
	0.68±0.12	31	
4			9.13
	0.59±0.09	39	
6			5.13
	0.60±0.11	30	
8			3.49
	0.41±0.07	34	
10			2.58

TABLE VIIIb. — *Differential size distribution $g(\psi)$ and its integral $h(\psi)$.*

ψ (")	h(ψ)	Σn	g(ψ)
0	1.00	74	
			0.20±0.04
2	0.80	54	
			0.11±0.03
4	0.69	36	
			≲ 0.18
6	0.51	35	
			0.10±0.04
8	0.41	29	
			0.10±0.04
10	0.31	22	
			0.04±0.02
12	0.27	19	
			0.04±0.02
14	0.23	16	
			≲ 0.02
16	0.21	15	
			0.03±0.02
18	0.18	13	
			0.06±0.03
20	0.12	9	
			≲ 0.01
22	0.11	8	
			0.03±0.02
24	0.08	6	
			0.0
26	0.08	6	
			0.0
28	0.08	6	
			≲ 0.01
30	0.07	5	
			0.006±.004
40	0.04	3	
			0.0
50	0.04	3	
			0.008±.005

TABLE IX. — *The $\theta_{MED}(S)$ relations for various 21 cm surveys.*

Survey	Range in $S_{1.4}$ (mJy)	Median S_{1412} (mJy)	θ_{MED} (arcsec)	Reference
GB	6420 - 2600	4040	45.3 ± 10.8	BDFL (1972)
	2600 - 1980	2310	24.6 ± 5.1	
5C	200 - 15	25	11.1 ± 2.3	Downes et al. (1981)
	200 - 20	41	7.0 ± 2.0	Fielden et al. (1983)
BGS	110 - 55	78	7.8 ± 1.0	Oosterbaan (1978)
2nd WBK	65 - 15	30	10.0 ± 1.9	Katgert & Spinrad (1974)
3rd WBK	85 - 25	46	13.1 ± 2.8	Katgert (1977)
LBDS	320 - 80	115	9.2 ± 3.5	this paper
	80 - 20	32	11.0 ± 3.1	"
	20 - 10	12	13.0 ± 3.5	"
	10 - 5.5	7.7	8.4 ± 1.9	"
	(100 - 10	21	12.0 ± 2.2)	"
Lynx.2	5.0 - 1.8	2 7	10.0 ± 3.8	Windhorst et al. (1983)
	1.8 - 0.9	1.35	7.6 ± 2.0	"
	(10 - P.0	5.9	8.3 ± 1.1)	"

TABLE Xa. — *Total 21 cm source count for the 1st, 2nd, and 3rd Westerbork survey and the Deep Westerbork survey.*

$S_{1.4}$ (mJy)	<S> (mJy)	n/n_o $ster^{-1}Jy^{-1}$	N	Surveys
196.6				Weighted average over:
	130.0	1.16 ±0.16	49	1st WBK (Katgert et al., 1973)
90.2				
	68.1	0.78 ±0.11	53	2nd WBK (Katgert & Spinrad, 1974)
51.4				3rd WBK (Katgert, 1975, 1976)
	42.1	0.61 ±0.11	51	
34.9				
	21.5	0.435 ±0.032	178	
13.3				
	11.0	0.290 ±0.037	60	
9.01				
48.1				Deep Westerbork Survey
	28.3	0.430 ±0.095	21	(Le Poole, private communication)
17.0				
	12.0	0.252 ±0.050	26	(see also Willis et al., 1977)
8.50				
	6.01	0.118 ±0.025	24	
4.25				
	3.01	0.068 ±0.016	22	
2.12				
	1.51	0.055 ±0.017	13	
1.06				

1984A&AS...58....1W

TABLE Xb. — *The 5 σ LBDS count based on the 3 km maps.*

S (MJY)	<S> (MJY)	NH NL	NOF NOF	<WT> +-ME	N(S) (/STER)	DN/DS (/STER/JY)	N/NO	N(>S) (/STER)
0.778								4.37×10^{5} 0.54
	1.10	15 0	2 0	5.11 1.39	1.86×10^{5} 0.51	2.39×10^{8} 0.65	0.042 0.011	
1.56								2.51×10^{5} 0.19
	1.85	32 2	9 6	3.72 0.71	7.04×10^{4} 1.35	1.09×10^{8} 0.21	0.071 0.014	
2.20								1.81×10^{5} 0.14
	2.62	33 1	9 9	2.41 0.47	4.40×10^{4} 0.87	4.83×10^{7} 0.95	0.075 0.015	
3.11								1.37×10^{5} 0.11
	3.70	36 1	9 9	1.60 0.29	3.19×10^{4} 0.58	2.48×10^{7} 0.45	0.091 0.017	
4.40								1.05×10^{5} 0.09
	5.23	40 1	9 9	1.36 0.27	2.99×10^{4} 0.59	1.64×10^{7} 0.32	0.144 0.028	
6.22								7.46×10^{4} 0.66
	7.40	31 1	9 9	1.12 0.21	1.94×10^{4} 0.36	7.52×10^{6} 1.39	0.156 0.029	
8.80								5.53×10^{4} 0.55
	12.4	43 1	9 9	1.02 0.16	2.43×10^{4} 0.38	2.76×10^{6} 0.43	0.207 0.032	
17.6								3.10×10^{4} 0.40
	24.8	27 0	9 9	0.97 0.19	1.41×10^{4} 0.27	7.99×10^{5} 1.55	0.338 0.066	
35.2								1.69×10^{4} 0.30
	49.6	17 0	9 9	0.89 0.22	8.19×10^{3} 2.03	2.33×10^{5} 0.58	0.558 0.138	
70.4								8.73×10^{3} 2.15
	116.8	12 0	9 9	1.00 0.29	6.46×10^{3} 1.87	5.02×10^{4} 1.45	1.019 0.294	
199.1								2.27×10^{3} 1.08
	328.2	3 0	9 9	1.00 0.58	1.62×10^{3} 0.93	4.44×10^{3} 2.56	1.212 0.700	
563.2								6.51×10^{2} 5.39
	921.3	1 0	9 9	1.00 1.00	5.39×10^{2} 5.39	5.23×10^{2} 5.23	1.921 1.921	
1593								1.12×10^{2} 0.11

TABLE Xc. — *The 5 σ LBDS count based on the 1.5 km maps.*

S (MJY)	<S> (MJY)	NH NL	NOF NOF	<WT> +-ME	N(S) (/STER)	DN/DS (/STER/JY)	N/NO	N(>S) (/STER)
1.10								3.42×10^{5} 0.43
	1.56	13 17	7 3	4.72 1.17	1.65×10^{5} 0.41	1.50×10^{8} 0.37	0.062 0.015	
2.20								1.77×10^{5} 0.14
	2.62	8 23	9 9	2.71 0.57	4.52×10^{4} 0.96	4.96×10^{7} 1.05	0.077 0.016	
3.11								1.32×10^{5} 0.10
	3.70	8 24	9 9	1.94 0.37	3.34×10^{4} 0.63	2.59×10^{7} 0.49	0.095 0.018	
4.40								9.83×10^{4} 0.78
	5.23	5 25	9 9	1.33 0.25	2.15×10^{4} 0.41	1.18×10^{7} 0.22	0.103 0.020	
6.22								7.68×10^{4} 0.67
	7.40	11 24	9 9	1.18 0.21	2.22×10^{4} 0.39	8.61×10^{6} 1.52	0.179 0.032	
8.80								5.46×10^{4} 0.54

TABLE Xd. — *The 7 σ LBDS count based on the 3 km maps.*

S (MJY)	<S> (MJY)	NH NL	NOF NOF	<WT> +-ME	N(S) (/STER)	DN/DS (/STER/JY)	N/NO	N(>S) (/STER)
1.56								2.10×10^{5} 0.22
	2.20	27 0	7 3	3.96 1.01	7.41×10^{4} 1.88	4.77×10^{7} 1.21	0.047 0.012	
3.11								1.36×10^{5} 0.11
	3.70	27 0	9 9	2.01 0.42	2.92×10^{4} 0.61	2.26×10^{7} 0.47	0.083 0.017	
4.40								1.07×10^{5} 0.10
	5.23	30 0	9 9	1.58 0.34	2.55×10^{4} 0.54	1.40×10^{7} 0.30	0.123 0.026	
6.22								8.14×10^{4} 0.79
	7.40	30 1	9 9	1.53 0.31	2.55×10^{4} 0.51	9.90×10^{6} 2.00	0.206 0.042	
8.80								5.58×10^{4} 0.60

FIGURE 1a. — Profile plot of the inner 1° × 1° of the 21 cm map of Lynx.1 before cleaning. The map flux of the strong point source is 150 mJy.

FIGURE 1b. — Profile plot after cleaning and restoration of the same map. Residual grating rings are due to calibration errors and due to aliasing of the 60′ ring (in the upper left) of 4C45.17.

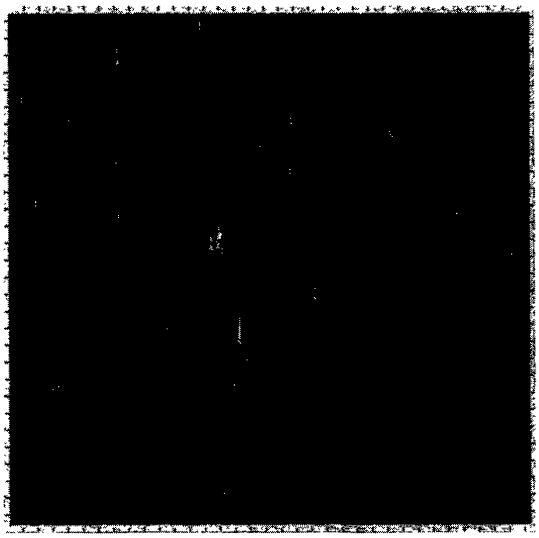

FIGURE 1c. — Profile plot after the strongest source components have been subtracted (before the FFT) and selfcalibration has been applied.

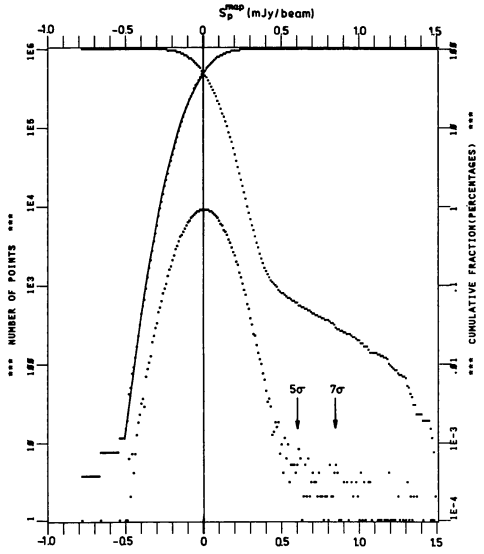

FIGURE 2. — Logarithmic histogram of intensities (0.01 mJy intervals) in the central 512^2 pixels of the cleaned and restored Lynx.2 map. At the negative side the histogram is perfectly Gaussian in shape.

FIGURE 3. — Contour plot of the inner 256^2 pixels of the same Lynx.2 map, superimposed on a grey scale plot, which illustrates the noise uniformity. The grey scale values are optimized to show largest contrast for $-1\,\sigma \leqslant S_p^{MAP} \leqslant +1\,\sigma$.

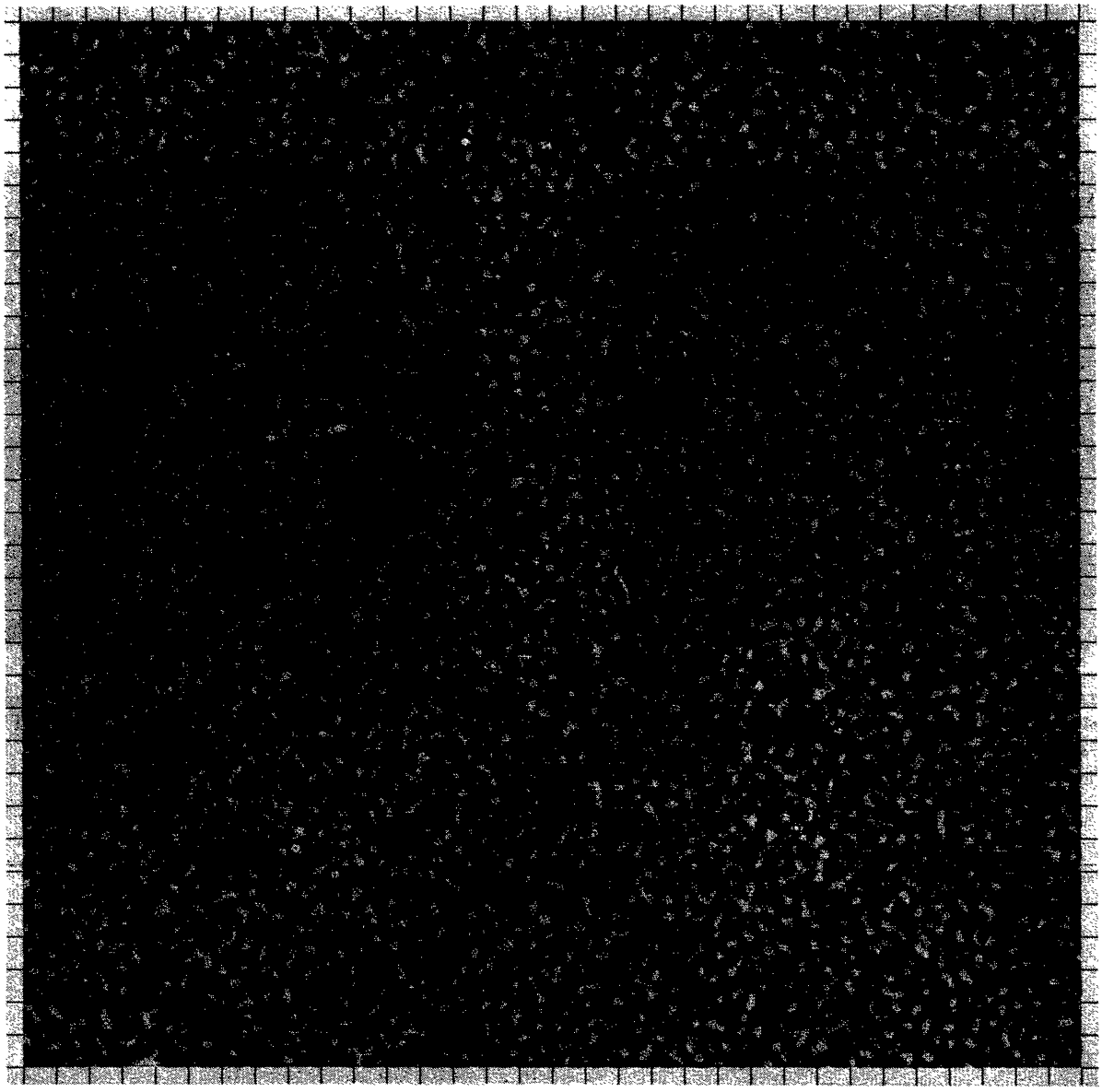

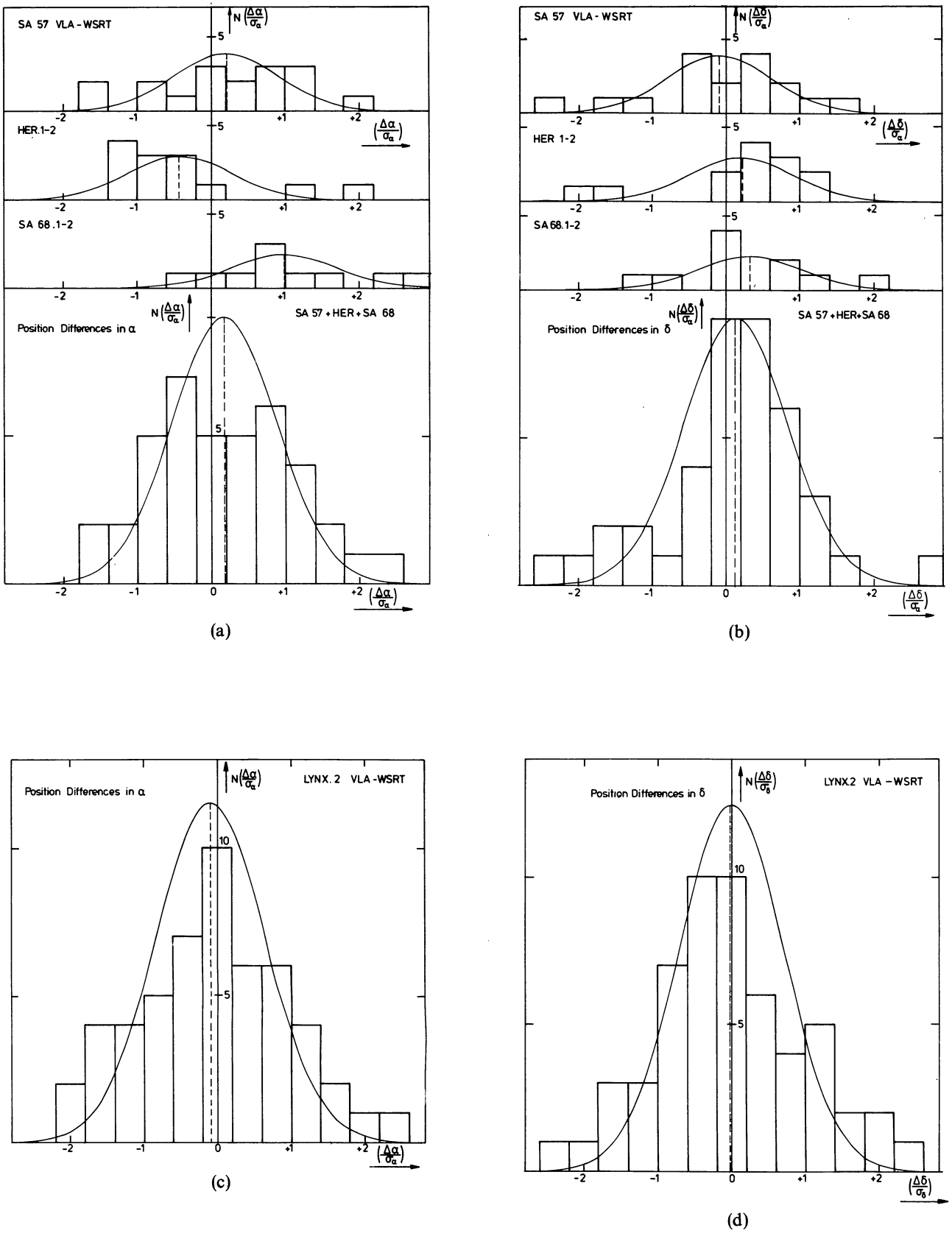

FIGURES 4a-d. — Position error distributions for sources in overlapping fields.

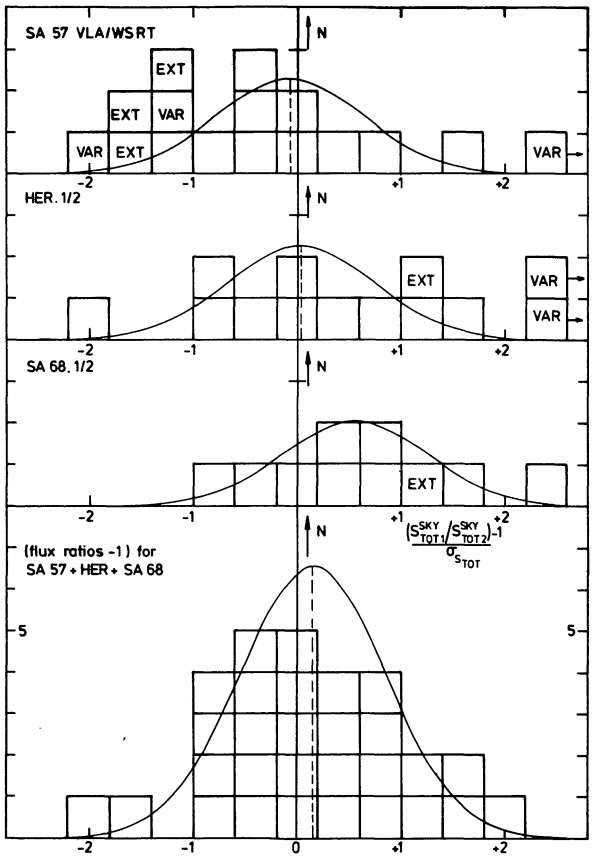

(e)

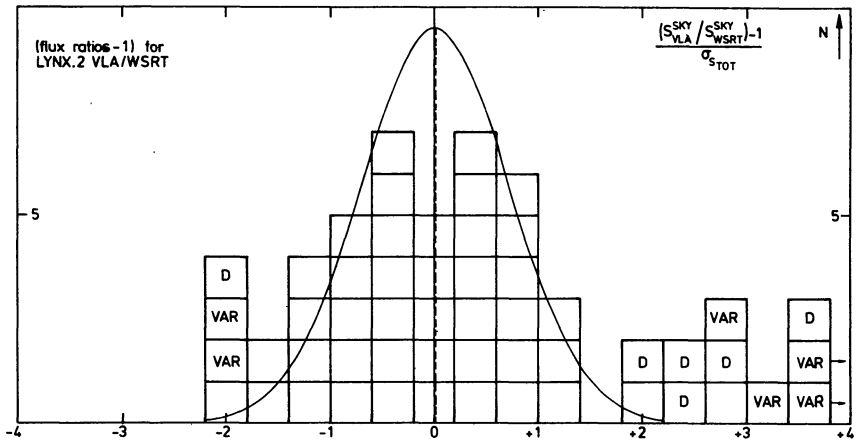

(f)

FIGURES 4e-f. — Flux error distributions in overlapping fields. The (flux ratios − 1) are normalized to their combined errors. Double, extended and variable sources are marked, but not included in the Gaussian expectations (drawn lines).

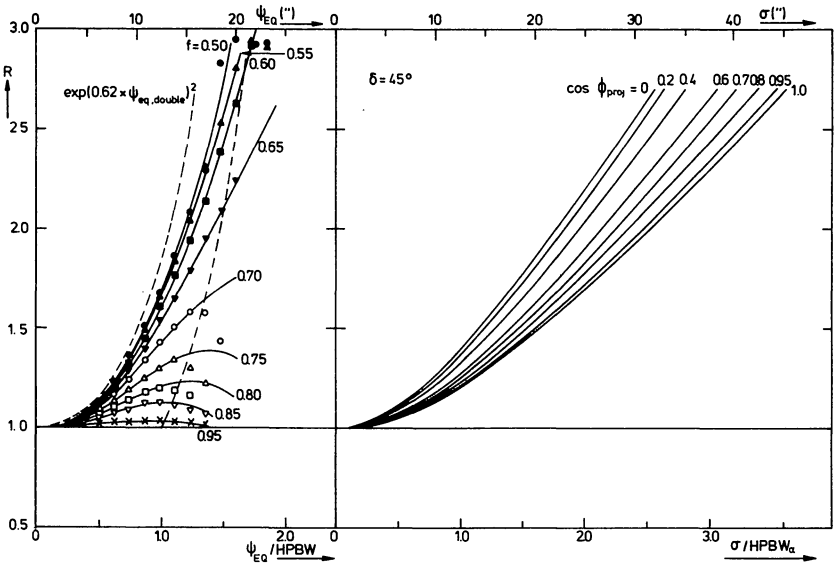

FIGURE 5a. — The relation between the normalized source area R and the equivalent angular size ψ_{EQ}, for various values of the component flux ratio f. The leftmost dashed line shows the behaviour of Willis *et al.*'s (1977) algorithm for an equal double source.

FIGURE 5c. — The relation between R and σ, for various values of the projected position angle ϕ_{proj} of the source in the map plane.

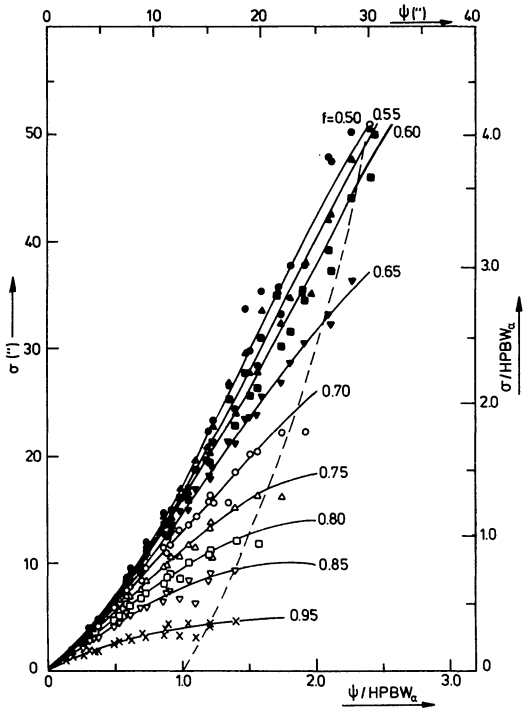

FIGURE 5b. — The relation between the deconvolved Gaussian halfwidth σ and the intrinsic angular size ψ for various values of f. In figures 5a and 5b the rightmost dashed line shows beyond which (ψ, f)-values the algorithm breaks down.

FIGURES 5a-c. — The relation between (R, σ, ϕ_{proj}) and (ψ, f, ϕ) in the limit $S_p/N \to \infty$.

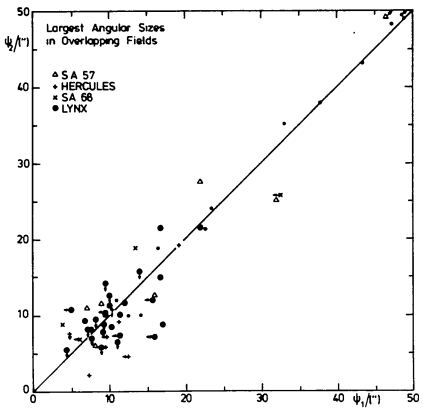

FIGURE 6a. — Comparison of the intrinsic largest angular sizes ψ. Arrows denote 1 σ upper limits. Angular sizes of individual components of extended sources are affected by blending and are not plotted.

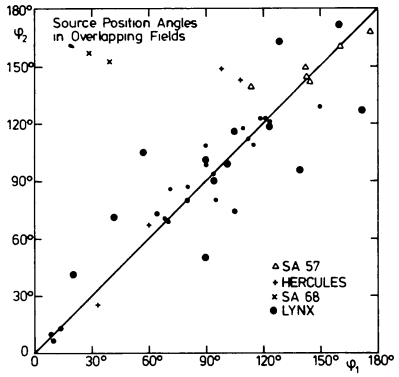

FIGURE 6b. — Comparison of the intrinsic source position angles ϕ, including the ones for individual components of extended sources.

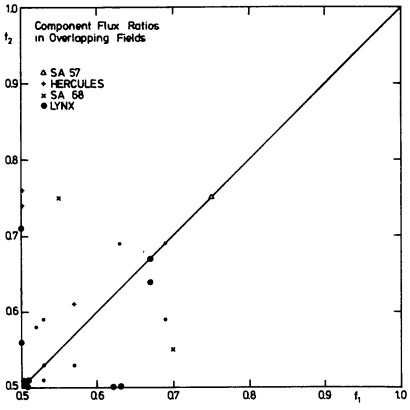

FIGURE 6c. — Comparison of the component flux ratio f. If f could not be determined in one of the maps, it was set to 0.5.

FIGURES 6a-c. — Comparison of intrinsic source parameters in overlapping fields. Thin circles are direct measurements for extended sources.

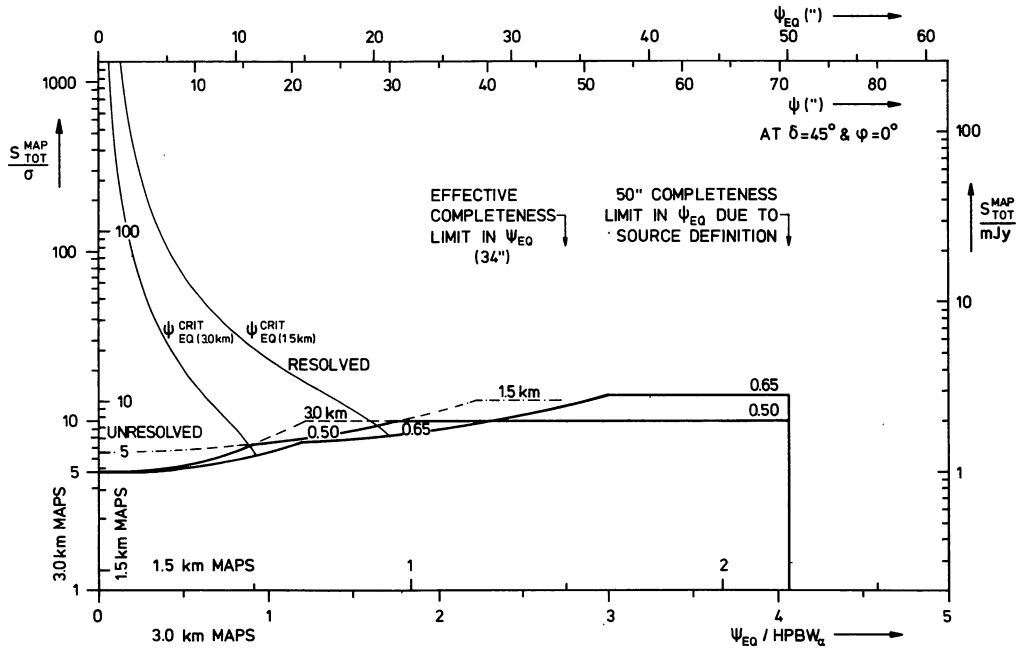

FIGURE 7. — The sample completeness in total map flux (the combined effect of the 3 and 1.5 km maps) as a function of east-west angular size and component flux ratio f. The curve with $f = 0.65$ represents the effective completeness limit for the whole survey. The two curves labelled ψ_{EQ}^{CRIT} separate unresolved and resolved sources.

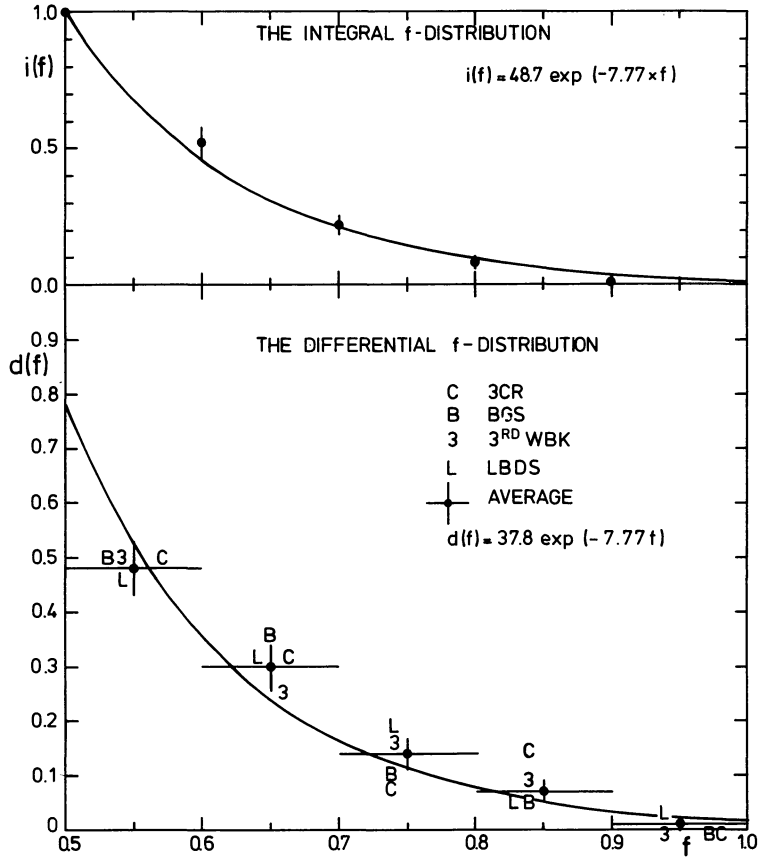

FIGURE 8. — The distribution of component flux ratios f.

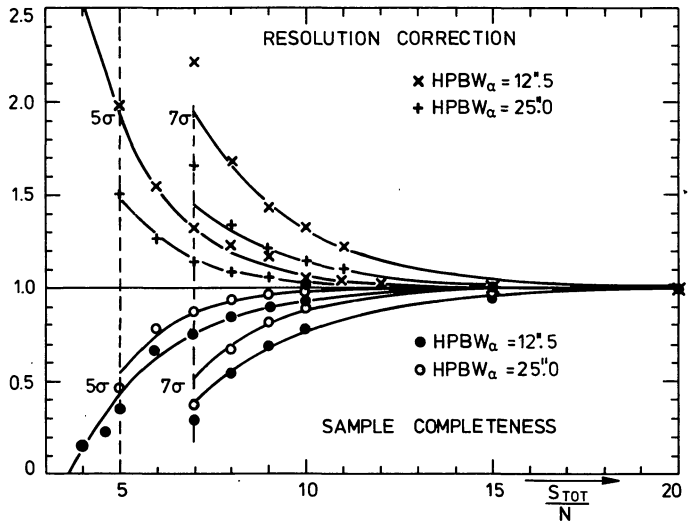

FIGURE 9a, b. — The resolution correction and sample completeness *versus* total map signal-to-noise for different HPBW$_\alpha$ and peak flux density cut-offs.

Following pages.

FIGURE 10. — Contour plots of 0°.03 × 0°.03 areas around individual radio sources, that were asymmetrically resolved, extended or complex. In each lower right corner the HPBW is marked. Little crosses denote the positions of optical identification candidates, given in paper II. Contour values are generally − 5, − 3, + 2, + 3, + 4, + 5, + 7.5, + 10, + 20, + 40, + 80, + 160, + 320 and + 640 × σ, where σ is in map units (Table Ib). Negative contours are dashed. For some strong sources only the following contour values are drawn : − 5, − 3, + 2, + 3.5, + 5, + 10, + 20, + 40, + 80, + 320 and + 640 × σ. Such sources are marked with a filled circle in the HPBW-cross. A contour for 55W172 has been given from both the Lynx.2 and Lynx.3 maps and shows how differential primary beam effects and minor differences in the synthesized beam may affect the apparent source morphology. The contour plot of 55W022 also contains 55W023, while that of 55W222 also contains 55W220.

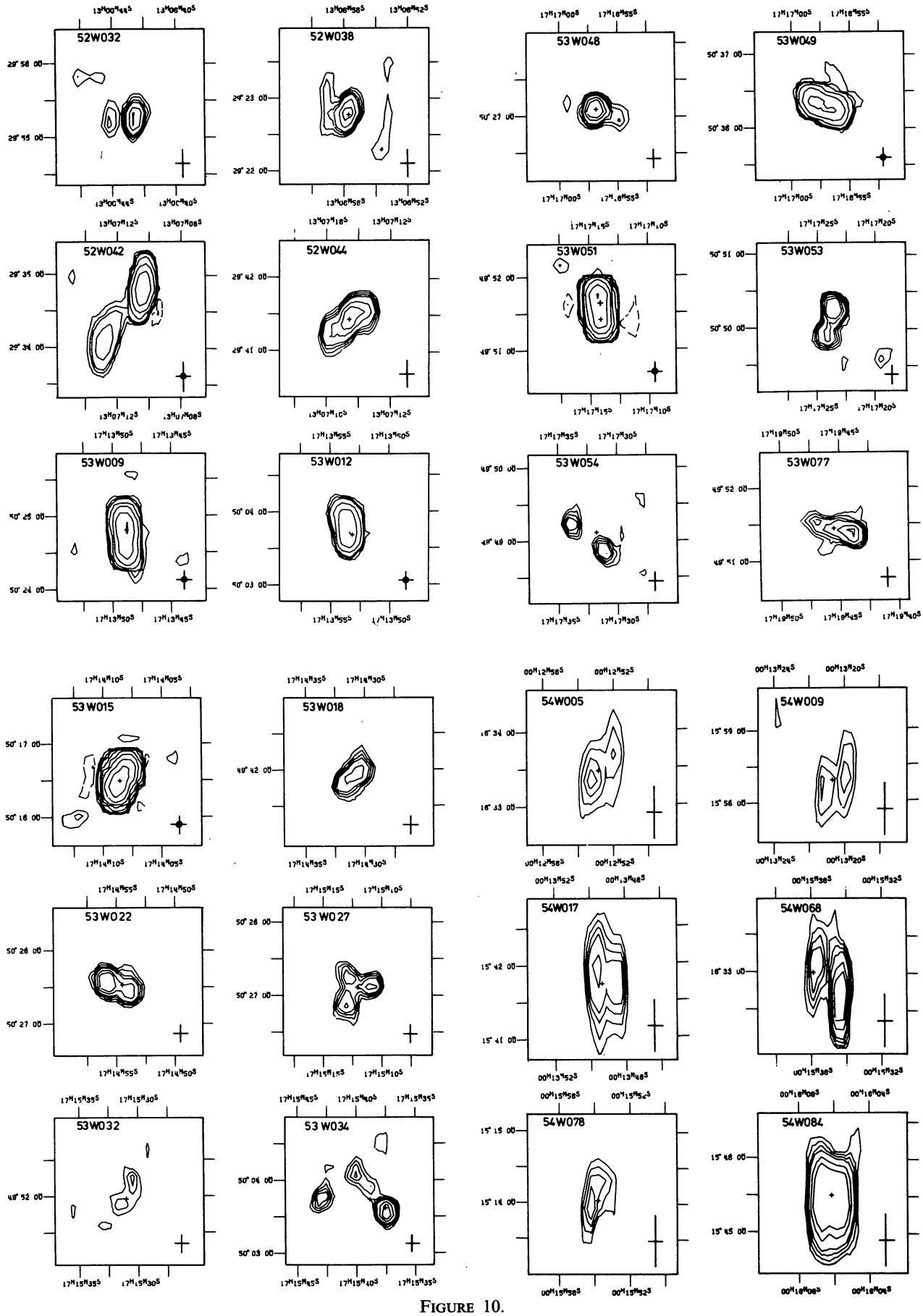

FIGURE 10.

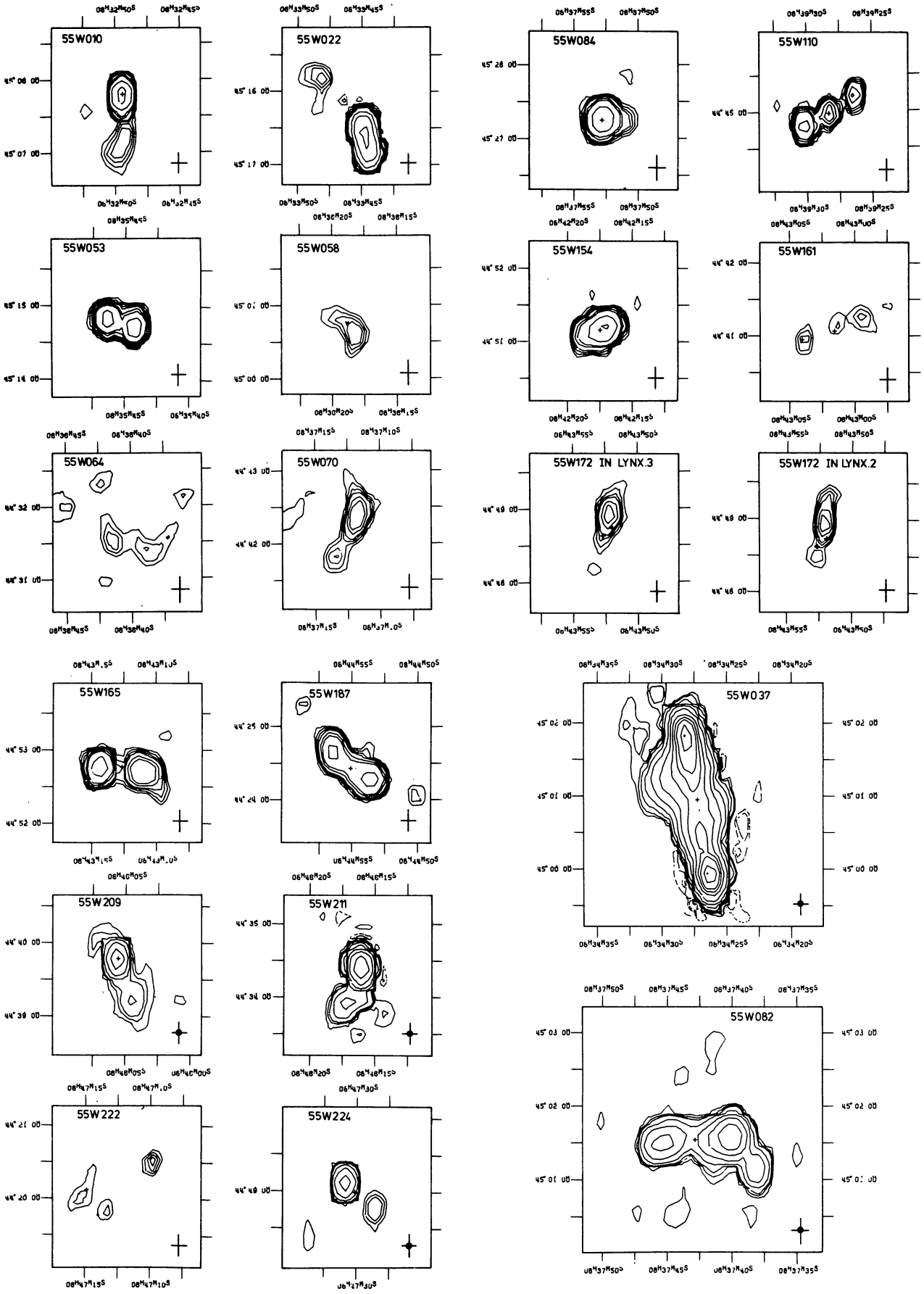

FIGURE 10 (*continued*).

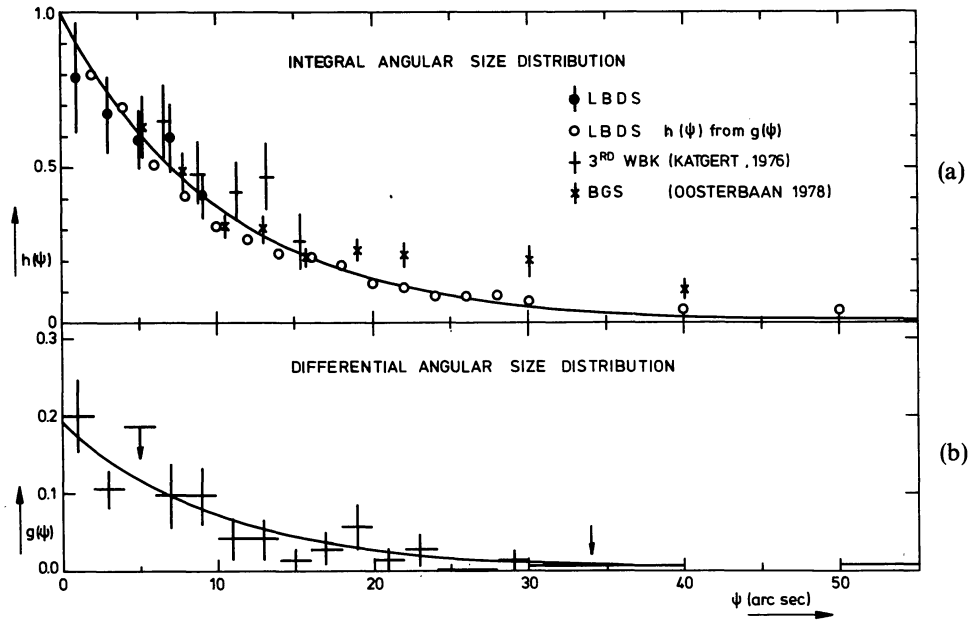

FIGURE 11. — (a) The integral angular size distribution $h(\psi)$. Filled circles are the independent points, open circles are derived from $g(\psi)$. The data from the BGS and 3rd WBK surveys ($S_{1.4} \gtrsim 60$ mJy) show a larger fraction of sources for $\psi \geqslant 20''$. (b) The differential angular size distribution $g(\psi)$. The arrow denotes the completeness limit of the LBDS in ψ.

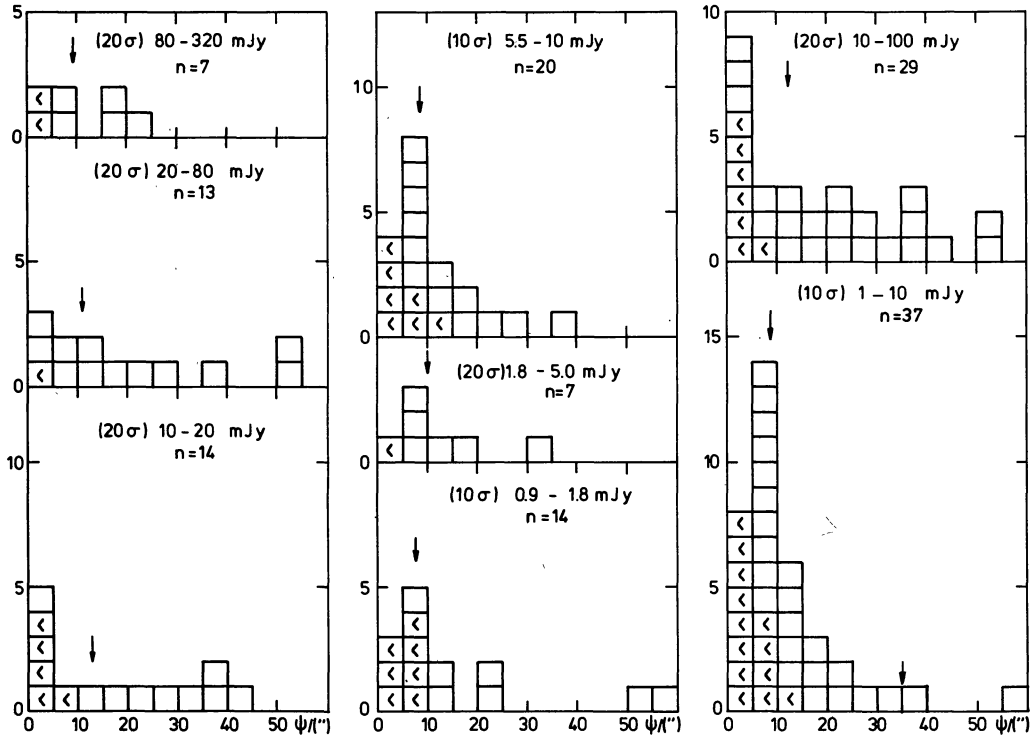

FIGURE 12. — The differential angular size distribution as a function of flux density. The arrows mark the median angular size θ_{MED}. There is a somewhat larger fraction of compact sources ($\psi \geqslant 10''$) in the flux density range 1-10 mJy than in the range 10-100 mJy.

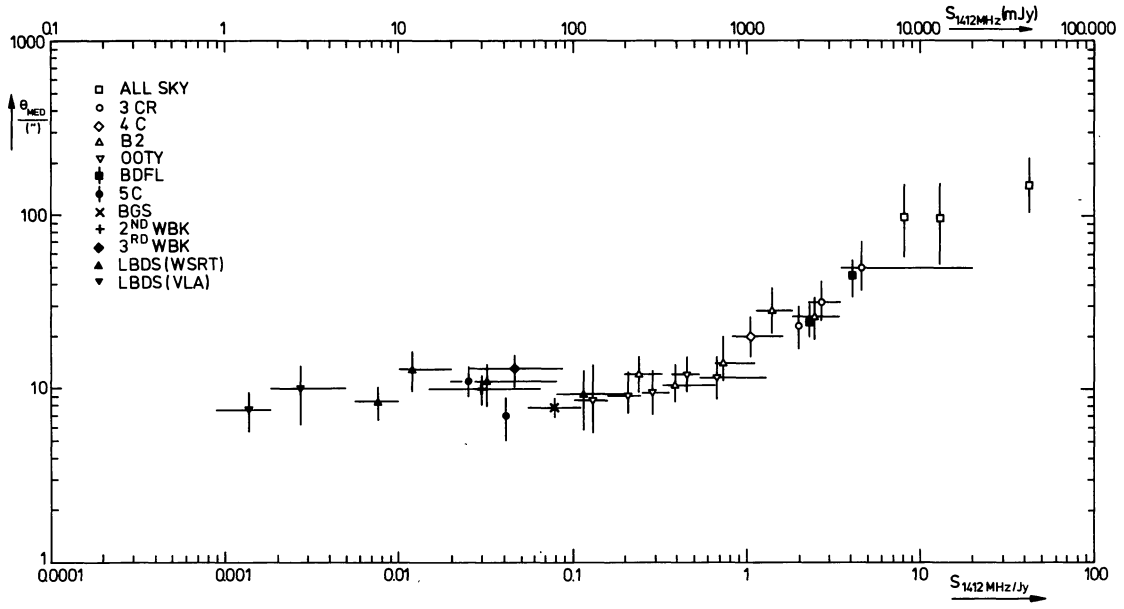

FIGURE 13. — The median angular size flux density relation at 1.4 GHz. Open symbols refer to surveys selected at low frequencies (mainly at 408 MHz). Filled symbols refer to surveys selected at 1.4 GHz, the filled triangles are from the LBDS. For 1-200 mJy the value of θ_{MED} remains almost constant ($\sim$ 10″).

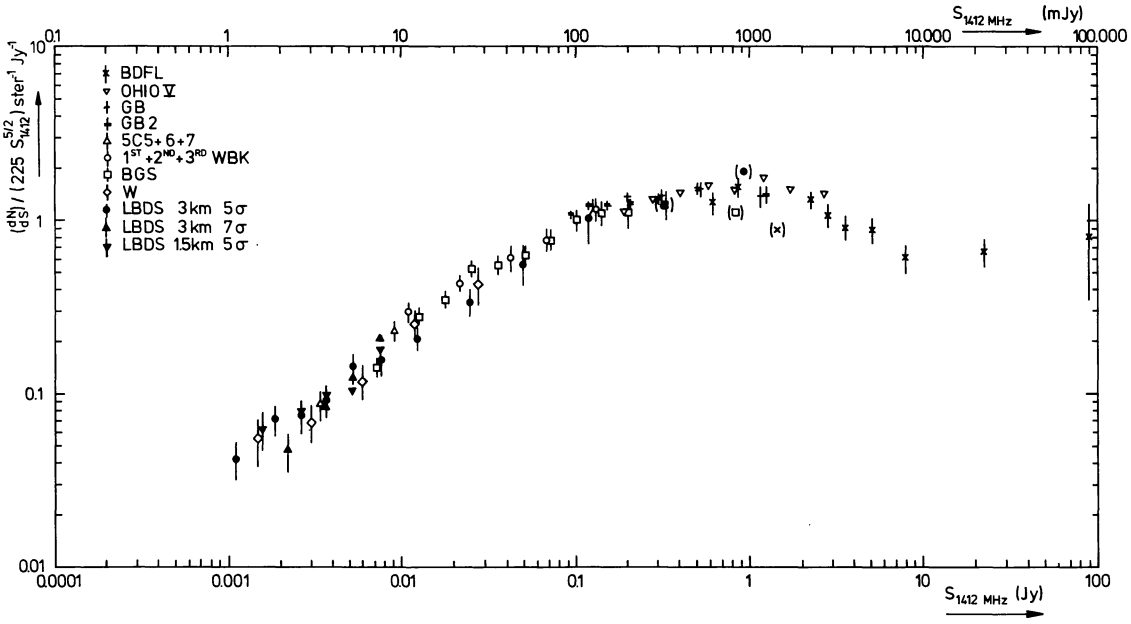

FIGURE 14. — The differential source counts at 1412 MHz. Open symbols are data from previous 1.4 GHz surveys. Filled symbols represent the 5 σ and 7 σ count from the current survey, based primarily on the 3 km maps. Also shown is the 5 σ count that is based mainly on the 1.5 km maps. The agreement of the LBDS counts at various significance levels and beam sizes shows that population and resolution bias were corrected for properly.